TNO Built Environment and Geosciences

Princetonlaan 6
P.O. Box 80015
3508 TA Utrecht
The Netherlands

www.tno.nl

T +31 30 256 42 56
F +31 30 256 44 75
wegwijzer@tno.nl

TNO report

TNO-034-UT-2010-01298 / A

Central Offshore Platform - Area NCP2E
Burial history, temperature, source rock maturity and hydrocarbon generation

Date	July 2010
Author(s)	J.M. Verweij M. Souto Carneiro Echternach N. Witmans
Customer	Ministry of Economic Affairs
Projectname	4DMod
Project number	034.22774
No. of copies	5
Number of pages	70 (incl. appendices)
Number of appendices	4

Contents

1 Introduction

1.1 Mapping of the deep subsurface of the Netherlands offshore (NCP-2 project)

The detailed mapping of seven offshore areas on the Netherlands Continental Shelf (Figure 1.1) was initiated in late 2005 and will be finalized in 2010. It builds on and goes one step beyond the previous regional mapping of the Netherlands onshore and offshore. In 2004 the publication of the Geological Atlas of the Subsurface of the Netherlands – onshore rounded off the onshore regional mapping project and a 'quick and dirty' offshore mapping (NCP-1 project) was completed in 2006 (viz. on the http://www.nlog.nl; Duin et al., 2006).

The main aim of the detailed mapping of seven sub-areas is to present a more comprehensive model of the subsurface to future and current operators in the oil industry and to governmental and non-governmental organizations for, amongst other things, the spatial planning of the Dutch subsurface. The deliverables include:

- 3D geological framework (depth and thickness grids)
- Rock and fluid parameters (petrophysical parameters, P, T, Vr)
- 3D burial histories
- Petroleum system analysis

All deliverables, such as maps, grids, graphs and reports, can be downloaded at the http://www.nlog.nl site. When applicable, regular updates will be made available on the site.

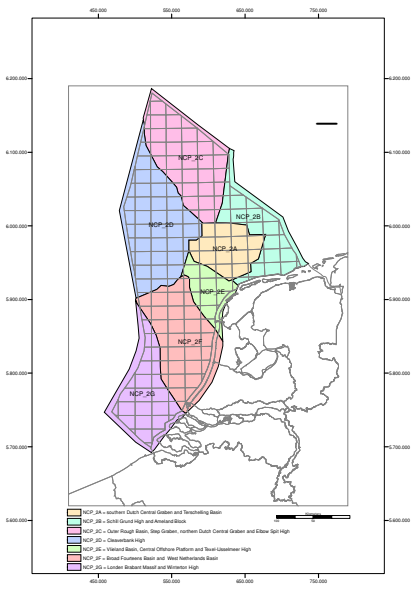

Figure 1.1 NCP-2 areas, including the location of the project area NCP-2E: Central Offshore Platform.

1.2 Definition of mapping areas in the Netherlands offshore

Based on consultation with the exploration departments of the oil companies operating in the Netherlands it was decided to divide the offshore area into seven sub-areas (Figure 1.1). These areas represent more or less

structural entities at the Late Jurassic to Early Cretaceous times (Figure 1.2). The detailed mapping project started with sub-area NCP-2A: Terschelling Basin and southern part of the Dutch Central Graben and was continued with sub-area NCP-2E, which comprises the Central Offshore Platform, Vlieland Basin, the northwestern part of the Texel-IJsselmeer High and the offshore extension of the Noord-Holland Platform.

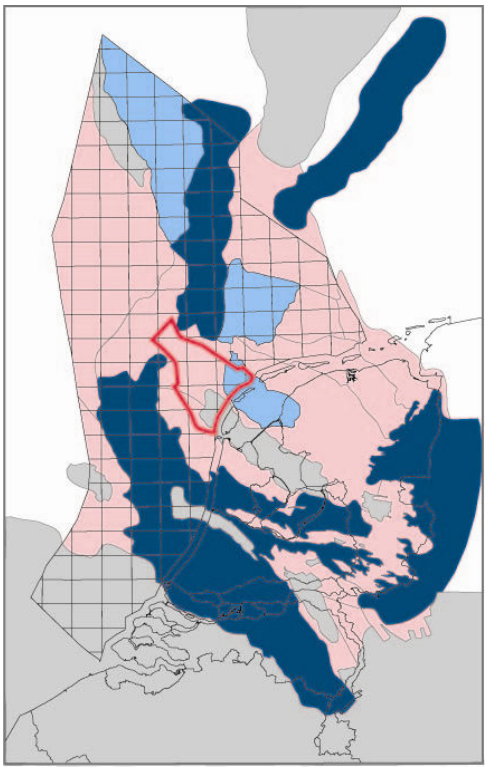

Figure 1.2 Structural setting at Late Jurassic-Early Cretaceous: highs (grey), platforms (pink), basins with Lower Jurassic units (dark blue) and basins without Lower Jurassic units (light blue).

1.3 Detailed mapping of the Central Offshore Platform

The detailed mapping was focused on the assessment of the present-day stratigraphic and structural framework of the sedimentary fill of the area as well as on the properties of rocks and fluids it contains, such as reservoir porosity, pore fluid pressure, formation water salinity, source rock maturity, characteristics of oil and gas.

Special attention was paid to improve the lithostratigraphic sub-division of the Upper Rotliegend Group and to provide new porosity data for the main reservoir units in this group. 3D basin modeling was used to integrate the data, visualize the geodynamic, geothermal and geofluid history the area, and herewith to provide additional information of importance for evaluating the petroleum systems.

1.4 Geological setting of the Central Offshore Platform

The dominant features of the present-day structural framework and lithostratigraphic buildup are summarized in Figures 1.3, 1.4 and 1.5. The main structural elements in the area are: Central Offshore Platform, Vlieland Basin, Texel-IJsselmeer High, and Noord-Holland Platform (Figure 1.4). The Namurian Epen Formation is the oldest unit included in the study (Figure 1.3). The Epen Formation covers the Dinantian paleogeography, which is characterized by inferred carbonate platforms and basinal areas (Geluk et al., 2007, Kombrink, 2008; Figure 1.6).

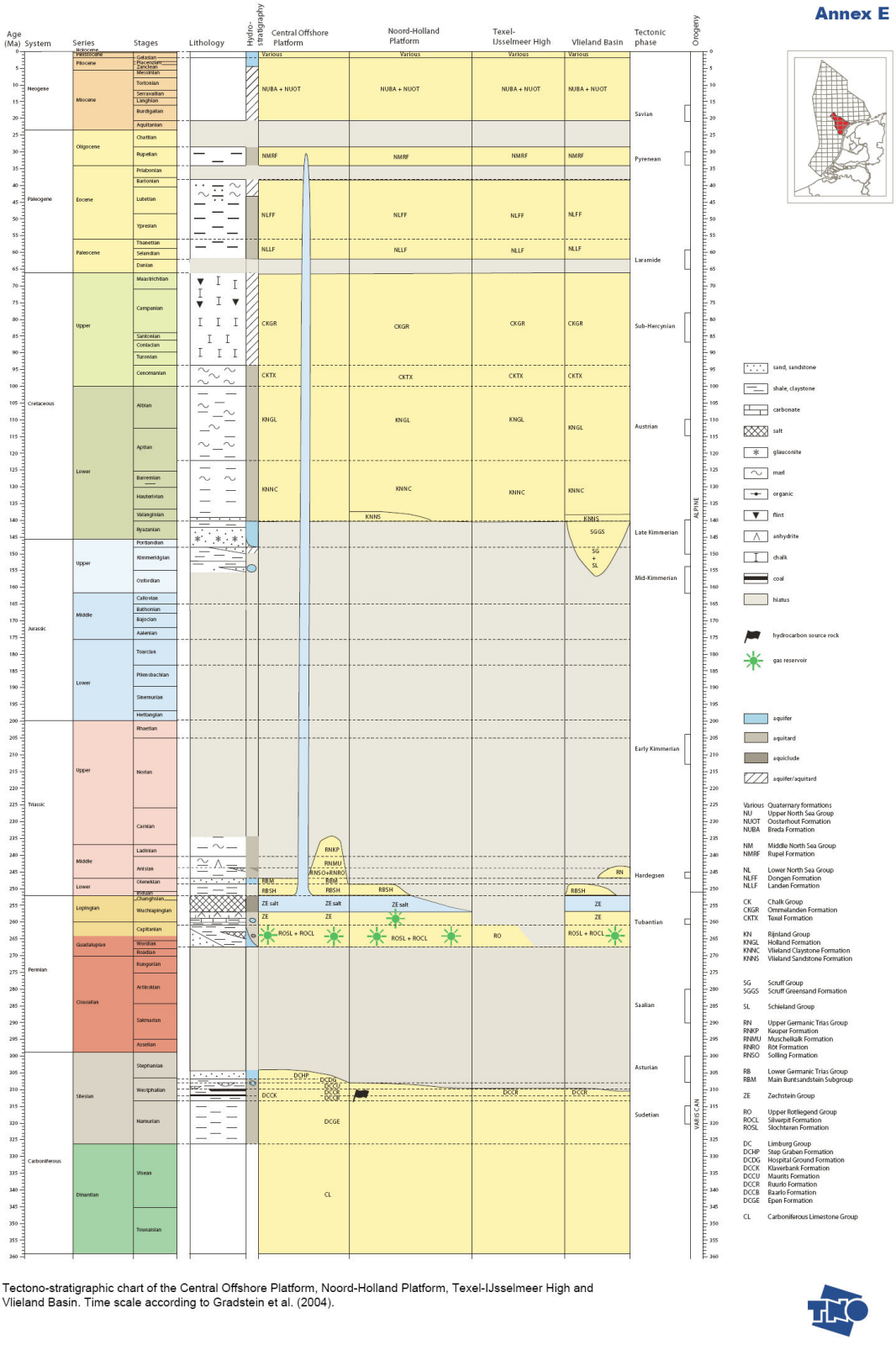

Tecto-stratigraphic chart of the Central Offshore Platform, Noord-Holland Platform, Texel-IJsselmeer High and Vlieland Basin. Time scale according to Gradstein et al. (2004).

Figure 1.3 Tectonostratigraphic chart of the Central Offshore Platform, Noord-Holland Platform, Texel-IJsselmeer High and Vlieland Basin.

The Carboniferous to present geological history of the area was strongly affected by the Saalian, Mid-Late Kimmerian and Subhercynian/Laramide tectonic phases. The Saalian phase in Early to Middle Permian induced strong uplift and regional erosion of the Carboniferous units. The Carboniferous units at the Texel-IJsselmeer High were also affected by later erosion phases. The Pre-Permian subcrop map (Figure 1.7 a) shows the regional variation in erosion of the Carboniferous units. Erosion affected the Ruurlo Formation in the southeast, while in the northwest the younger units of the Step Graben are preserved. After the Saalian uplift and erosion, the Carboniferous was covered by Rotliegend and subsequently by Zechstein, Triassic and Early Jurassic sediments. The Mesozoic tectonic phases induced a differential dynamic development of the main structural elements in the area: while sediments accumulated in the subsiding Vlieland Basin during the Late Jurassic-Early Cretaceous time (Kimmerian tectonic phases), the adjacent Central Offshore Platform, Noord-Holland Platform and Texel-IJsselmeer High were uplifted and eroded. Late Cretaceous Subhercynian inversion reduced the deposition of Chalk in the Vlieland Basin. Halokinesis has affected post-Permian units in the northwestern part of the area.

Detailed information on the present-day stratigraphic and structural framework of the sedimentary fill of the area is given in Witmans et al. (2010).

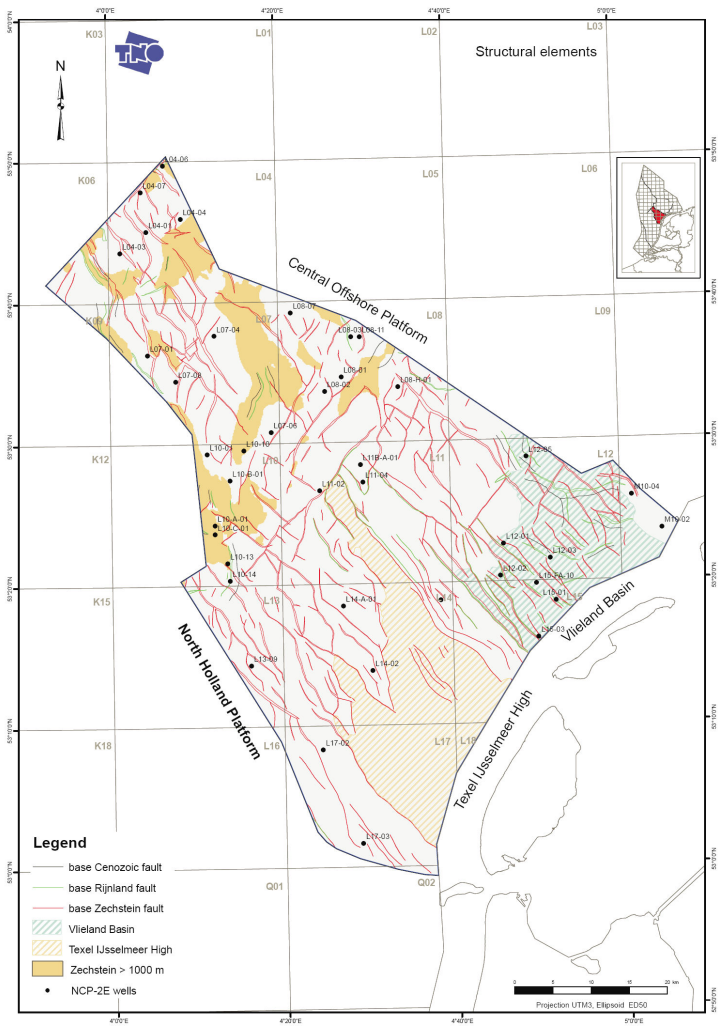

Figure 1.4 Structural elements

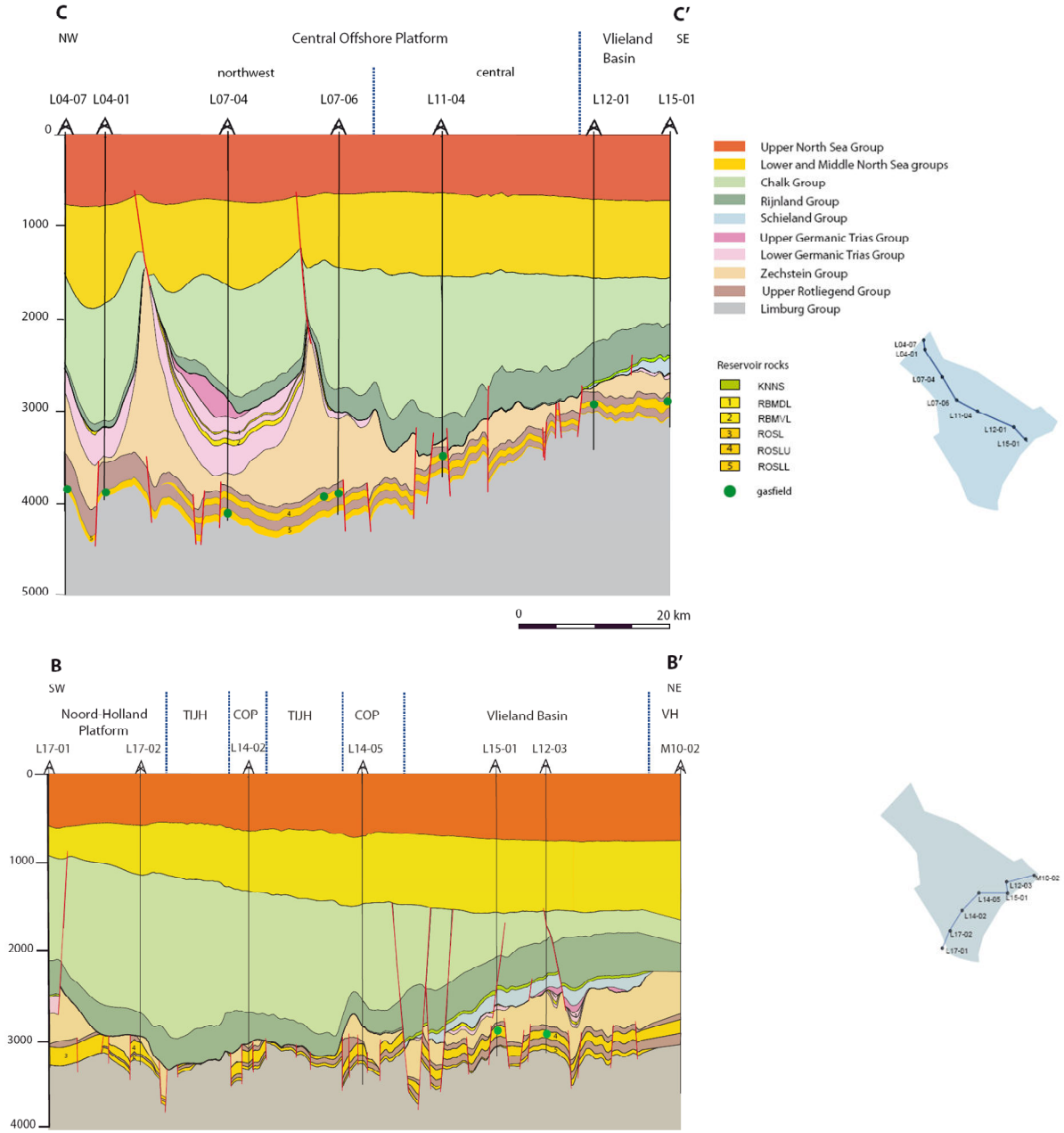

Figure 1.5 Cross-section C-C' shows the pinch-out of the Upper Slochteren Sandstone reservoir in northerly direction. Halokinesis has affected the post-Permian units in the northwestern part of the Central Offshore Platform. In the depletion areas Triassic units have been preserved. In the Vlieland Basin Upper Jurassic and Lower Cretaceous units rest on a remnant of the Lower Germanic Trias Group.
Cross-section B-B' shows the variation in present-day stratigraphic build-up in the southern part of the area. On the Texel-IJsselmeer High the Upper Rotliegend Group is locally missing and Zechstein, Germanic Trias and Schieland Groups are absent. Triassic units are thin or absent in the Platform areas. A very thick Chalk sequence is present on the platforms and highs. In the Vlieland Basin, Upper Jurassic Schieland Group have been preserved and are overlain by the Lower Cretaceous Friesland Member. Late Cretaceous inversion affected the thickness of the Chalk Group in the basin. The overlying Upper North Sea Group increases in thickness towards the north.

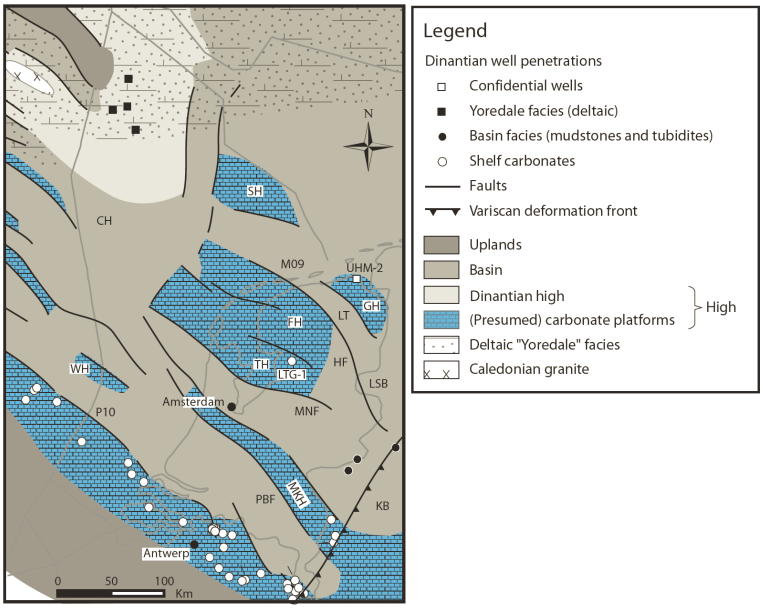

Figure 1.6 Dinantian paleogeography. Dinantian highs around the London-Brabant Massif and on Groningen High are characterized by carbonate platforms (Kombrink, 2008), a carbonate platform is inferred to occur on the Texel-IJsselmeer High (Kombrink et al., 2010b).

1.5 Petroleum systems of the Central Offshore Platform

The three main elements of the Westphalian-Upper Rotliegend gas system in the NCP2E area are: the Westphalian source rocks, the Upper Rotliegend reservoirs and the Zechstein evaporites as ultimate top seal (Figure 1.7).

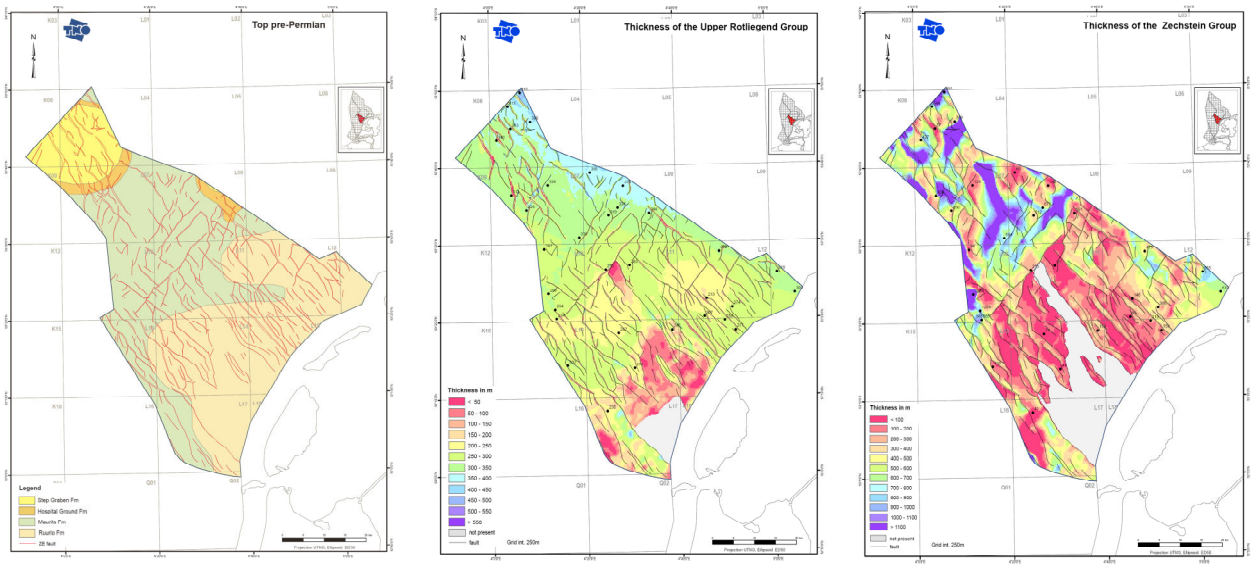

Figure 1.7 Distribution of the three main elements of the Westphalian-Upper Rotliegend gas system in the NCP2E area; a. Westphalian source rocks are present in the whole area; b. the Upper Rotliegend (reservoir) is present in large part of the area, but is locally absent in the southernmost part of the area, on the Texel-IJsselmeer High; c. the Zechstein (seal) is present in large part of the Central Offshore Platform, but is missing on the Texel-IJsselmeer High.

Distribution of gas accumulations

Figure 1.8 shows the distribution of the gas fields in the area. The gas fields occur in the reservoir units of the Slochteren Formation of the Upper Rotliegend Group (Lower and Upper Slochteren Members, Figures 1.5

and 1.7b). To a minor extent gas was also encountered in the Ten Boer Member of the Silverpit Formation (ROCLT, well L12-01) and in Zechstein Carbonates (e.g. well L14A-01).

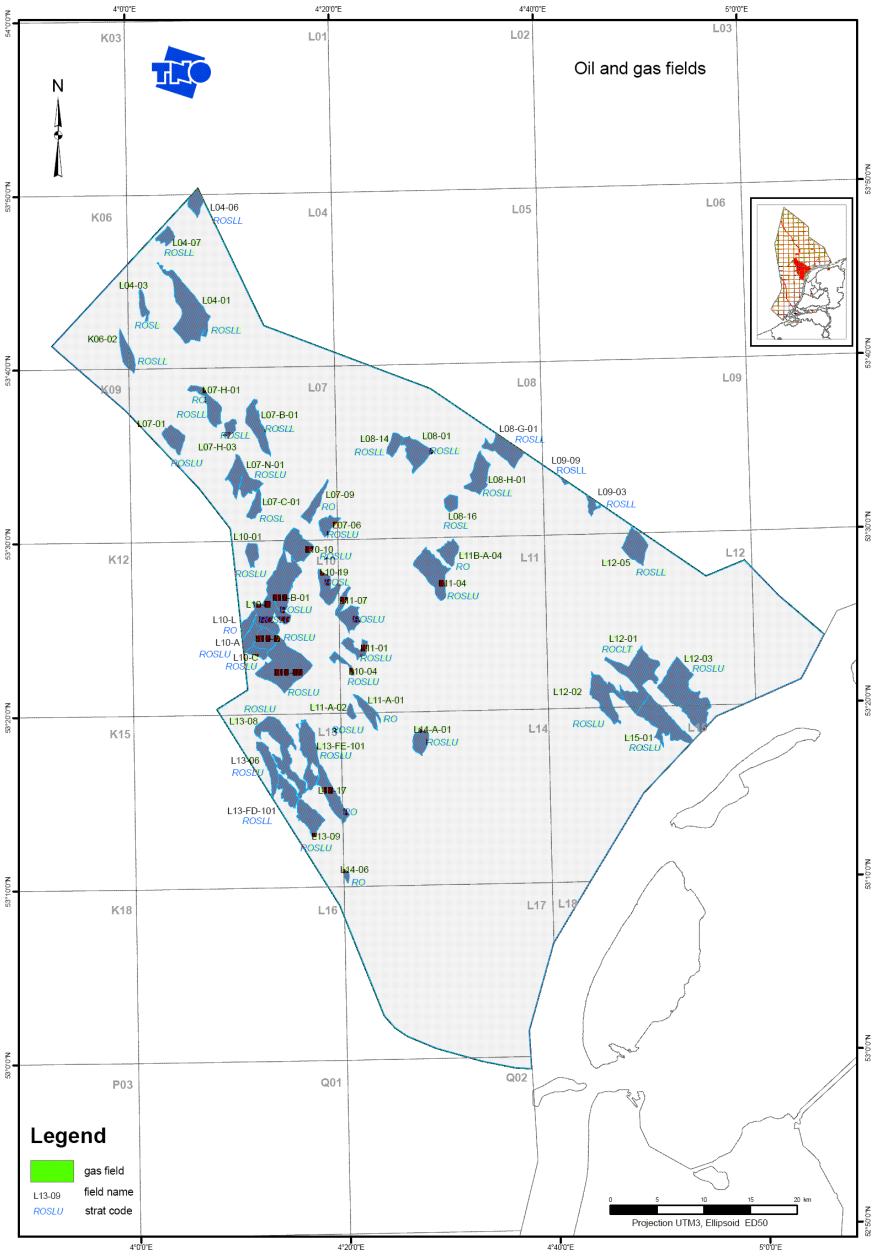

Figure 1.8 Gas fields in NCP2E area / the Central Offshore Platform and Vlieland Basin.

Geochemical gas composition

The gas in the Upper Rotliegend reservoirs is wet (Figure 1.9). The wetness ratio (C1/(C2+C3)) of the gas varies between 9 and 68. Very wet gases with wetness ratios of 10-18, and 1-5 Mol% CO2 and less than 3 Mol% of N2, are encountered in the Vlieland Basin. In block L08 at the northeastern border of the area gas is of intermediate wetness with a wetness ratio between 27 and 50, a CO2 content of 2-6 Mol% and N2 content of less than 2 Mol%. In the remainder of the area the wetness of the gas is variable and the gas is mostly less wet in comparison with the gas in the Vlieland Basin.

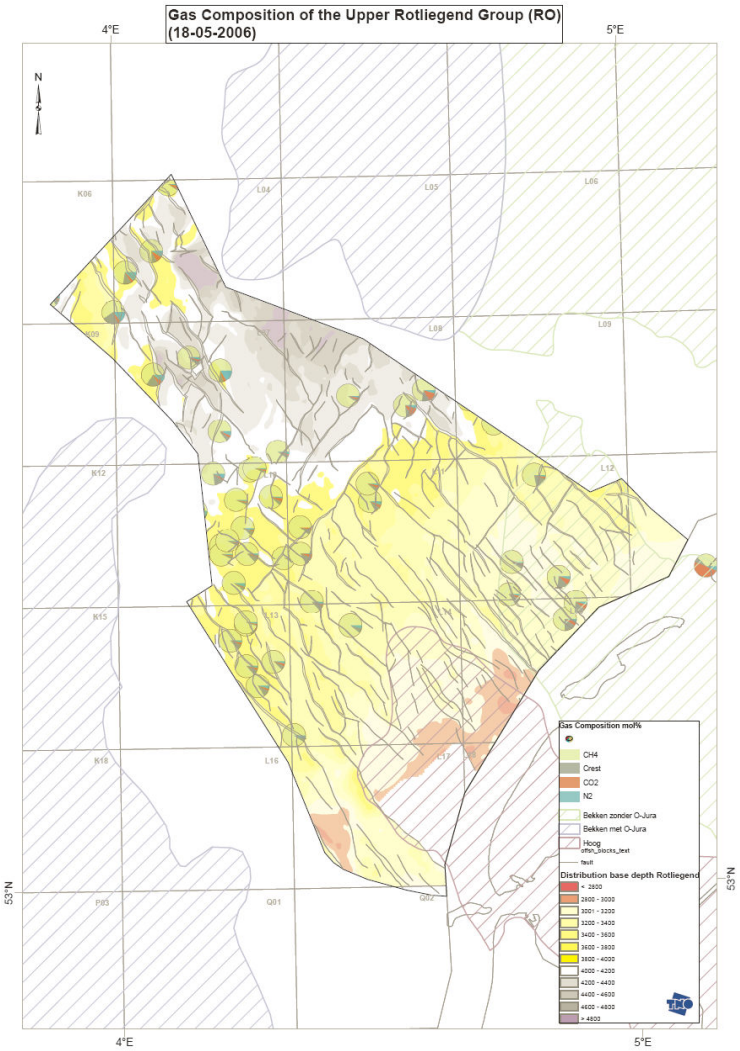

Figure 1.9 Geochemical compositions of the natural gas accumulations. This map is also included in Annex 1.

Fluid overpressure condition

The present-day fluid pressure and flow condition in the Westphalian-Upper Rotliegend gas system influences present-day migration and accumulation of the gas in various ways, amongst other things it exerts an influence on present-day gas column heights. The fluids (pore water and gas) in the Limburg, Upper Rotliegend and Zechstein groups are overpressured (Figure 1.10). The distribution of the all fluid overpressures in the Upper Rotliegend Group are presented in Figure 1.11 (all fluid overpressures include overpressures of pore water and gas). Relatively high values of overpressure occur along the northeastern border of the area (for example gas fluid overpressure reach values of 14.7 MPa at L12-05, 8.2 MPa at L08-G-01, and 9.2 MPa at L04-06). The overpressures decrease southward and reach their lowest values around the Texel-IJsselmeer High (for example gas fluid overpressures of 4.0 MPa at L15-FA101, 3.6 MPa at L14-06, and water overpressure of 3.3 MPa at L14-06).

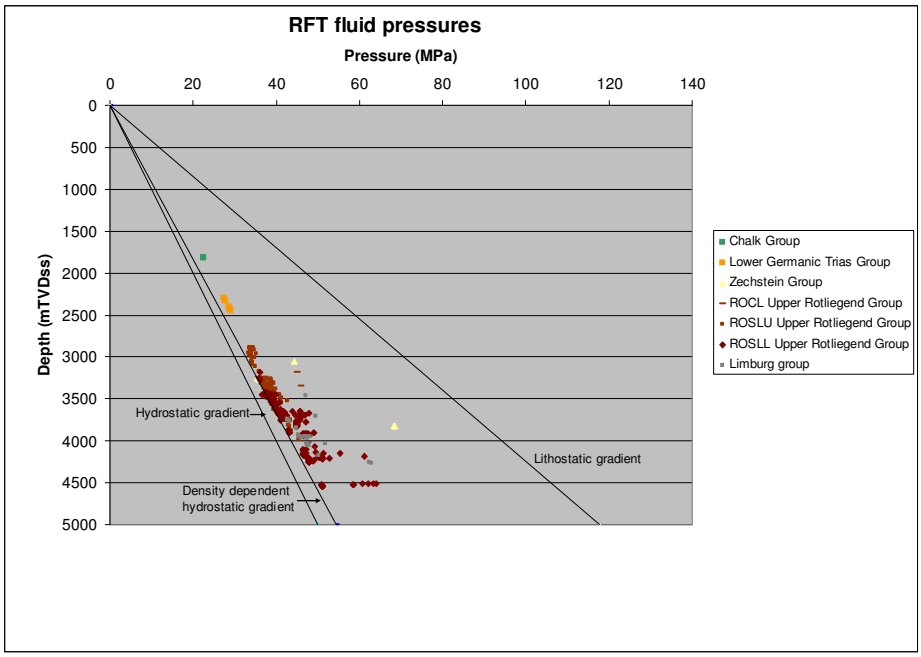

Figure 1.10 Multiwell plot of selected fluid pressures versus depth in different stratigraphic units in the NCP2E area.

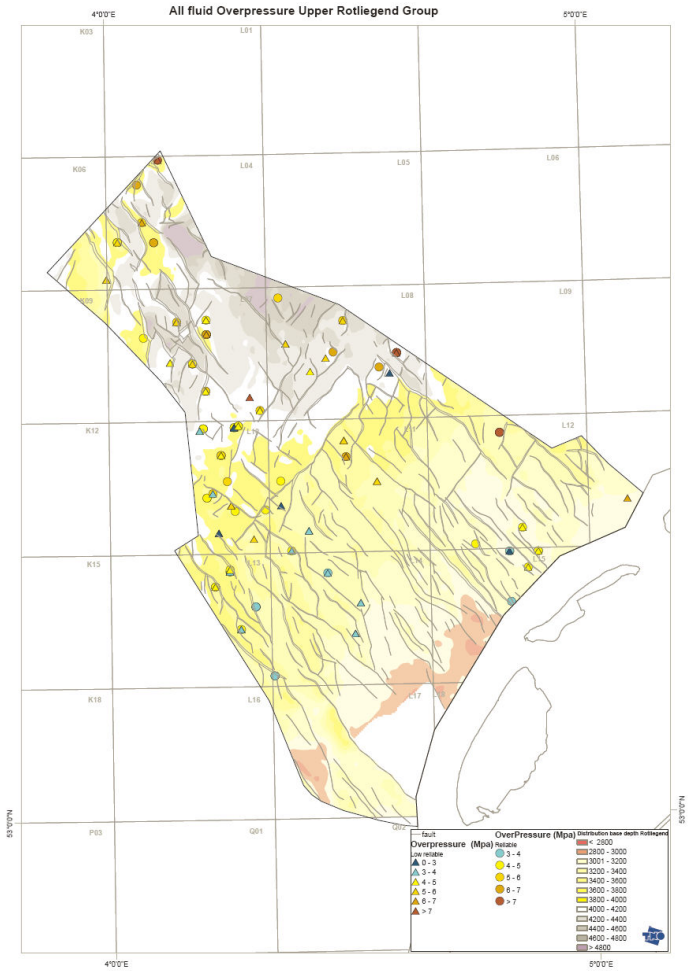

Figure 1.11 Distribution of all fluid overpressures in the Upper Rotliegend Group. All fluid = water, oil, gas; overpressure = measured pore fluid pressure at a certain depth minus hydrostatic pressure of pore water (calculated for a water density of 1020 kg/m3 at that depth). This map is also included in Annex 1.

Source rocks
The main source rocks for gas are the Westphalian coals and carbonaceous shales of the Limburg Group. These source rocks of kerogen type III include the Baarlo, Ruurlo and Maurits formations. The present-day burial depth of the top of the Limburg Group increases from southeast to northwest and reaches depths between 3000 and 4500 m. The Baarlo and Ruurlo Formations occur throughout the area; the Maurits Formation is absent in the southeast (Figures 1.3 and 1.7a).

In the Netherlands secondary Carboniferous source rocks occur in basal Namurian organic rich shales (e.g. Lokhorst, 1998; NITG, 1998; Gerling et al., 1999, Doornenbal and Stevenson, 2010). These black organic rich shales developed in an anoxic environment and are suggested by Van Buggenum and De Jager (2007) to be present throughout the central and deeper part of the Carboniferous Basin. The organic rich shales are known to occur immediately to the north of the London Brabant Massif, onlapping the Dinantian carbonates to the south (e.g. Doornenbal and Stevenson, 2010). A Dinantian Carbonate platform was also inferred to be present below the Epen Formation in the Texel-IJsselmeer High area (Figure 1.6).
Organic rich black shale of the bituminous Geverik Member of the Epen Formation was encountered in onshore well GVK-1. In the southern Netherlands, Namurian shale source rocks have TOC's up to 10% and are mainly of kerogen type II. It is not known if the Namurian source rock (Geverik Member) also extends as far north as the study area, as the deepest wells in the study area only penetrate the top part of the Carboniferous and do not reach the Namurian.
In addition to the basal organic rich shale, dispersed organic matter occurs locally in the Namurian A and B shales of the Epen Formation.
Interest in Namurian source and reservoir characteristics is increasing. This relates to three different issues:

- The role of the Namurian in explaining the occurrence of nitrogen in gas fields. The Namurian is thought to have contributed significantly to the nitrogen charge of natural gas accumulations in the Netherlands (De Jager and Geluk, 2007). The nitrogen content in the Central Offshore Platform varies, the highest contents are encountered in gas fields in the western part of the area (Figure 1.9); no published information is available explaining these variations;
- The unknown Namurian shale gas prospectivity;
- The unknown propectivity of the Dinantian carbonate play (based on the assumptions that 1. Dinantian carbonate platforms were charged with hydrocarbons generated and migrated from Basal Namurian sources; and 2. accumulated hydrocarbons were preserved through geological history).

1.6 Basin modeling of the Central Offshore Platform

TNO uses 1D, 2D and 3D basin modeling to integrate the wealth of data and information gathered and mapped in its detailed mapping program of subareas of offshore Netherlands and to evaluate the interdependencies of the different processes that affect rocks and fluids during its geological history. Special attention is paid to processes and conditions affecting hydrocarbon potential. Here we present selected results from a full 3D reconstruction of the burial history, and the history of temperature, source rock maturity and timing of hydrocarbon generation in the Central Offshore Platform from 320 Ma to present-day (using basin modeling program Petromod, version 10, of IES/Schlumberger). More detailed insight in the timing of hydrocarbon generation in the Carboniferous-Rotliegend petroleum system is much needed as a basis to improve understanding of the geochemical compositions of gas (content of non-hydrocarbons, such as nitrogen) and to assess drainage areas of undrilled prospects. In addition, there is a need for information on burial, temperature and maturity histories of the Namurian in order to improve the evaluation of, for example, its propectivity as a shale gas. For these objectives we used, in addition to the latest mapping results, also recently constructed thermal boundary conditions and we investigated different kinetics and source rock properties for the Westphalian and assumed Namurian source intervals.

2 Basin modeling: Workflow, input data and boundary conditions

2.1 Assumptions and conditions underlying the basin modeling approach

General assumptions and conditions inherent in basin modeling:

- Geological history:
  - the model is laterally constrained: no horizontal compression or extension of the basin fill is taken into account
  - vertical movement only (no lateral deformation of the sediments in the model, except for salt movement)
  - salt movement has no direct relation to changes in stress
  - compaction of the basin fill is vertical
  - compaction is mechanical according to vertical effective stress-based rock property model
- History pore water fluids
  - density of pore water is constant
- Thermal history
  - conductive heat flow

The basin modeling scenarios presented here are based on a geological model without faults and hydrostatic conditions are assumed in all scenarios.

In addition to the above listed general limiting assumptions and conditions, default set-ups of the modeling package influence simulation results. Such default set-ups include default relations between standard lithologies and properties through compaction approaches, porosity-permeability relations, thermal models, kinetic models; mixing rules lithology. The selection of the proper set-up is an important part of the basin modeling workflow.

2.2 Data base

The basic data requirements for the 3D modeling involve: present-day geometry (stratigraphy; property/facies boundaries within stratigraphic units, water depth); lithological properties (lithological composition of each stratigraphic unit and eroded – part of – unit and of each facies); quantified uninterrupted time-sequence of events during geological history (3D history of sedimentation, uplift and erosion; estimated thickness of erosion; 3D history of water depth, basal heat flow, surface temperature; timing of salt movement); calibration data (such as present-day temperatures, porosities, permeabilities, pressures, vitrinite reflectance measurements).

The results of the detailed mapping of the Central Offshore Platform (Witmans et al., 2010) provided the basic 3D stratigraphic model required for the numerical modeling.

2.3 Basin modeling workflow

Initially 1D simulations at well locations were carried out to verify the conceptual models of subsidence and erosion history; calibration with porosity, temperature and vitrinite reflectance data.

The general workflow with respect to the full 3D basin modeling of the Central Offshore Platform and Vlieland Basin, as described here, included the following three phases and steps:

<u>Phase 1 Building geological model, simulating burial history, calibration:</u>

- Building 3D geological model;

- Selection proper Petromod default porosity-depth and porosity-permeability relations;
- Running 3D model for reconstructing burial history;
- Selection of proper surface temperature boundary condition, by comparing two scenarios for the Cenozoic history of sediment water interface temperatures;
- Selection proper thermal conductivity model (using measured temperature data and published information on thermal conductivities); the default Sekiguchi model of Petromod was selected;
- Running 3D model for reconstructing history of temperature and maturity (using kinetic model Sweeney and Burnham, 1990 and a constant basal heat flow boundary condition of 60 mW/m2); calibration with temperature and vitrinite reflectance data;

Phase 2 Simulating history of temperature, source rock maturity and timing hydrocarbon generation of Westphalian source rocks:

- Running 3D model for reconstructing the history of temperature, source rock maturity and timing of hydrocarbon generation for the Westphalian Baarlo, Ruurlo and Maurits Formations, initially using the Burnham (1989)_T3 kinetic model and later the Pepper & Corvi (1995)_TIII-IV(F) kinetic model for the Westphalian source rocks, the selected SWIT boundary condition (SWIT=sediment water interface temperature), a basal heat flow of 60 mW/m2, and a set of source rock parameters;
- Evaluation of simulation results; the Pepper & Corvi (1995)_TIII-IV(F) kinetic model was selected for subsequent modeling;
- Running 3D model for reconstructing the history of temperature and timing of hydrocarbon generation for the Westphalian Baarlo, Ruurlo and Maurits Formations, using the Pepper & Corvi (1995)_TIII-IV(F) kinetic model for the Westphalian source rocks, the selected SWIT boundary condition, tectonic basal heat flow, and a set of source rock parameters;
- Comparison of simulation results for the two different basal heat flow boundary conditions; the constant basal heat flow of 60 mW/m2 was selected for subsequent modeling.

Phase 3 Simulating history of temperature, source rock maturity and timing hydrocarbon generation of Westphalian and Namurian source rocks:

- Extension of the 3D geological model with assumed thicknesses of the Namurian Epen Formation;
- Running 3D model for reconstructing the history of temperature, source rock maturity and timing of hydrocarbon generation for Baarlo, Ruurlo and Maurits Formations (using the Pepper & Corvi (1995)_TIII-IV(F) kinetic model) as well as for the assumed Namurian source rocks (using the Burnham(1989)_T2 kinetic model), for the selected SWIT boundary condition, a basal heat flow of 60 mW/m2, and a set of source rock parameters. The 3D model was run for two different sets of parameters for the Namurian source rocks;
- Evaluation of simulation results.

2.4 Input: Present-day geometry

The present-day 3D stratigraphic model was the basic input for the 3D modeling. Depth and thickness maps of 20 stratigraphic units were loaded from Petrel into Petromod and horizons were adjusted. The mapped stratigraphic units comprise the main stratigraphic groups and subdivisions thereof based on their reservoir properties: Upper North Sea, Middle and Lower North Sea groups; Chalk Group (CK); Rijnland Group (KN) and the Vlieland Sandstone Formation (KNNS); Schieland Group (SL) and Scruff Group (SG); Upper Germanic Triassic Group (RN) and the Basal Solling Sandstone Member of the Solling Formation (RNSOB); Detfurth Claystone Member (RBMDC), Lower Detfurth Sandstone Member (RBMDL), Volpriehausen Clay-Siltstone Member (RBMVC), Lower Volpriehausen Sandstone Member (RBMVL) and the Lower Buntsandstein Formation (RBSH) of the Lower Germanic Triassic Group; Zechstein Group (ZE); Rotliegend Group (RO), and Slochteren Formation (ROSL), Upper Slochteren Member (ROSLU) and Lower Slochteren Member (ROSLL).

The present-day stratigraphic model was extended to greater depth with the Step Graben, Hospital Ground, Maurits, Ruurlo and Baarlo Formations of the Limburg Group (model Scenario 1) ; and later also with the

Namurian Epen Formation and Geverik Member (model Scenario 2). The thicknesses of the Westphalian Formations were derived from the subcrop map of the base Permian unconformity and regional mapping studies (Witmans et al., 2010). The total thickness of the Namurian was estimated from regional information given in Kombrink (2008) and Kombrink et al. (2008).

The Upper North Sea Group was split into 3 layers (Quaternary, Pliocene and Miocene) to incorporate the more detailed changes in sedimentation rate during late Tertiary and Quaternary times.

The initial 3D model includes 27 layers plus basement (Figure 2.1, Table 2.1)

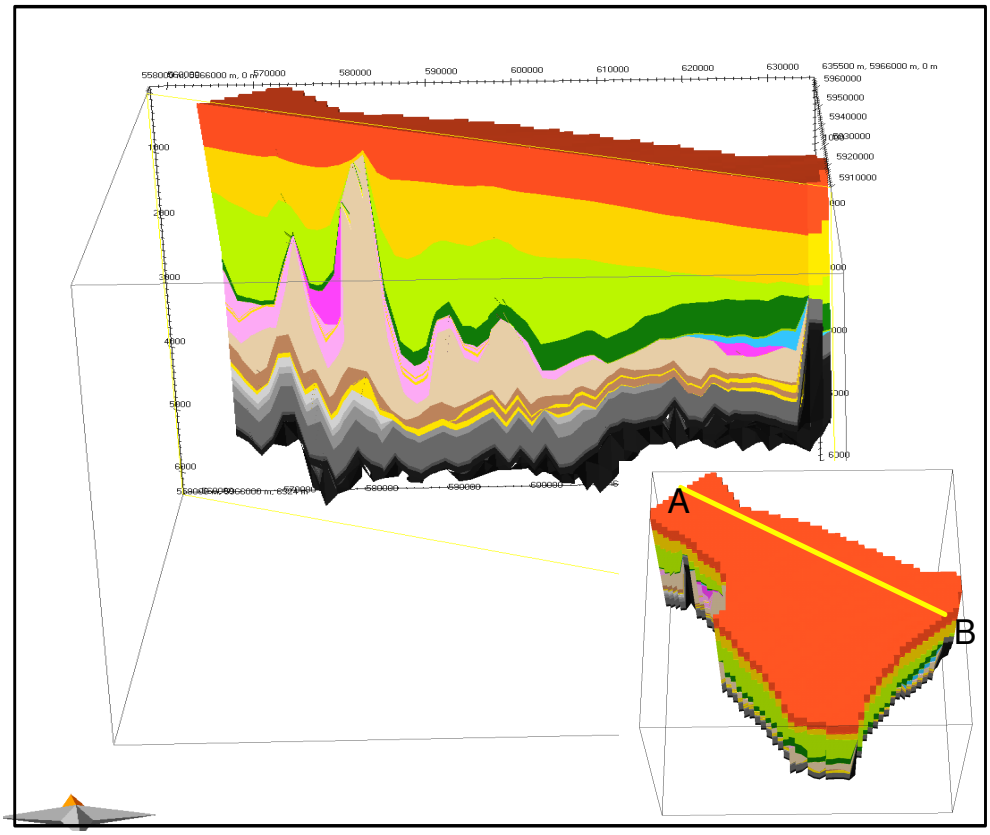

Figure 2.1 Present-day 3D geometrical model of the Central Offshore Platform and Vlieland Basin.

2.5 Input: Properties

Lithology: Lithological compositions were assigned to each layer (Tables 2.1 and 2.2).

Table 2.1 Model stratigraphy (Scenario 1): 28 layers and assigned lithological composition in Central Offshore Platform and Vlieland Basin.

Layer	Layer Code	Lithology
		Facies
1 Upper North Sea Group_Quaternary	NU	75% Shale 25% Sand
2 Upper North Sea Group_Pliocene	NU	50% Sand 50% Shale
3 Upper North Sea Group_Miocene	NU	50% Sand 50% Shale
4 Middle & Lower North Sea group	NM & NL	90% Shale 10% Sand
5 Chalk Group	CK	100% Chalk
6 Rijnland Group	KN	75% Shale 25% Silt
7 Rijnland Group_Vlieland Sandstone Formation	KNNS	90% Sand 10% Shale
8 Schieland & Scruff groups	SL&SG	100% Shale
9 Upper Germanic Trias Group	RN	75% Shale 25% Silt
10 Basal Solling Sandstone Member	RNSOB	75% Sand 25% Shale
11 Detfurth Claystone Member	RBMDC	100% Shale
12 Lower Detfurth Sandstone Member	RBMDL	75% Sand 25% Shale
13 Volpriehausen Clay-Siltstone Member	RBMVC	50% Sand 50% Shale
14 Lower Volpriehausen Sandstone Member	RBMVL	80% Sand 20% Shale
15 Lower Buntsandstein Formation	RBSH	80% Shale 15% Silt 5% Limestone
16 Zechstein Group	ZE	100% Salt
17 Rotliegend Group	RO	80% Shale 20% Sand
18 Slochteren Formation	ROSL	80% Sand 20% Shale
19 Rotliegend Group_01	RO	80% Shale 20% Sand
20 Upper Slochteren Member	ROSLU	80% Sand 20% Shale
21 Rotliegend group_02	RO	80% Shale 20% Sand
22 Lower Slochteren Member	ROSLL	80% Sand 20% Shale
23 Step Graben Formation	DCHP	60% Sand 20% Silt 18% Shale 2% Coal
24 Hospital Ground Formation	DCDG	49% Shale 49% Sand 2% Coal
25 Maurits Formation	DCCU	80% Shale 15% Sand 5% Coal
26 Ruurlo Formation	DCCR	78% Shale 20% Sand 2% Coal
27 Baarlo Formation	DCCB	48% Shale 25% Silt 25% Sand 2% Coal
28 Basement		basement

Table 2.2 Additional model stratigraphy (Scenario 2): Epen Formation and assigned lithological composition.

Layer	Layer Code	Lithology
		Facies
Epen Formation_top	DCGE	65% Shale 25% Sand 10% Silt
Epen Formation_main	DCGE	80% Shale 15% Sand 5% Silt
Geverik Member	DCGEG	100% Shale

Source rock properties. Model scenario 1 includes the Westphalian coal measures of the Limburg Group. The gas-prone source rocks of the Baarlo, Ruurlo and Maurits Formations were defined as source rocks of kerogen type III. Model scenarios 2a and 2b assume the presence of Namurian source intervals of kerogen type II in the area.

Table 2.3 shows the source rock parameter values used for simulating the timing of hydrocarbon generation from these source rocks.

Table 2.3 Source rock parameters used for simulating timing of hydrocarbon generation.

Source rock	TOC (wt%)average	HI (mgHC/gTOC)
Scenario 1		
Maurits Formation	5	250
Ruurlo Formation	2	250
Baarlo Formation	2	250
Scenario 2a		
Maurits Formation	5	250
Ruurlo Formation	2	250
Baarlo Formation	2	250
Geverik Member	10	500
Scenario 2b		
Maurits Formation	5	250
Ruurlo Formation	2	250
Baarlo Formation	2	250
Epen Formation_Main	2	200
Geverik Member	2	200

Pore water/formation water properties. In the model the pore water is of constant density, that is the density of the water is independent of changes in temperature and salinity. The water is incompressible.

Rock properties. The solid rock is incompressible. Salt is impermeable (k = 10^-16 mD).

2.6 Input: Quantified uninterrupted time-sequence of events

Table 2.4 shows the timing and duration of periods of sedimentation, erosion and non-deposition from Late Carboniferous to present-day (scenario 1). The geological evolution includes 2 main phases of erosion, namely the Saalian and Mid-Kimmerian phases, and additional periods of non-deposition, for example in the Tertiary.

Table 2.4 Timing and duration of periods of sedimentation, erosion and nondeposition.

Layer	Layer Code	Deposition age (Ma)		Erosion age (Ma)	
		From	To	From	To
Upper North Sea Group_Quaternary	NU	2,4	0	0	0
Upper North Sea Group_Pliocene	NU	5,33	2,4	0	0
Upper North Sea Group_Miocene	NU	20,1	5,33	0	0
Middle & Lower North Sea group	NM & NL	56,8	28	0	0
Chalk Group	CK	99,1	61,7	0	0
Rijnland Group	KN	124	99,1	0	0
Rijnland Group_Vlieland Sandstone Formation	KNNS	140,7	124	0	0
Schieland & Scruff groups	SL&SG	153,87	140,7	0	0
Altena (deposition & erosion)		203,7	173	173	168
Upper Germanic Trias (depostion and erosion)		204,02	203,7	168	161
Upper Germanic Trias Group	RN	246	204,02	0	0
Basal Solling Sandstone Member	RNSOB	246,2	246	0	0
Lower Germanic Trias (deposition and erosion)		246,5	246,2	161	154
Detfurth Claystone Member	RBMDC	247,6	247,5	0	0
Lower Detfurth Sandstone Member	RBMDL	247,7	247,6	0	0
Volpriehausen Clay-Siltstone Member	RBMVC	248,7	247,8	0	0
Lower Volpriehausen Sandstone Member	RBMVL	249	248,7	0	0
Lower Buntsandstein Formation	RBSH	251	249	0	0
Zechstein Group	ZE	258	251	0	0
Rotliegend Group	RO	259	258	0	0
Slochteren Formation	ROSL	260	259	0	0
Rotliegend Group_01	RO	261	260	0	0
Upper Slochteren Member	ROSLU	262	261	0	0
Rotliegend group_02	RO	263	262	0	0
Lower Slochteren Member	ROSLL	263,99	263	0	0
Step Graben Formation	DCHP	304	300	300	292
Hospital Ground Formation	DCDG	308	304	292	288
Maurits Formation	DCCU	310	308	288	280
Ruurlo Formation	DCCR	312	310	280	278
Baarlo Formation	DCCB	316,5	312	0	0
Basement		320	316,5	0	0

Salt deformation. Deformation of Zechstein salt is incorporated in the 3D simulation of the burial history (workflow phase 1). The 'salt movement' tool of Petromod was used to simulate the movement of Zechstein salt, taking the calculated original thickness of the Zechstein Group as original depositional thickness. This original constant thickness of the Zechstein Group over the whole area was derived from the present-day volume of the Zechstein Group. The calculated original thickness of the Zechtein Group is 396 m. Salt movement was set to start in the Triassic. The simulations during phase 2 and 3 did not incorporate salt movement.

Erosion. The 3D thickness of the eroded sediments was reconstructed for each main period of erosion. For that purpose, we first estimated the original thicknesses of missing stratigraphic units using the top Carboniferous map, the new thickness maps of the stratigraphic units and detailed stratigraphic information from the new well log interpretations in the study area (Witmans et al., 2010), in combination with regional knowledge and information on paleogeography, sedimentary and structural history (e.g. De Jager, 2007, Geluk, 2007, Van Buggenum and Den Hartog Jager, 2007). Estimated erosional thicknesses were verified

with 1D basin modeling at well locations. The following estimated initial thicknesses of stratigraphic units and erosional thicknesses were used in the 3D modeling:

Saalian erosion. This erosion phase affected the Step Graben, Hospital Ground, Maurits and Ruurlo formations (original thicknesses of 300, 100, 200 and 100 m, respectively). The erosion decreases from southeast to northwest over the area: at present-day the Ruurlo Formation subcrops the Upper Rotliegend Group in the southeastern part of the area, while the Step Graben Formation is present in the northwest (Figure 2.2; Witmans et al., 2010).

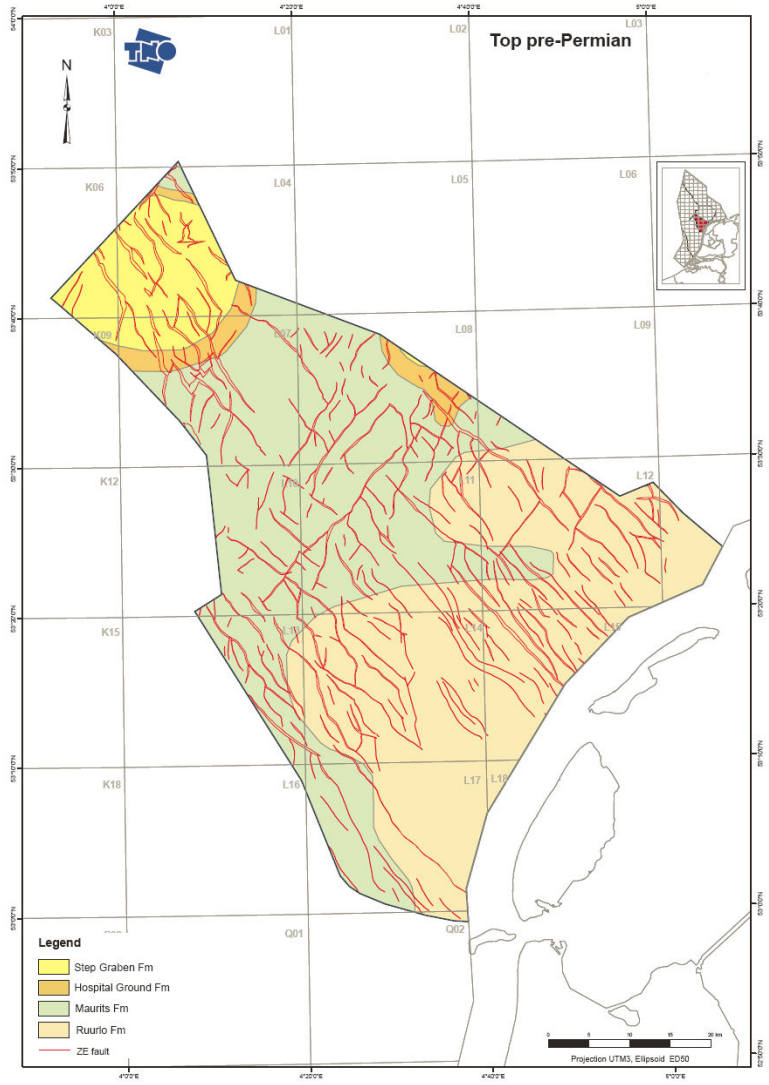

Figure 2.2 Sub-crop map of the base Permian unconformity.

Mid-Kimmerian erosion. The Mid-Kimmerian uplift caused deep erosion and complete removal of the Altena Group and affected the Upper and Lower Germanic Trias Groups. The Trias Groups in the northwestern part of the area were least affected by erosion The original minimum thickness of the Altena Group was estimated at 200 m; the minimum original thickness of the Lower and Upper Germanic Trias Groups were each set at 400 m.

We created 7 erosion maps (corresponding to the 7 stratigraphic layers affected by erosion) for input into the 3D model (Annex 2). Figure 2.3 shows an example of a map for the Saalian erosion of the Maurits Formation.

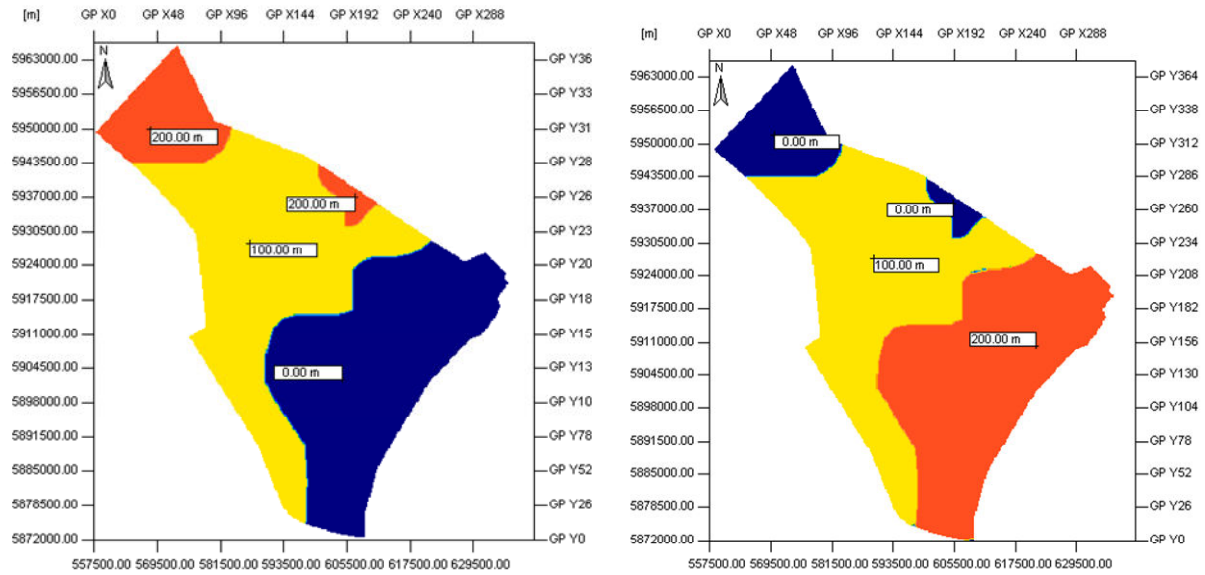

Figure 2.3 Present-day thickness and erosional thickness of the Maurits Formation (left and right figure, respectively). The reconstruction of the erosional thickness is based on an assumed minimum original thickness of the Maurits Formation of 200m.

Paleo water depths. Present-day water depths used in the modeling correspond to measured water depths. The paleo water depths were allowed to vary in time but were kept constant over the entire area at a certain time (Figure 2.4).

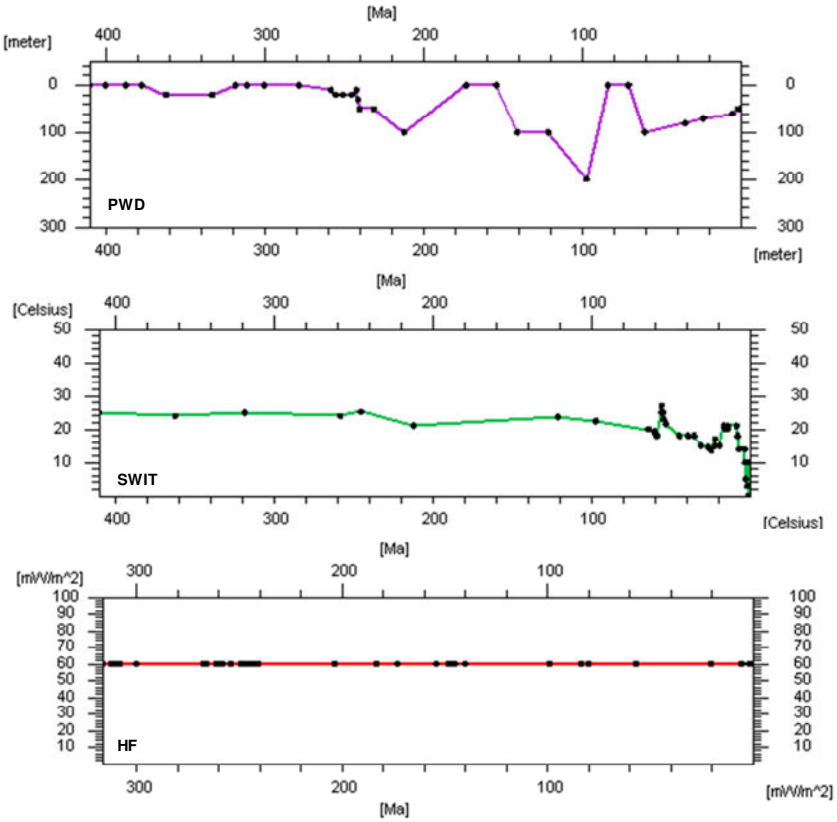

Figure 2.4 History of water depth (paleo water depth =PWD), sediment water interface temperature (SWIT) and basal heat flow (HF); PWD and SWIT are representative for the whole area.

Sediment water interface temperature (SWIT): The paleo surface temperature at the sediment water interface was calculated with an integrated Petromod tool that takes into account the paleo water depth and the evolution of ocean surface temperatures through time depending on paleolatitude of the area. For the Tertiary and Quaternary history of SWIT's more detailed temperature boundary conditions were reconstructed. The temperatures at a certain time are kept constant over the entire area.

Initially two scenarios were used for the paleo sediment water interface temperatures during Tertiary and Quaternary times (Figure 2.5). The selected SWIT scenario used for final simulations is shown in Figure 2.4. Cenozoic climate history has been studied in detail worldwide the past few years, including the reconstruction of paleo sea surface and continental temperatures using geochemical and geobiological techniques. These studies revealed long time trends of global warming (e.g., Paleocene to Early Eocene warming) and cooling (e.g., Eocene), as well as geologically brief episodes of globally elevated temperatures superimposed on these long-term trends (Sluijs et al., 2006, Zachos et al., 2008). The most well known hyperthermal is the Paleocene-Eocene Thermal Maximum (PETM), ~ 55.5 million years ago, that was marked by a 5-8 ^{o}C warming during 170000 years (Sluijs et al., 2006, Sluijs and Brinkhuis, 2008). Tertiary climate reconstructions are now becoming available for the Netherlands and surrounding areas (Donders et al., 2009 and Mosbrugger et al., 2005, respectively). We used the results of these studies in combination with published paleo climate data from other parts of the world (Sluijs et al., 2006, Pearson et al., 2007 and Zachos et al., 2008) to tentatively compile different scenarios for the evolution of SWIT during the Tertiary in the Dutch North Sea area (Verweij et al. 2010). Both scenarios include a thermal maximum at Mid Miocene times. The scenario that takes into account the relatively low temperatures during Pleistocene times provided the best fit of measured temperatuture data with the 1D and 3D simulation results. The two boundary conditions resulted in similar calculated present-day maturities at source rock levels.

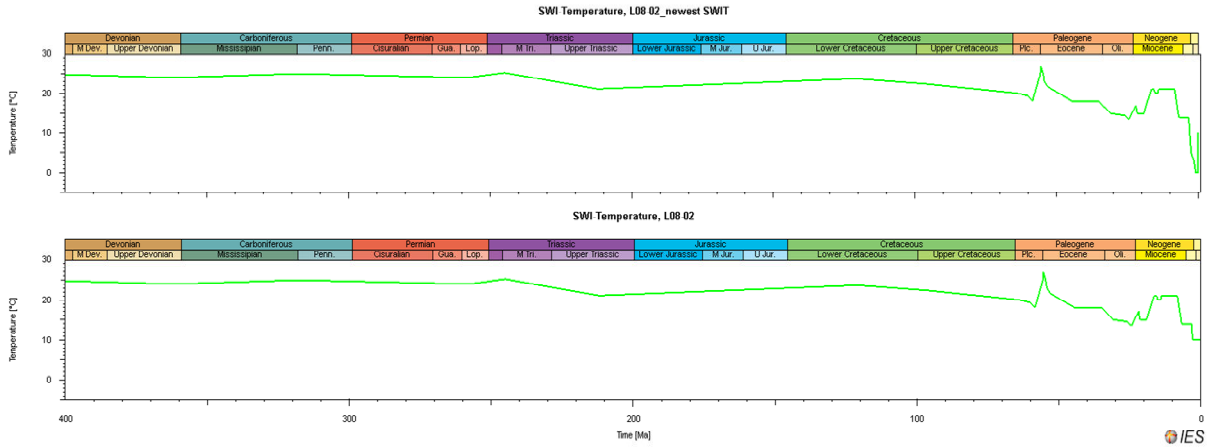

Figure 2.5 Two scenarios for the Quaternary histories of the sediment water interface temperatures. Scenario (top figure) was selected for final simulations.

Paleo basal heat flow. Basal heat flow was kept constant at 60 mW/m^2 (Figure 2.4). Phase 2 of the modeling workflow included a comparison of simulation results for the constant heat flow boundary condition of 60 mW/m^2 and a variable paleo basal heat flow. Section 4.3 presents the results.

2.7 Default set-ups, calibration

The Petromod program provides an extensive suit of default set-ups. Default set-ups that were used in the simulations concern the lithology and mixed lithology and their associated default properties (thermal conductivity, radiogenic heat production, and heat capacity), default mechanical compaction equations and default porosity-permeability relations (Annex 3). We selected the Sekiguchi model to calculate the thermal conductivity (Sekiguchi, 1984). The heat capacity is calculated with the Waples model (Waples and Waples, 2004), and Athy's Law is used to derive the mechanical compaction. Measured porosities and permeabilities provided the basis for selecting the proper compaction and porosity-permeability relations. Present-day temperature data and vitrinite reflectance data (Annex 4) were used to calibrate the 1D and later the 3D input model.

3 Modeling results: Burial history and thermal history

3.1 Burial history

The 3D burial history and maturity history was reconstructed and calibrated with temperature and vitrinite reflectance data during the first phase of the project. A selection of calibration results and simulated burial histories is shown here for the final scenario that was based on boundary conditions given in Figure 2.4, using the salt movement tool, and the kinetic model Sweeney and Burnham (1990) for calculating maturities. Figures 3.1 and 3.2 show a selection of the calibration at 3 well locations.

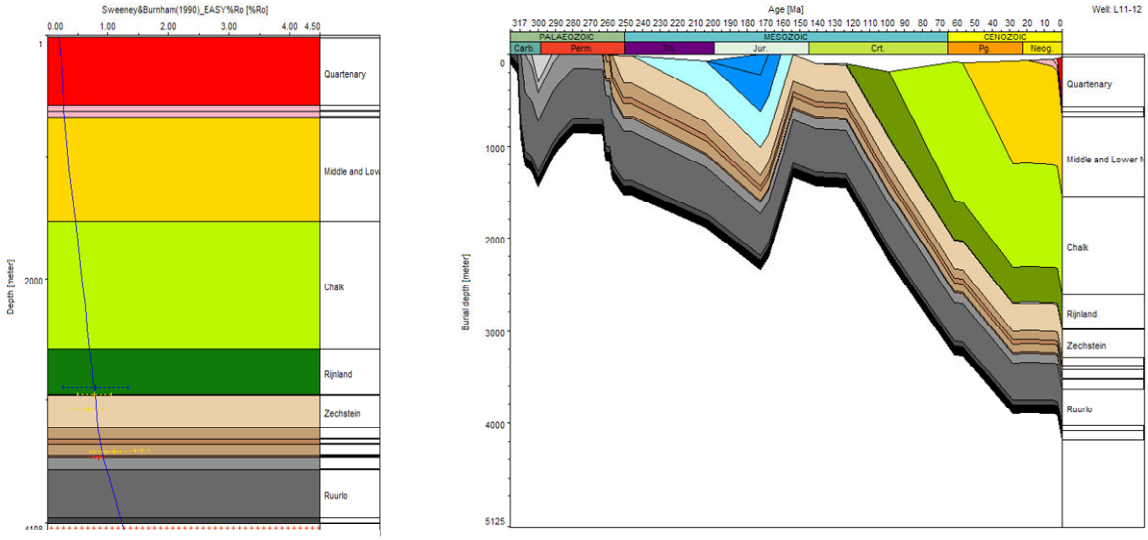

Figure 3.1 1D extraction at well L11-12 of the 3D simulation of burial history and present-day maturity. The figure at the left hand side shows that the simulated maturity fits nicely with the measured values of maturity.

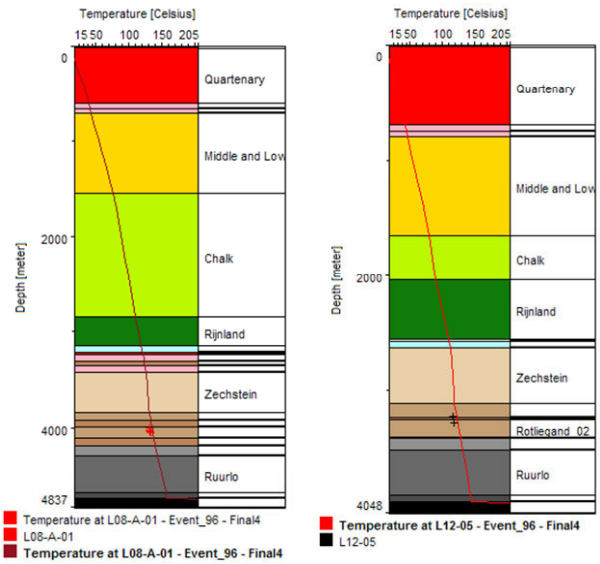

Figure 3.2 1D extraction at wells L08-A-01 and L12-05 of the 3D simulation of burial and temperature history, showing the simulated temperature distribution at present-day and reliable temperature data (DSText temperatures).

The simulated burial history clearly reveals that the whole area was affected by three phases of relatively rapid subsidence and sedimentation, namely during the Late Carboniferous, Late Permian and Pliocene-Quaternary (Figure 3.1). The whole area was affected to a greater or lesser extent by Kimmerian uplift and erosion. Large part of the area underwent continued subsidence since the start of deposition of the Rijnland Group (at approximately 140 Ma). The burial history of the Vlieland Basin deviates from the platforms and high in the area by a) the start of the subsidence of the Vlieland Basin, and the contemporaneous deposition of the Schieland Group, in Late Jurassic times and b) the relatively thinly developed Chalk Group in the inverted basin (Figure 3.3; location 6).

Zechstein salt movement has affected the sedimentation and erosional history of the basin, especially in the northwestern part of the area where salt structures reach thicknesses of more than 1100 m.

The Westphalian source rocks are at their maximum depth of burial at present-day (Figure 3.3).

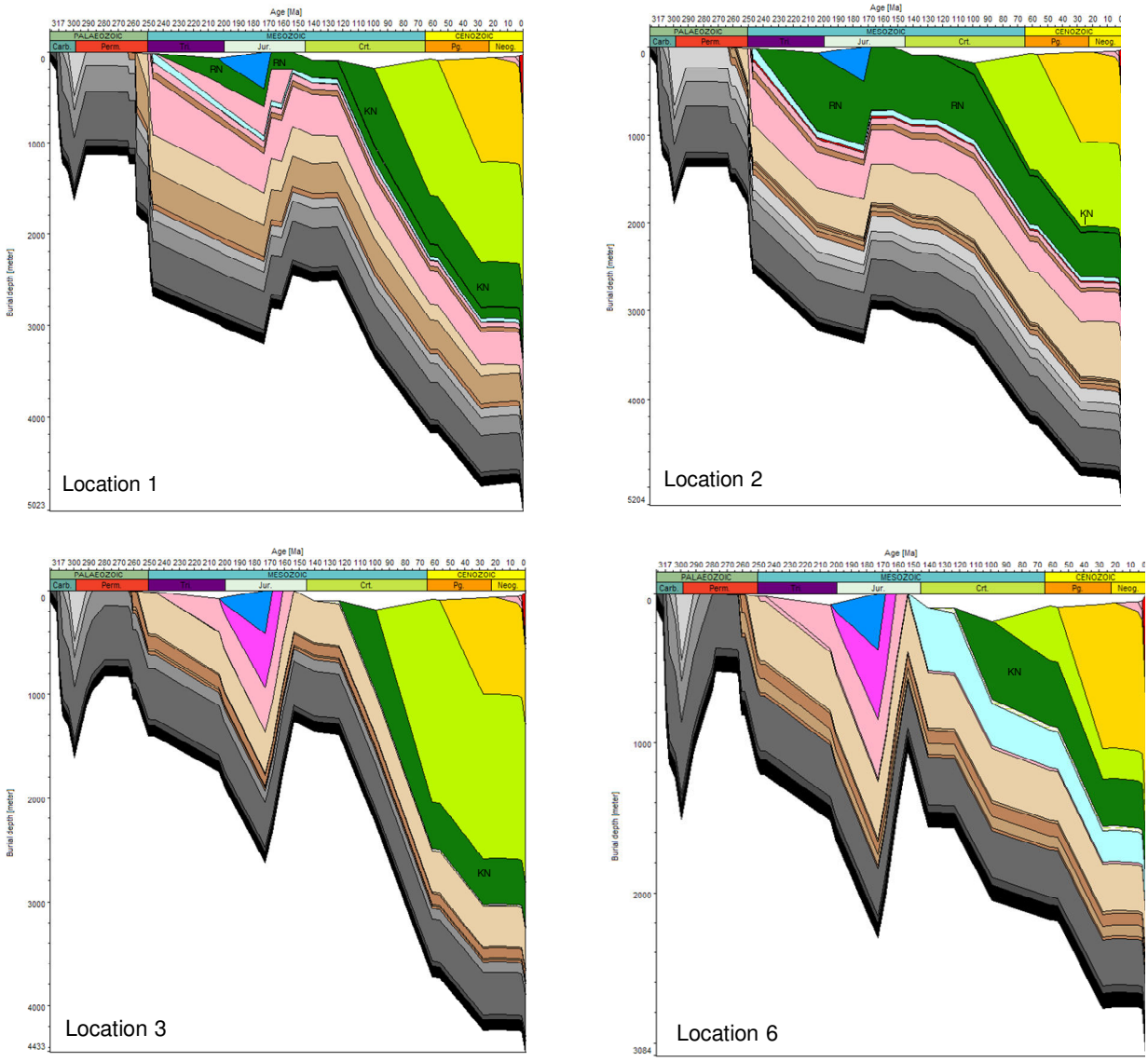

Figure 3.3 Selected 1D extractions of the 3D simulation of burial history of the NCP2E area (Note: dark green RN= Lower Germanic Trias group; dark green KN = Rijnland Group; Figure 3.6 shows location of the 1D extractions).

3.2 Thermal history

The 3D temperature history was reconstructed using a constant heat flow boundary condition of 60 mw/m^2, in combination with the sediment water interface temperatures and paleo water depths given in Figure 2. 4. Figures 3.1 and 3.2 show examples of calibration results for 1D extractions at well locations of 3D temperature simulations.

The temperature distribution in a sedimentary basin at a certain time during history, assuming steady state conditions, principally depends on the spatial variation in basal heat flow input (assumed to be constant in the simulations), the distribution of the bulk thermal conductivities of the subsurface and the sediment water interface temperatures. Bulk thermal conductivities of clastic sedimentary units and carbonates broadly range between 1.5 and 3.5 mW^{-1}K^{-1}. The bulk thermal conductivities of halites and anhydrites vary between approximately 2.8 and 5 Wm^{-1}K^{-1}. Because the thermal conductivities of salt decreases as a function of increasing temperature, and therefore depth, the deeper salt units tend to act thermally similar to the sediments. Within the shallower part of a basin, salt diapiric structures can significantly disturb heat flow. Focusing of heat flow through salt structures will increase temperatures in the top part of the salt structures and in adjacent lithostratigraphic units, while decreasing the temperatures in units immediately underlying the salt structures. Figure 3.4 shows simulation results of the 3D modeling and clearly illustrates the effect of salt structures in the northwestern part of the area on the temperature distribution.

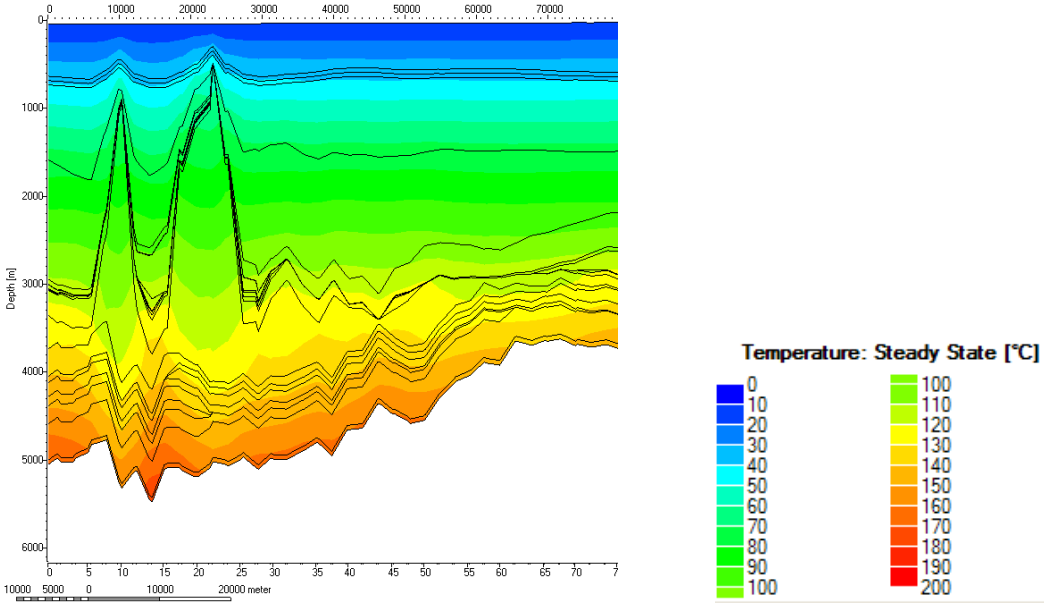

Figure 3.4 Influence of salt structures on present-day temperature distribution (2D NW-SE extraction of 3D simulation results; see Figure 3.5 for location cross section). High heat flows through salt structures are associated with increased temperatures in sediments close to the top of the salt structures and reduced temperatures below the salt structures. The reduction of temperatures below salt structures also affects the Rotliegend reservoir units and the Westphalian source rocks.

For steady state simulations the regional variations in temperature in a stratigraphic unit at a certain time in history mainly result from regional variation of: depth of burial and the bulk thermal conductivity of the sedimentary sequence, assuming basal heat flow is constant. Figure 3.5 shows the simulated present-day steady state temperature distribution in map view for the top of the Baarlo Formation.

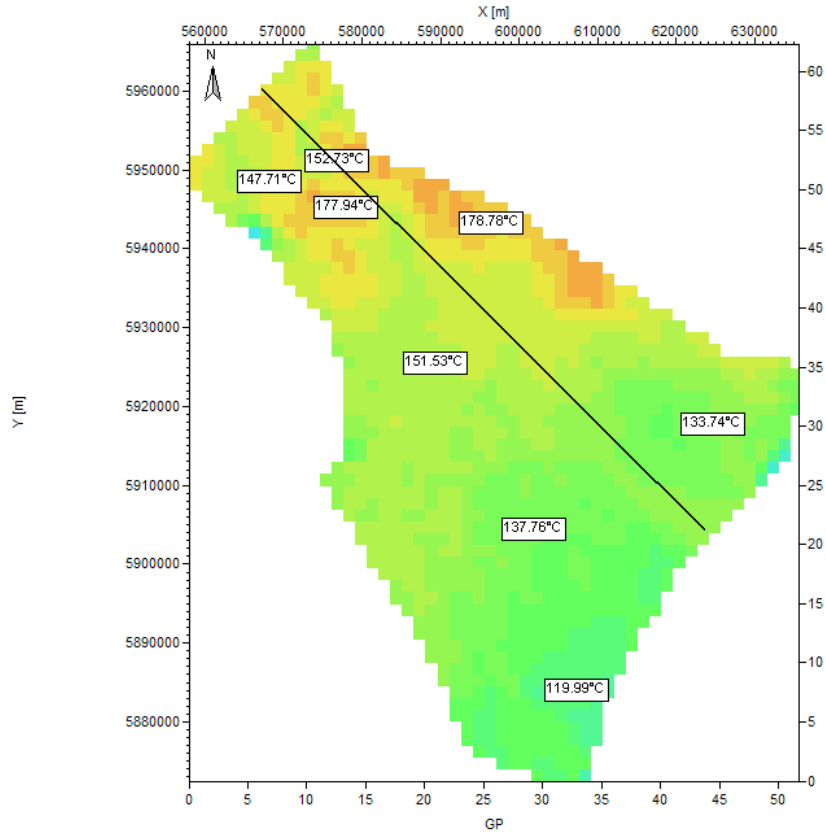

Figure 3.5 Simulated present-day steady state temperature distribution at the top of the Baarlo Formation. The lateral variations in temperature are the combined result of burial depth and differences in bulk thermal conductivity of sedimentary fill. Location of cross-section shown in Figure 3.4.

Transient simulations incorporate effects of paleo boundary conditions (e.g. paleo surface temperatures) and effects of rapid sedimentation or uplift on the temperature distribution at a certain time.

Representative results of transient 3D simulations of temperature evolution of the Westphalian source rocks are summarised below.

3.2.1. Thermal history of Westphalian source rocks

The simulated regional variations in calculated temperature history of the Maurits, Ruurlo and Baarlo Formations will result mainly from differences in burial history and more locally from differences in position relative to salt structures. The burial history and related temperature histories of the Maurits and the Baarlo Formations are shown in Figures 3.7 and 3.8, respectively.

The characteristics of the calculated temperature history at the different locations are broadly similar in the NCP2E area: the temperature increase and decrease follow the burial histories of the Westphalian source rocks for large part of geological history. Temperatures increase from Late Permian up to the start of the Kimmerian uplift and erosion phase in the Jurassic; after a period of temperature decrease during this Kimmerian period of erosion, the temperatures start to increase again, reaching pre-uplift values in Mid Cretaceous times and increase continuously to maximum values during the Miocene. These maximum temperatures coincide with the thermal maximum of surface temperatures during the Miocene (Figure 2.4). The temperatures of the Westphalian source rocks decrease from Miocene to Pliocene –Pleistocene times, reflecting the steep drop of surface temperatures in combination with the lack of subsidence during that time.

Simulated present-day temperatures are still lower than the maximum temperatures experienced during Miocene times.

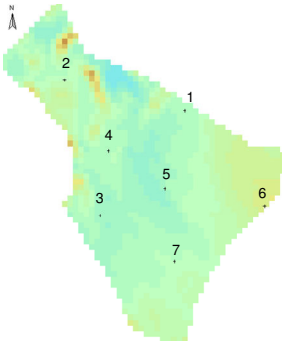

Figure 3.6 Location of the 1D extractions of the 3D simulation of the NCP2E area.

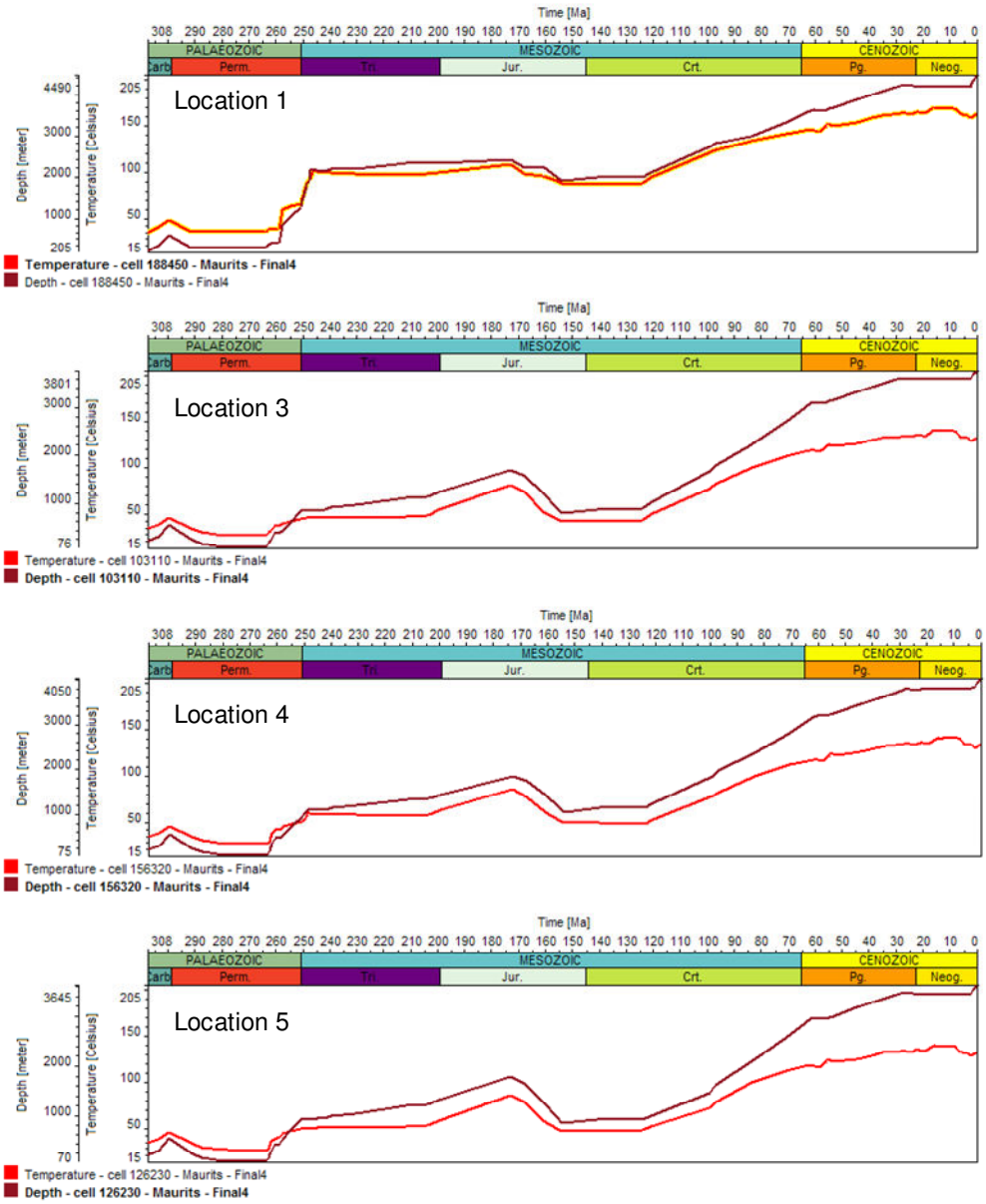

Figure 3.7 Selected 1D extractions of the 3D simulated burial history (brown line) and temperature history (red line of the Maurits Formation (see Figure 3.6 for locations). Maximum temperatures of the Maurits Formation were reached during the Mid-Miocene.

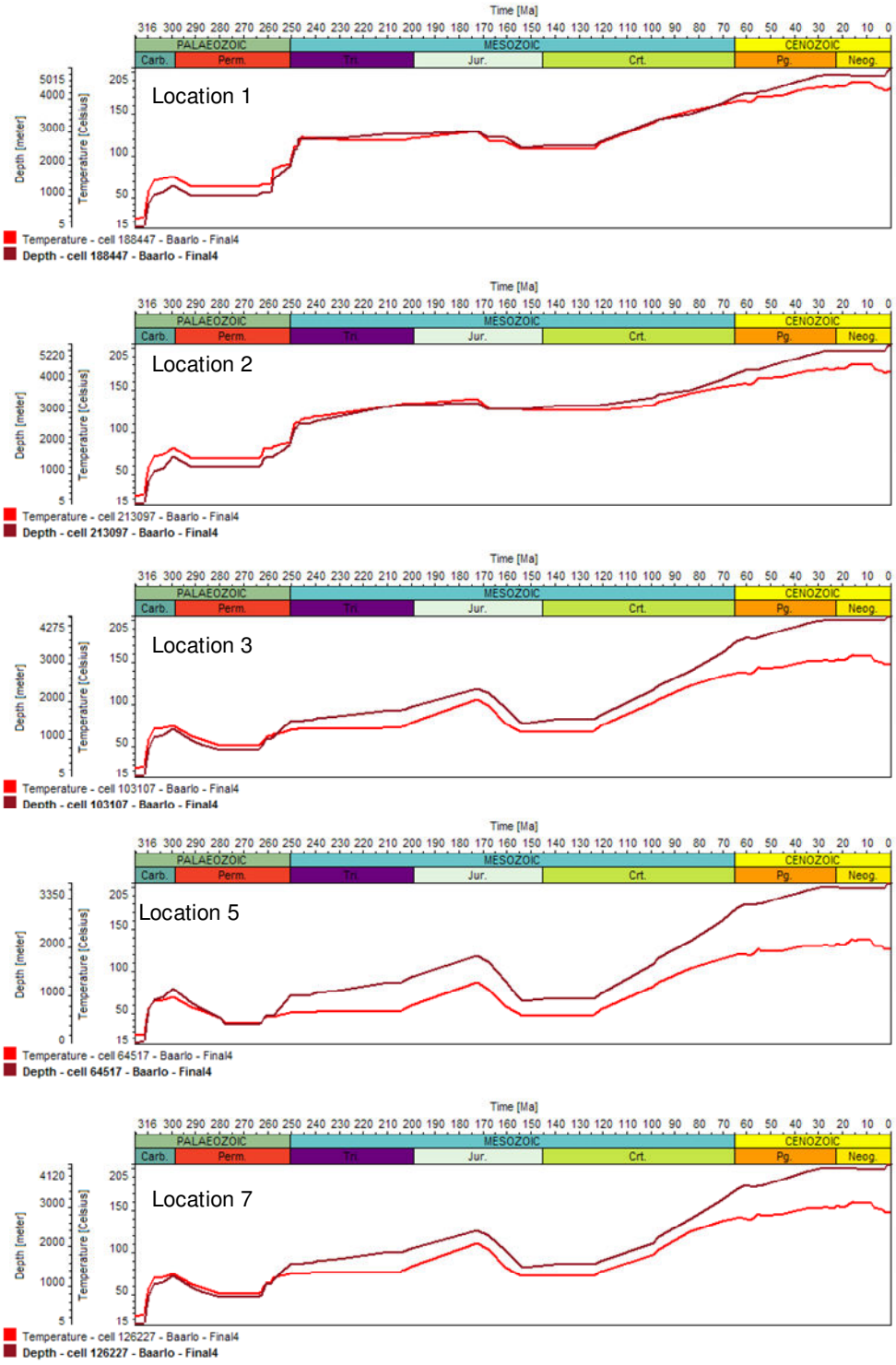

Figure 3.8 Selected 1D extractions of the 3D simulated burial history (brown line) and temperature history (red line) of the Baarlo Formation (see Figure 3.6 for locations). Maximum temperatures were reached during the Mid Miocene.

Figure 3.9. shows that from Permian times onward, the temperatures of the Westphalian source rocks in the northern part of the area (locations 1 and 2) were higher than the temperatures in the central (locations 3 and 5) and southern (location 7) part of the area. These differences are related to the differences in burial depth of the source rocks during geological history in the regions.

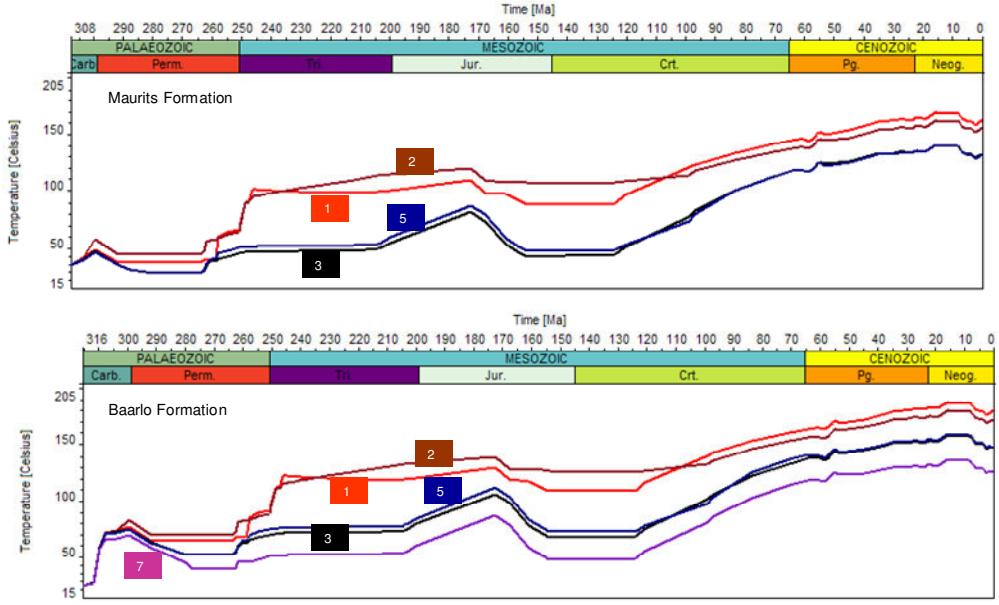

Figure 3.9 Selected 1D extractions of the 3D simulated temperature history of the Maurits Formation and the Baarlo Formation (see Figure 3.6 for the locations 1,2,3, 5 and 7). At all locations present-day temperatures are less than the maximum temperatures that were reached during Mid Miocene times.

4 Modeling results: History of maturity and hydrocarbon generation of Westphalian source rocks

The 3D reconstruction of the maturity history of the area provides information on the 3D distribution of maturity indicators such as vitrinite reflectance values (according to Sweeney and Burnham 1990) and tranformation ratios. Vitrinite reflectance values are calculated for all stratigraphic units. The transformation ratio is the ratio of generated petroleum to potential petroleum in a source rock. The transformation ratio provides information on the timing of hydrocarbon generation and is calculated for the source rock units.

Initially we used the Burnham (1989)_T3 kinetic model for simulating the hydrocarbon generation from the Westphalian Baarlo, Ruurlo and Maurits Formations. As a second scenario for these Westphalian source rocks we used the Pepper & Corvi (1995)_TIII-IV(F) kinetic model (section 4.1). After extension of the 3D geological model with assumed thicknesses for the Namurian Epen Formation in phase 3 of the project the source rock maturity and hydrocarbon generation were simulated for the Westphalian source rocks (using the Pepper & Corvi (1995)_TIII-IV(F) kinetic model) (Section 4.2) and the Namurian source rocks (using the Burnham(1989)_T2 kinetic model) (Chapter 5).

4.1 Kinetic models

The Burnham (1989)_T3 kinetic model and Pepper & Corvi (1995)_TIII-IV(F) kinetic model were used for simulating the hydrocarbon generation from the Westphalian Baarlo, Ruurlo and Maurits Formations, using similar boundary conditions (evolution of sediment water interface temperatures and paleo water depths, a basal heat flow of 60 mW/m^2; Figure 2.4), and set of source rock parameters (Table 2.3).

Figures 4.1, 4.2 and 4.3 show the strong influence of the kinetic models on the simulated history of hydrocarbon generation.

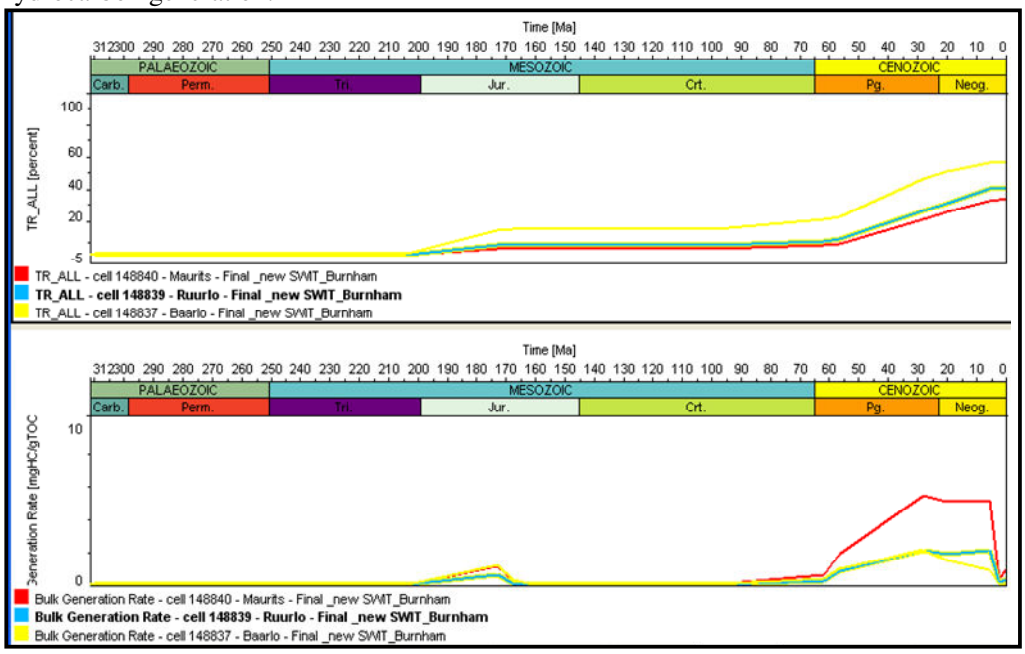

Figure 4.1 1D extraction of 3D simulated history of transformation ratios and the bulk generation rates of hydrocarbons for the Maurits, Ruurlo and Baarlo Formations, using the Burnham (1989)_T3 kinetic model (location L11-12).

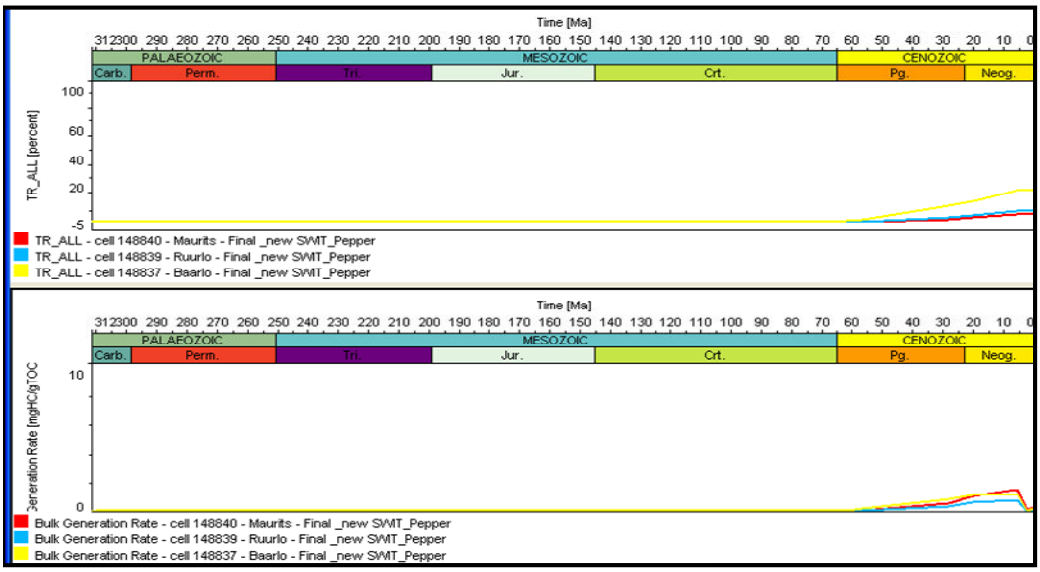

Figure 4.2 1D extraction of 3D simulated history of transformation ratios and the bulk generation rates of hydrocarbons for the Maurits, Ruurlo and Baarlo Formations, using the Pepper & Corvi (1995)_TIII-IV(F) (location L11-12).

Burnham (1989)_T3

	Dry Gas	Medium Oil	Sum
Maurits	4912.93	2061.74	6974.67
Ruurlo	6219.08	2381.13	8600.21
Baarlo	910.773	309.834	1220.61
Sum Generated	**12042.8**	**4752.7**	**16795.5**
Maurits	1866.96	1727.2	3594.16
Ruurlo	2374.45	1897.3	4271.75
Baarlo	288.138	229.56	517.698
Sum Accumulated in Source	**4529.54**	**3854.06**	**8383.6**
Maurits	3045.97	334.54	3380.51
Ruurlo	3844.63	483.83	4328.46
Baarlo	622.635	80.274	702.909
Sum Expelled	**7513.24**	**898.644**	**8411.88**
Sum Accumulated in Reservoir	**0**	**0**	**0**
Migration Losses	0	0	0
Sec. Cracking Losses	7513.24	898.644	8411.88
Sum Outflow Top	0	0	0
Sum Outflow Side	0	0	0
Sum HC Losses	**7513.24**	**898.644**	**8411.88**

Pepper & Corvi (1995)_TIII-IV

	Dry Gas	Medium Oil	Sum
Maurits	1475.02	862	2337.02
Ruurlo	2418.92	859.8	3278.72
Baarlo	455.134	99.59	554.724
Sum Generated	**4349.07**	**1821.39**	**6170.46**
Maurits	400.378	862	1262.38
Ruurlo	452.4	859.71	1312.11
Baarlo	63.0548	99.594	162.649
Sum Accumulated in Source	**915.833**	**1821.3**	**2737.13**
Maurits	1074.64	0	1074.64
Ruurlo	1966.52	0.09	1966.61
Baarlo	392.079	-0.004	392.075
Sum Expelled	**3433.24**	**0.086**	**3433.33**
Sum Accumulated in Reservoir	**0**	**0**	**0**
Migration Losses	0	0	0
Sec. Cracking Losses	3433.24	0.086	3433.33
Sum Outflow Top	0	0	0
Sum Outflow Side	0	0	0
Sum HC Losses	**3433.24**	**0.086**	**3433.33**

Legend

Expelled = Generated - Accu. in Source (incl. Adsorption)
= Accu. in Reservoir + HC Losses
HC Losses = Outflow Top/Side + Migration Losses
+ Sec. Cracking Losses

Figure 4.3 Calculated masses of generated and expelled hydrocarbons (in 10^9 kg) from the Maurits, Ruurlo and Baarlo Formations using two different kinetic models: the kinetic model of Burnham (1989)_T3 and Pepper & Corvi (1995)_TIII-IV(F), respectively.

The application of the Burnham (1989)_T3 kinetic model results in two phases of hydrocarbon generation, a Jurassic and a Cenozoic phase, while the kinetic model of Pepper & Corvi (1995)_TIII-IV(F) calculates that the Westphalian source rocks start to generate hydrocarbons in the Tertiary (Figures 4.1 and 4.2) . In addition, the calculated bulk generation rates of hydrocarbons are higher for the Burnham (1989)_T3 kinetic model in comparison with those calculated with the Pepper & Corvi (1995)_TIII-IV(F) model (Figures 4.1 and 4.2).

The kinetic parameters of the Pepper and Corvi model are based on depositional environment and stratigraphic age: their organofacies F relates to a terrigeneous, non marine, coastal environment of late paleozoic and younger age, including the Westphalian coals. The Pepper & Corvi (1995)_TIII-IV(F) kinetic model was selected for subsequent modeling.

4.2 Maturity and hydrocarbon generation

The burial and temperature histories of the Westphalian source rocks are reflected in the maturity histories of these source rocks (maturity according to Sweeney and Burnham, 1990; Figure 4.4). The simulated maturity histories reveal that the largest increase in maturity occurs in late Cretaceous-Tertiary times.

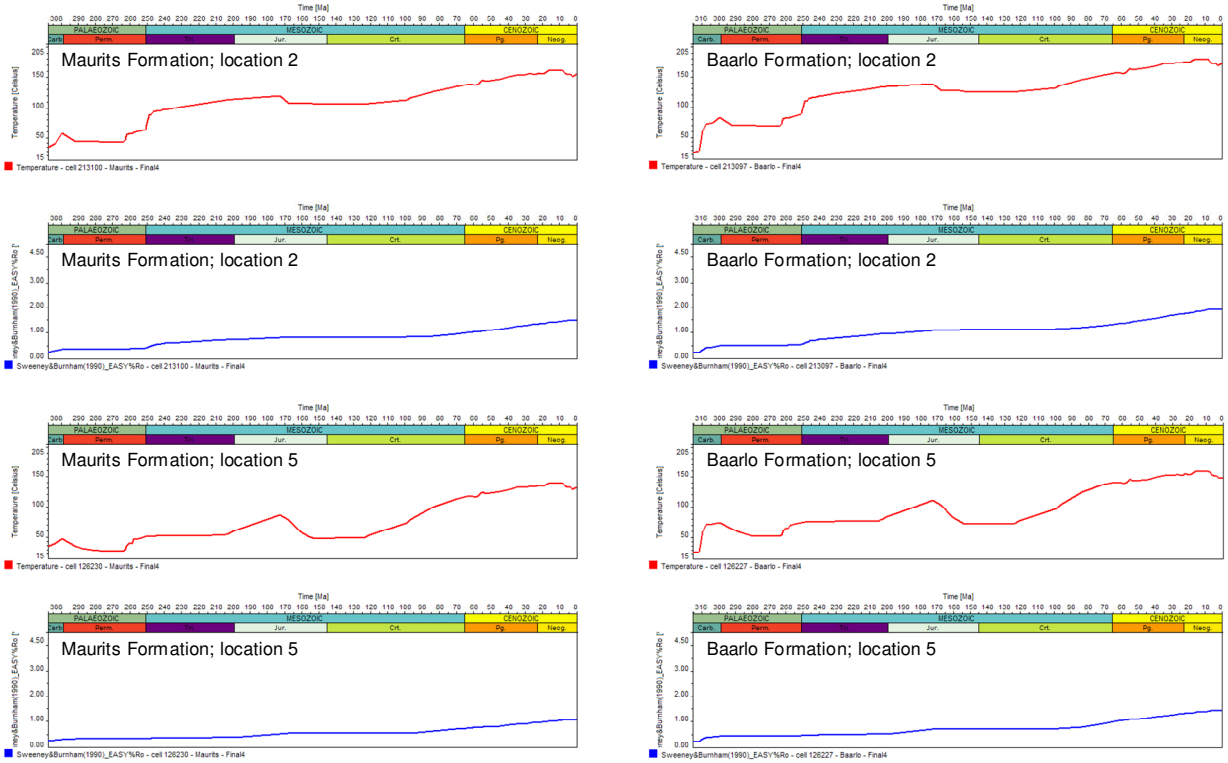

Figure 4.4 Selected 1D extractions of the 3D simulated temperature and maturity history of the Maurits and Baarlo Formations (see Figure 3.6 for locations).

The map views of the simulated maturity history of the Maurits and Baarlo Formations show this increase in maturity in greater detail (Figures 4.5 and 4.6), and reveal that there is hardly any increase in source rock maturity from 5.33 Ma to present-day. Figure 4.5 shows that the Maurits Formation reaches wet gas conditions along the northeastern boundary of the area in Late Tertiary times. The simulated present-day maturities of the Maurits Formation range from less than 1 Ro% around the Texel-IJsselmeer High to values of approximately 1.3 – 1.5 %Ro in a rather narrow zone along the northeastern border of the area and locally in the northwest (Figure 4.5). These calculated relatively low maturities of the Maurits Formation are in accordance with published maturity maps at top Carboniferous (e.g. Figure 6.19 in Kombrink et al. 2010). The maturity of the Baarlo Formation reaches wet gas conditions in most of the area in Late Tertiary times, while dry gas conditions develop locally along the northeastern border of the area (Figure 4.6).

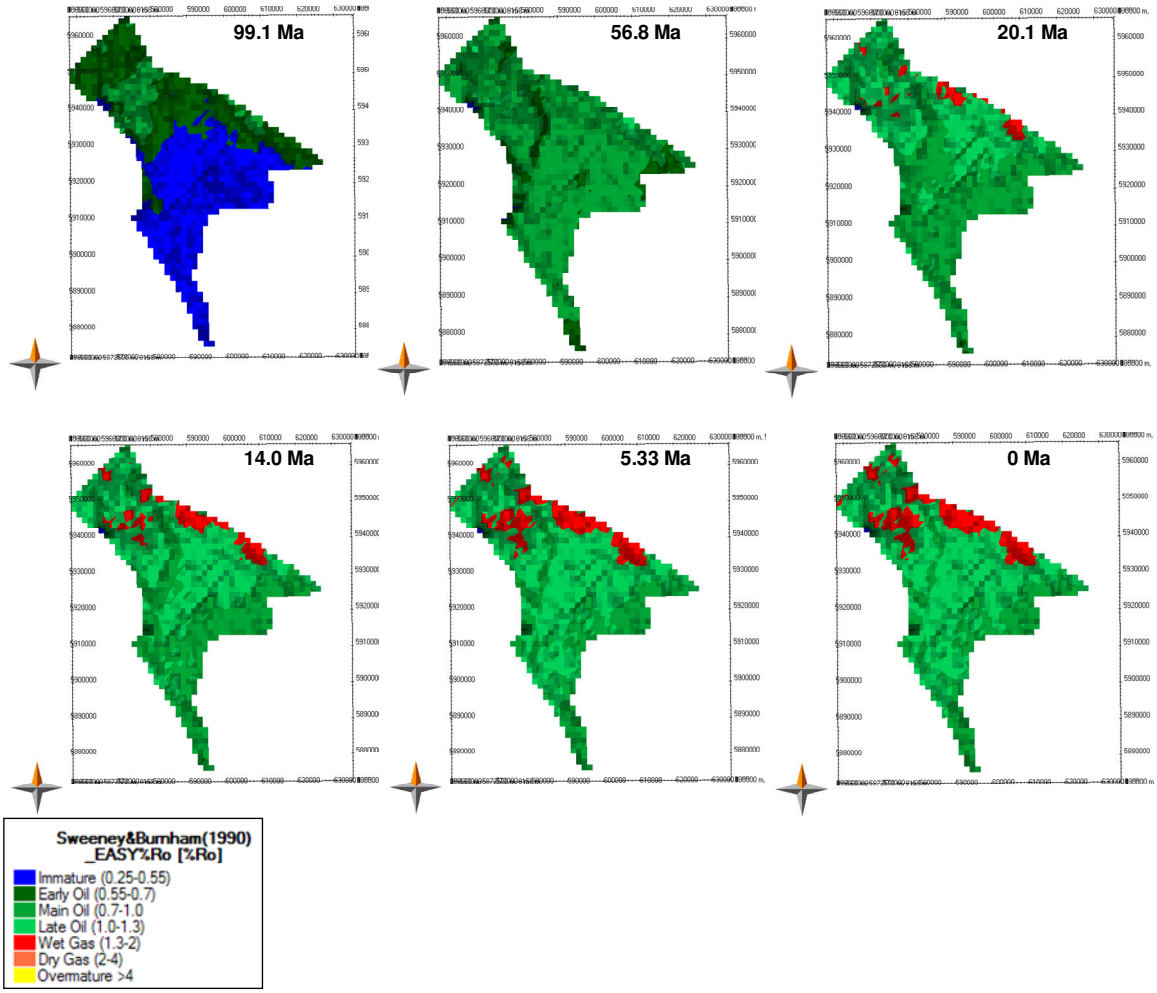

Figure 4.5 Map view of the simulated maturity history of the Maurits Formation from 99.1 Ma to present-day.

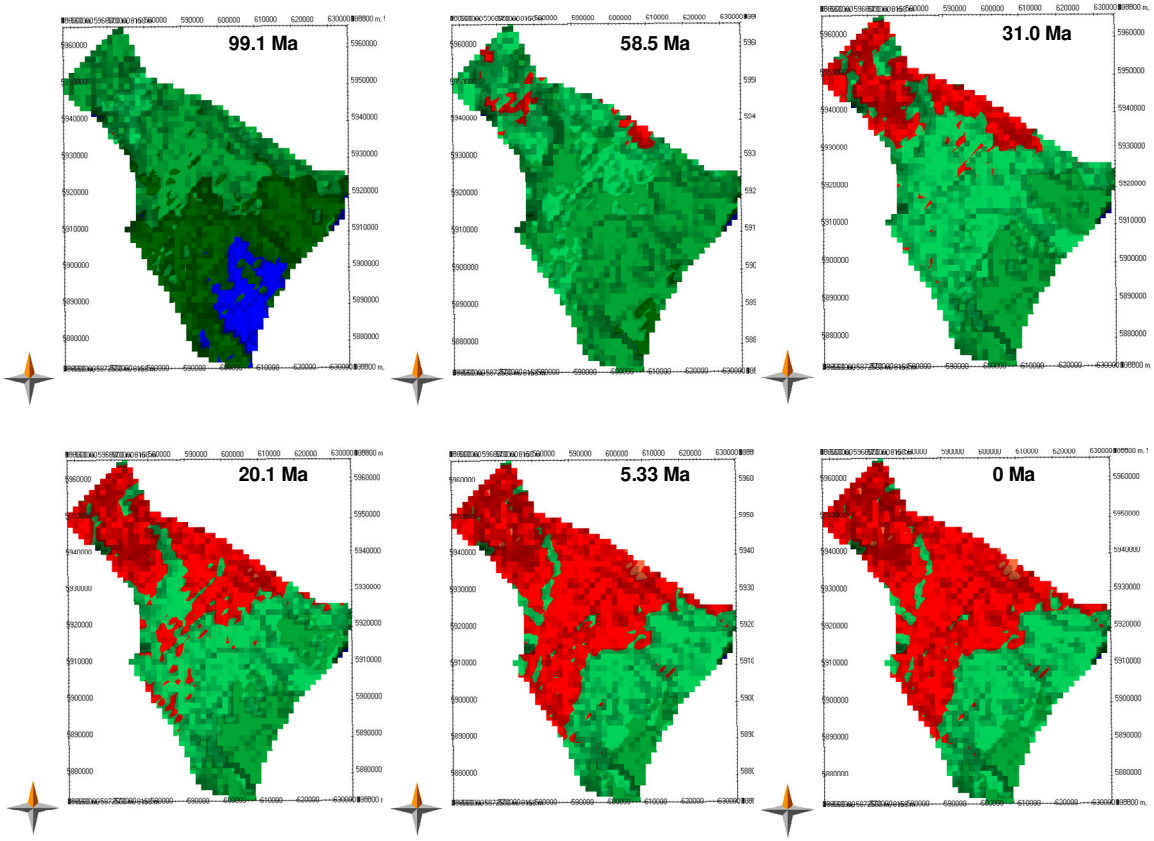

Figure 4.6 Map view of the simulated maturity history of the Baarlo Formation from 99.1 Ma to present-day (see Figure 4.5 for legend).

The transformation ratio (%) and the bulk hydrocarbon generation rates (mg HC/gTOC/My) are calculated for the source rock units only, using the Pepper & Corvi (1995)_TIII-IV(F) kinetic model. It provides more detailed insight in the timing of hydrocarbon generation. Figures 4.7 and 4.8 illustrate the history of transformation ratios of the source rocks at a 1D extraction of the 3D simulation (corresponding to location of well L08-10) and in map view, respectively. These simulation results show that hydrocarbon generation from Westphalian source rocks is concentrated in Tertiary times.

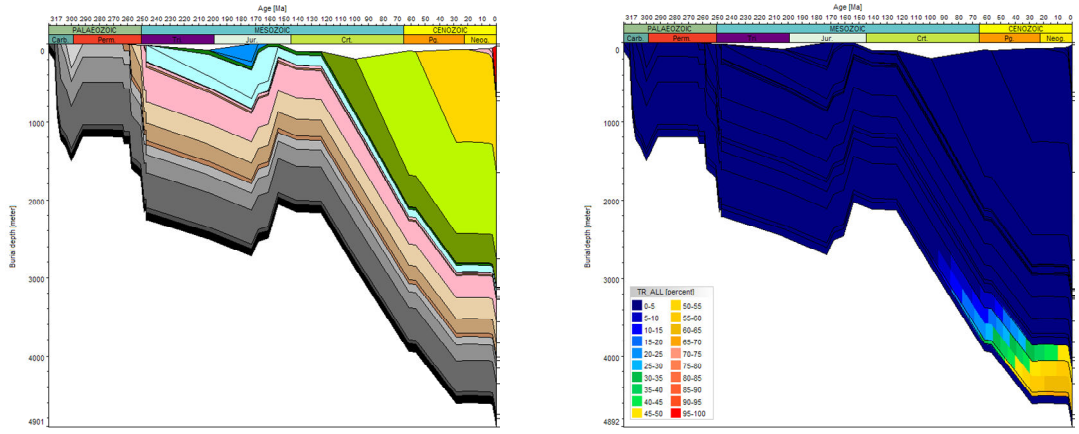

Figure 4.7 Burial history and associated history of transformation ratios at well location L08-10 (Figure 5.1 shows the well location).

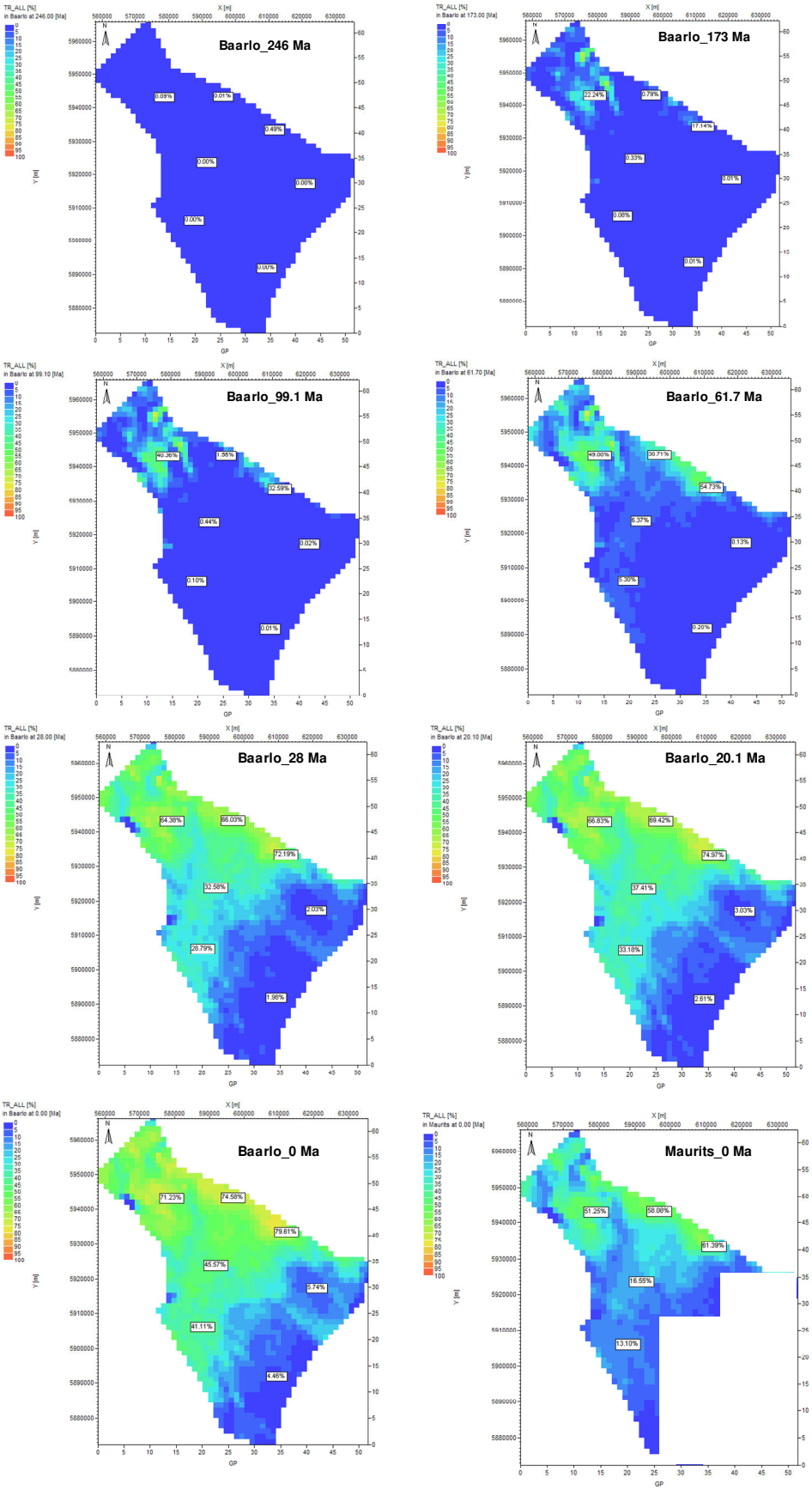

Figure 4.8 Map view of the evolution of transformation ratios of the Baarlo Formation between 246 Ma and present-day; also present-day distribution of transformation ratios of the Maurits Formation.

The 1D extractions of the 3D simulations of the transformation ratio and the bulk generation rates of hydrocarbons show that in the northern part of the area the Maurits source rock starts to generate in Late Cretaceous times and peak generation rates were reached in Late Paleogene times (Figure 4.9). In contrast, in the more southern part of the area hydrocarbon generation starts in the Paleogene and peaks in Late Neogene times. This Neogene peak in hydrocarbon generation rate coincides with a period of only minor changes in burial depth of the source rock and the Mid-Miocene thermal maximum of the surface temperatures. The relatively high Mid Miocene surface temperatures are reflected in the changes in source rock temperatures (Figure 3.9) and in the hydrocarbon generation rates (Figure 4.9): hydrocarbon generation in the Maurits source rock increases in response to these changes in surface temperature. The sharp drop in surface temperatures since the Mid-Miocene and the low to very low surface temperatures during the Quaternary reduce the temperatures in the source rocks and slow down hydrocarbon generation from the source rocks (see also maps transformation ratios). Only very recently hydrocarbon generation starts to increase again.

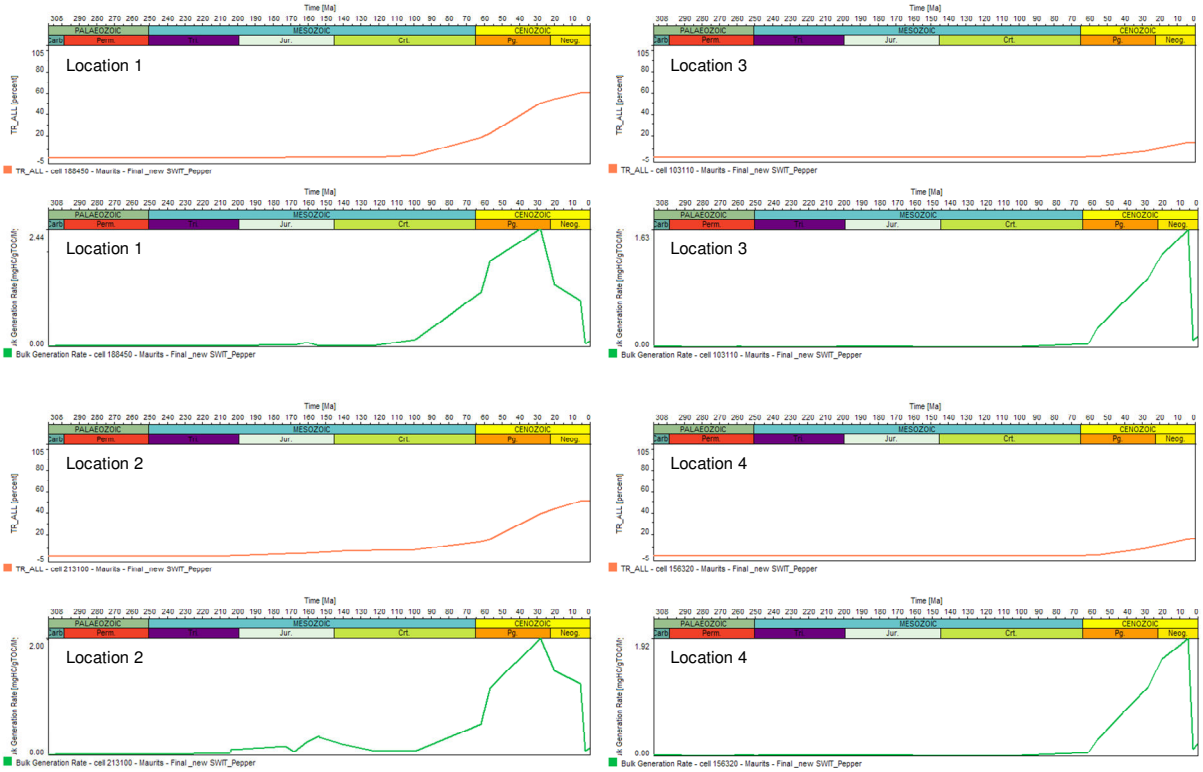

Figure 4.9 Selection of 1D extractions of the 3D simulation of the transformation ratio and the bulk generation rate of hydrocarbons of the Maurits Formation. Note the difference in timing of the maximum bulk generation rates between locations 1 and 2 (left side of figure) and locations 3 and 4 (see figure 3.6 for location of the 1D extractions).

Comparison of the distribution of the gas fields and the geochemical composition of the gases in the area (Figures 1.8 and 1.9, respectively) with the distribution of simulated maturities and regional variations in timing and rates of hydrocarbon generation for the Westphalian source rocks (Figures 4.6 and 4.8, respectively) reveals some interesting features. For example, the gas fields with the very wet gases in the Vlieland Basin (located in southern L12 and northern L15 blocks, Figure 1.8) are outside the main region where the Westphalian source rocks are mature for – wet – gas generation (Figures 4.5 and 4.6). The Maurits Formation is missing in the Vlieland Basin.The calculated maturities of the Baarlo Formation are below the wet gas generation window, transformation ratios of the Baarlo Formation do not exceed 10% in large part of the Vlieland Basin and the hydrocarbon generation from the Baarlo Formation peaks late, in Mid Miocene times. The simulated maturity and hydrocarbon generation histories of the source rocks suggest that the charging of the gasfields in the Vlieland Basin can only be explained to a limited extent by local sourcing from the low mature Westphalian source rocks and probably requires a lateral component of gas migration towards the Vlieland basin.The region with the intermediate wet gases in block L08 at the northeastern border

of the area (with wetness ratios between 27 and 50) coincides with the area of source rock maturities in the wet gas range (locally reaching dry gas maturity in the Baarlo Formation) and transformation ratios of the Baarlo and Maurits Formations of approximately 80 and 60 %, respectively.

The hydrocarbon generation in the area is concentrated in Cenozoic times, i.e. expulsion from the source rock and subsequent migration from Westphalian source to Upper Rotliegend traps occurred after the main periods of tectonic activity and deformation in the area. Present-day geometry of the top Rotliegend and fluid overpressure distribution in the Upper Rotliegend provide indications of the general direction of the main driving forces for lateral gas migration through the Upper Rotliegend reservoirs (Figure 1.11). Under the present-day conditions the driving forces are directed southwards and towards the Texel-IJsselmeer High. Gas migration through the Upper Rotliegend reservoirs was and still is influenced by the faulted nature of the Carboniferous-Upper Rotliegend units, as indicated by stepwise changes in fluid overpressures and the geometry of the gas fields in the area. Simulation of gas migration and charging requires the incorporation of faults and fault properties in the geological model. This will be subject of future studies.

4.3 Thermal boundary conditions

The foregoing section clearly showed that the surface temperature variations during Tertiary and Quaternary times exert an important influence on hydrocarbon generation history of the Westphalian source rocks. In order to investigate the influence of variations in basal heat flow boundary condition on the timing of hydrocarbon generation, the 3D model was also run with a tectonic heat flow boundary condition. Because there was no tectonic reconstruction of the basal heat flow boundary condition available for the Central Offshore Platform area itself, we used the basal heat flow reconstructed for well K01-02 (located on Cleaverbank High) (Figure 4.10).

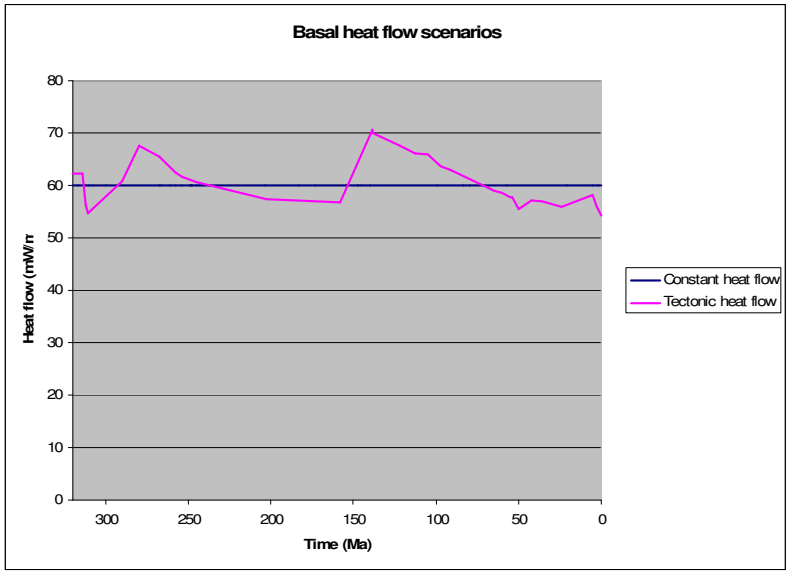

Figure 4.10 Two scenarios for the basal heat flow boundary condition: 1. constant basal heat flow of 60 mW/m^2; 2. variable tectonic heat flow reconstructed for well K01-02.

Comparison of the simulation results for the tectonic heat flow and the constant heat flow boundary condition of 60 mW/m^2 revealed differences in hydrocarbon generation rates from the source rocks, but no to only minor changes in timing of hydrocarbon generation. Figures 4.11 and 4.12 show examples of these results for the Maurits Formation.

Because the focus of the study was on investigating the timing of hydrocarbon generation and given the fact that there was not a tectonic heat flow boundary condition available for the area itself, we continued to use the constant basal heat flow boundary condition in the subsequent modeling exercises.

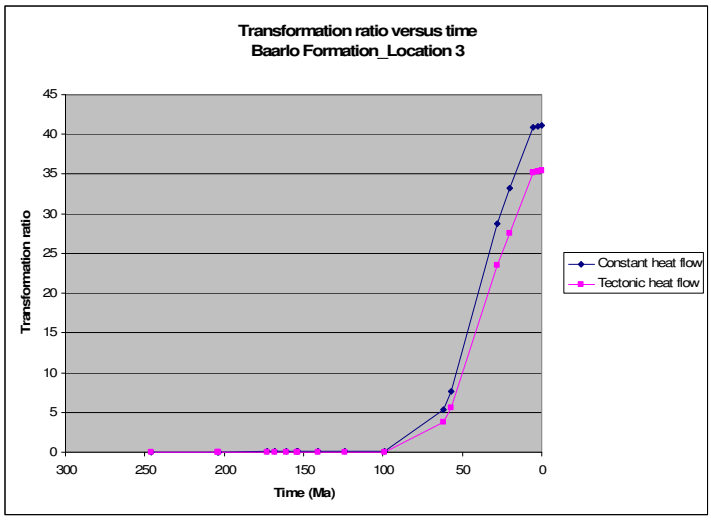

Figure 4.11 1D extraction at location 3 of the 3D simulation of the history of transformation ratios (%) of the Baarlo Formation using two different basal heat flow boundary conditions (see Figure 3.6 for location 3).

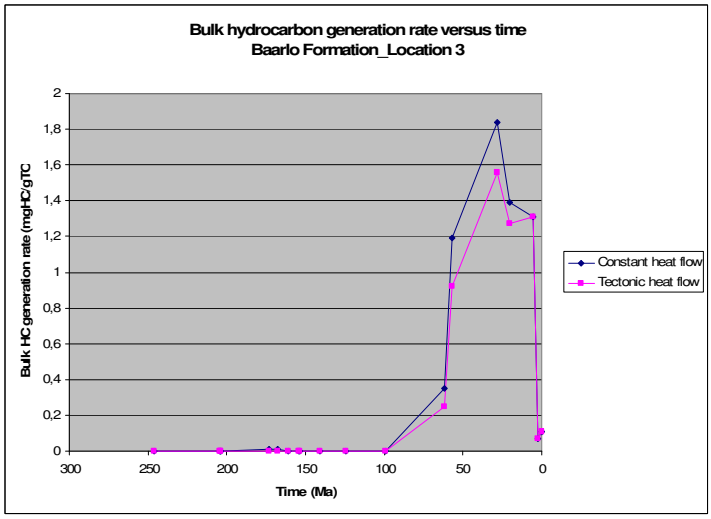

Figure 4.12 1D extraction at location 3 of the 3D simulation of the history o bulk hydrocarbon generation rates (mg HC/gTOC/My) of the Baarlo Formation using two different basal heat flow boundary conditions (see Figure 3.6 for location 3).

5 Modeling results: History of maturity and hydrocarbon generation of Westphalian and Namurian source rocks

In the third phase of the project we studied the history of temperature, source rock maturity and timing hydrocarbon generation of both Westphalian and Namurian source rocks. For this purpose the 3D geological model (Chapter 4) was extended to greater depth with the Namurian Epen Formation. The total thickness of the Namurian (1500 m) was estimated from regional information given in Kombrink (2008) and Kombrink et al. (2008). The Namurian was subdivided into three layers: 'Epen Top' (175 m), 'Epen Main' (1300 m) and Geverik (25 m).

The 3D history of temperature, source rock maturity and timing of hydrocarbon generation was simulated for the Baarlo, Ruurlo and Maurits Formations (using the Pepper & Corvi (1995)_TIII-IV(F) kinetic model) as well as for the assumed oil-prone Namurian source rocks of kerogen type II (using the Burnham(1989)_T2 kinetic model). We used the paleo water depth, selected SWIT boundary condition and a basal heat flow of 60 mW/m^2 given in Figure 2.4, and the set of source rock parameters listed in Table 2.3. The 3D model was run for two different sets of parameters for the Namurian source rocks (scenarios 2a and 2b in Table 2.3)...

5.1 Maturity and hydrocarbon generation Scenario 2a

Scenario 2a is based on the assumption that the Geverik Member of the Namurian Formation is present in the area and it is the only Namurian source rock (TOC=10wt%, HI = 500 mgHC/gTOC).

The results of the 3D simulation of maturity and hydrocarbon generation of the Westphalian source rocks and the Namurian Geverik source rock are shown in Figures 5.2, 5.3 and 5.4. Figure 5.2 reveals that hydrocarbon generation from the Geverik Member starts and ends in the Carboniferous and that transformation ratios reach 100 % at the end of the Carboniferous. The source rock maturity of the Geverik at the end of the Carboniferous is broadly similar to its present-day maturity. The calculated present-day maturity (Figure 5.3) is classified as dry gas.

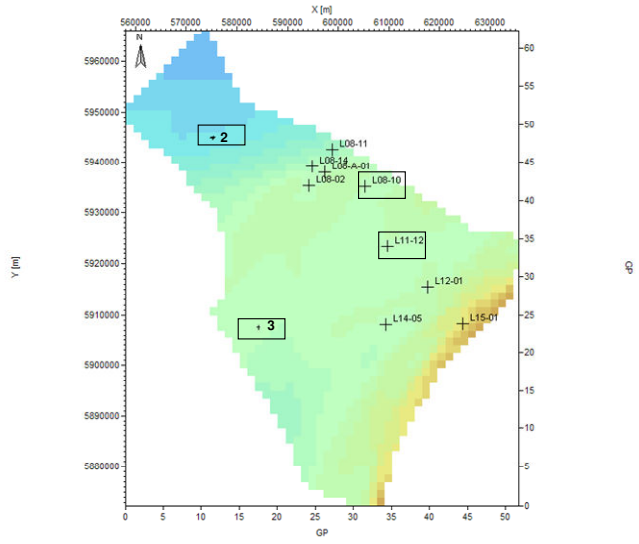

Figure 5.1 Location of 1D extractions of the 3D model (wells L08-10 and L11-12; locations 2 and 3).

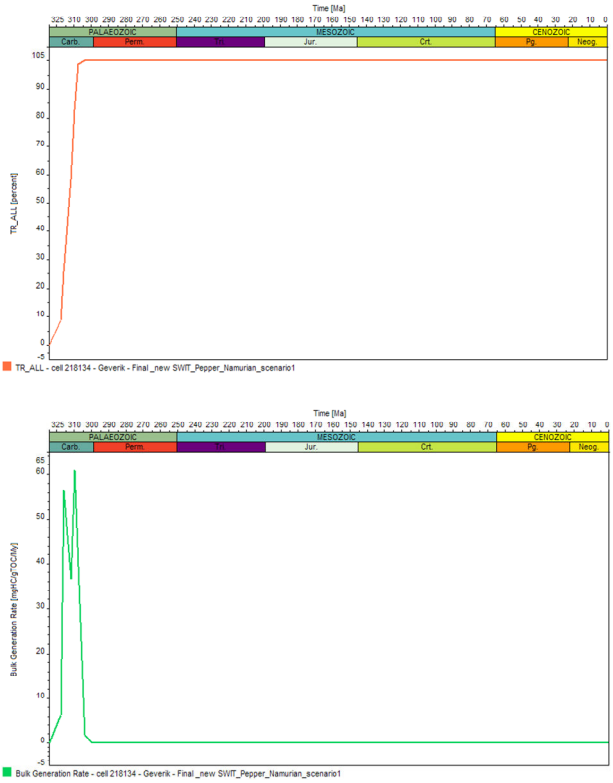

Figure 5.2 1D extraction at well location L08-10 of the 3D simulated history of transformation ratio and bulk hydrocarbon generation rate of the Namurian Geverik Member. Hydrocarbon generation from the Geverik Member starts and ends in the Carboniferous (see Figure 5.1 for location of well L08-10).

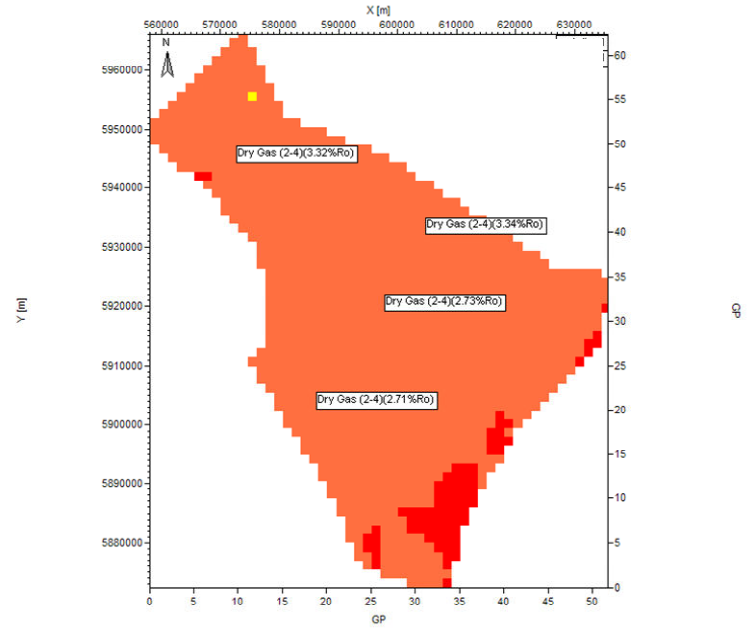

Figure 5.3 Calculated present-day maturity of the assumed Namurian source rock (Geverik Member).

The above simulation results suggest that oil generation from the Geverik source rock of kerogen type II, and the subsequent cracking of oil to gas, occurred before deposition of the Upper Rotliegend reservoirs and Zechstein seals.

The assumed constant thickness of 1500 m of generally low permeable Epen Formation and the overlying Westphalian mudrocks would have hampered effective vertical upward migration. In theory, downward expulsion of oil from the Geverik in Late Carboniferous times could have charged underlying Dinantian reservoir units (such as the inferred Dinantian carbonates surrounding the Texel-IJsselmeer High, Figure 1.6); the Namurian Epen Formation/Geverik Member acting as top seal. Ongoing burial will have cracked the residual oil in the Geverik and the expelled oil to gas. The subsequent history of assumed oil and gas accumulations in Dinantian Carbonates is characterized by a long history of deformation, starting with the Saalian deformation and erosion. These most likely will have induced remobilization to a greater and lesser extent by restructuration and by e.g. gas/oil driven out of traps by decompression expansion during erosion.

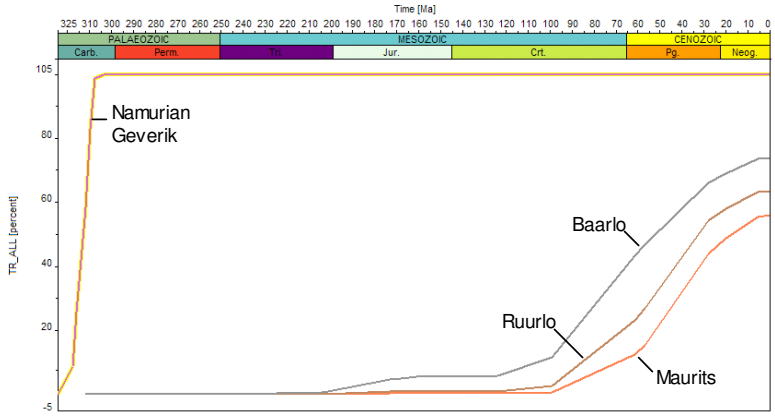

Figure 5.4 Calculated histories of transformation ratio of the Namurian Geverik Member, and the Westphalian Baarlo, Ruurlo and Maurits Formations at well location L08-10 (see Figure 5.1 for location).

Figures 5.4 and 5.5 show the differences between the history of transformation ratio of the Westphalian and the assumed Namurian Geverik source rocks, respectively.

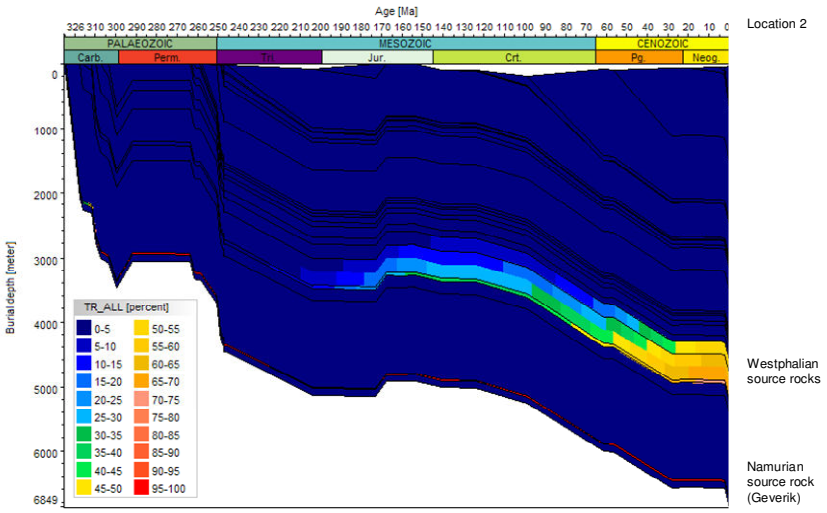

Figure 5.5 1D extraction at location 2 of the 3D simulated burial histories and history of transformation ratios of the assumed Namurian source rock 'Geverik' and the Westphalian source rocks (modeling scenario 2a)(see Figure 5.1 for location of the 1D extraction).

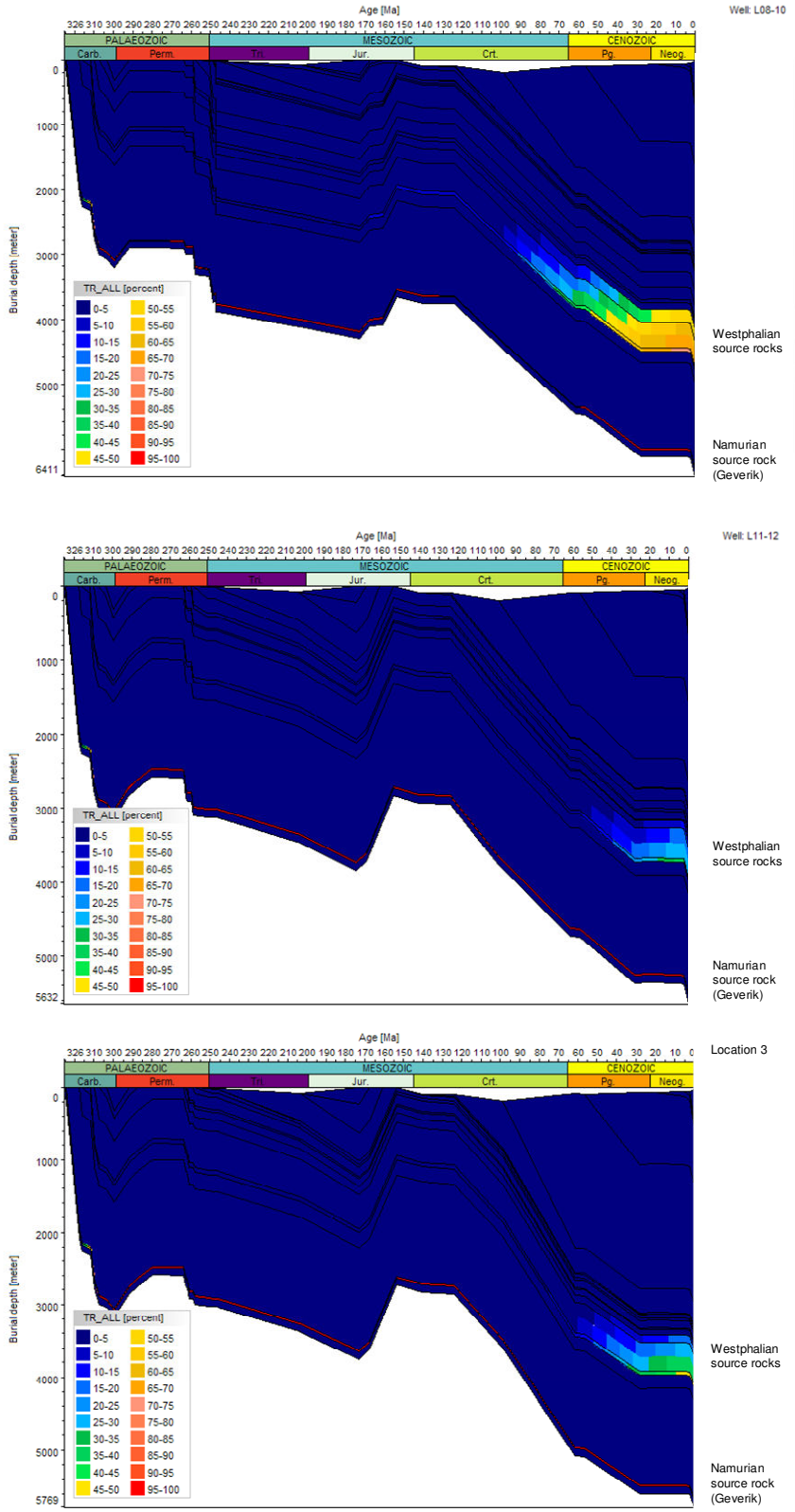

Figure 5.5(continued) 1D extraction at 3 locations of the 3D simulated burial histories and history of transformation ratios of the assumed Namurian source rock 'Geverik' and the Westphalian source rocks (modeling scenario 2a)(see Figure 5.1 for location of the 1D extractions).

The assumed Geverik source rock reaches a 100% transformation ratio already in the Carboniferous, while the Westphalian source rocks show the largest increase in transformation ratio during Late Cretaceous and Tertiary times and do not reach maximum values.

Figure 5.6 also illustrates the difference in timing of hydrocarbon generation between the assumed Geverik source rock and the Westphalian source rocks. The difference in bulk hydrocarbon generation rate between these two source intervals results from the combined effect of the differences in duration of hydrocarbon generation (relatively short for the Geverik) and in applied source rock properties (HI Geverik = 500 mgHC/gTOC; HI Westphalian = 250 mgHC/gTOC), in addition also source rock types and kinetic models differ.

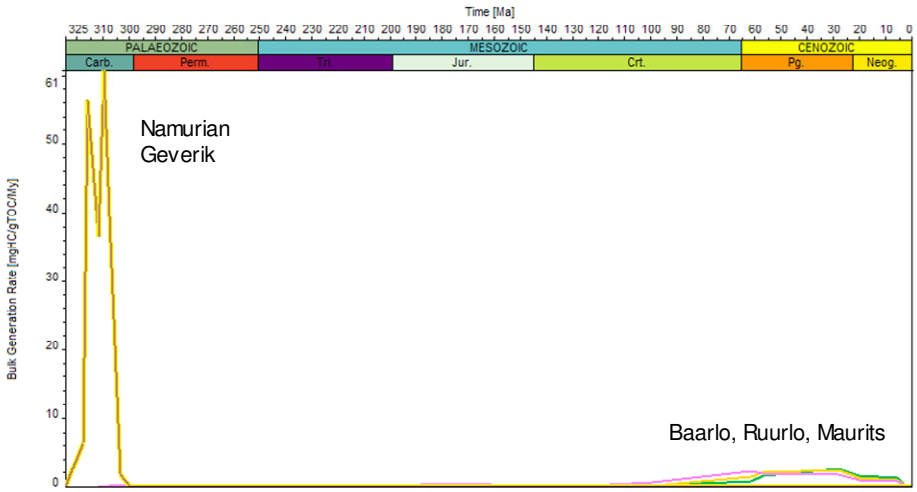

Figure 5.6 Calculated histories of bulk hydrocarbon generation rate of the assumed Namurian source rock ' Geverik', and the Westphalian Baarlo, Ruulo and Maurits source rocks at well location L08-10 (see Figure 5.1 for location).

5.2 Maturity and hydrocarbon generation Scenario 2b

Scenario 2b for the Namurian source rocks is based on the assumption that the Epen Formation contains different intervals with dispersed organic matter (Epen Formation_Main + Geverik : TOC = 2wt%, HI = 200 mg HC/gTOC); Table 2.3).

The general objective of running this scenario was to investigate the differences in timing of hydrocarbon generation depending on: 1) different depths of assumed source intervals in the Epen Formation and 2) the structural location of the source rock interval.

Figure 5.7 shows 1D extractions of the 3D simulated burial history and history of transformation ratio of 5 source rock depth intervals in the assumed Namurian and of the Westphalian source rocks at four locations. The deepest source interval is the first one to reach a 100 % transformation ratio at all locations. The shallower the position of the source interval, the later the hydrocarbon generation starts. At all four locations the combined Namurian Epen_Main + Geverik source rock reaches a transformation ratio of > 90 % before the Tertiary.

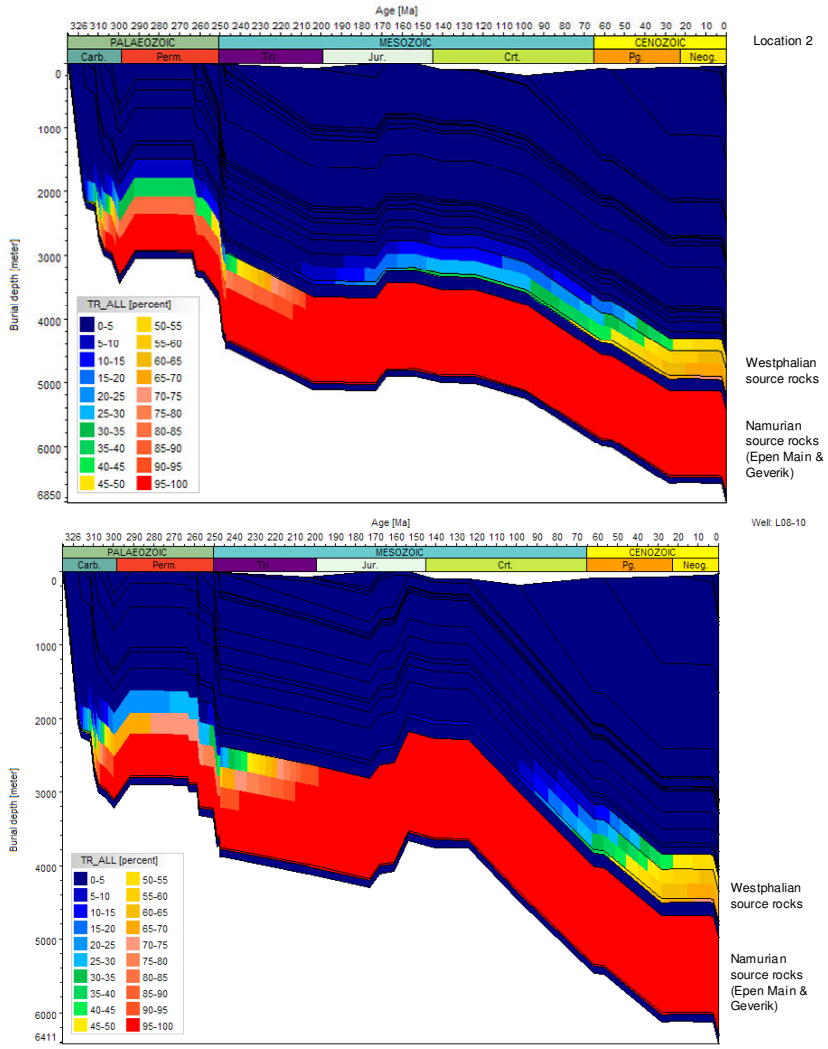

Figure 5.7 1D extraction at location 2 and at well L08-10 of the 3D simulated burial histories and history of transformation ratios of the assumed Namurian source rocks ('Epen Main' and Geverik) and the Westphalian source rocks modeling (scenario 2b) (see Figure 5.1 for location of the 1D extractions).

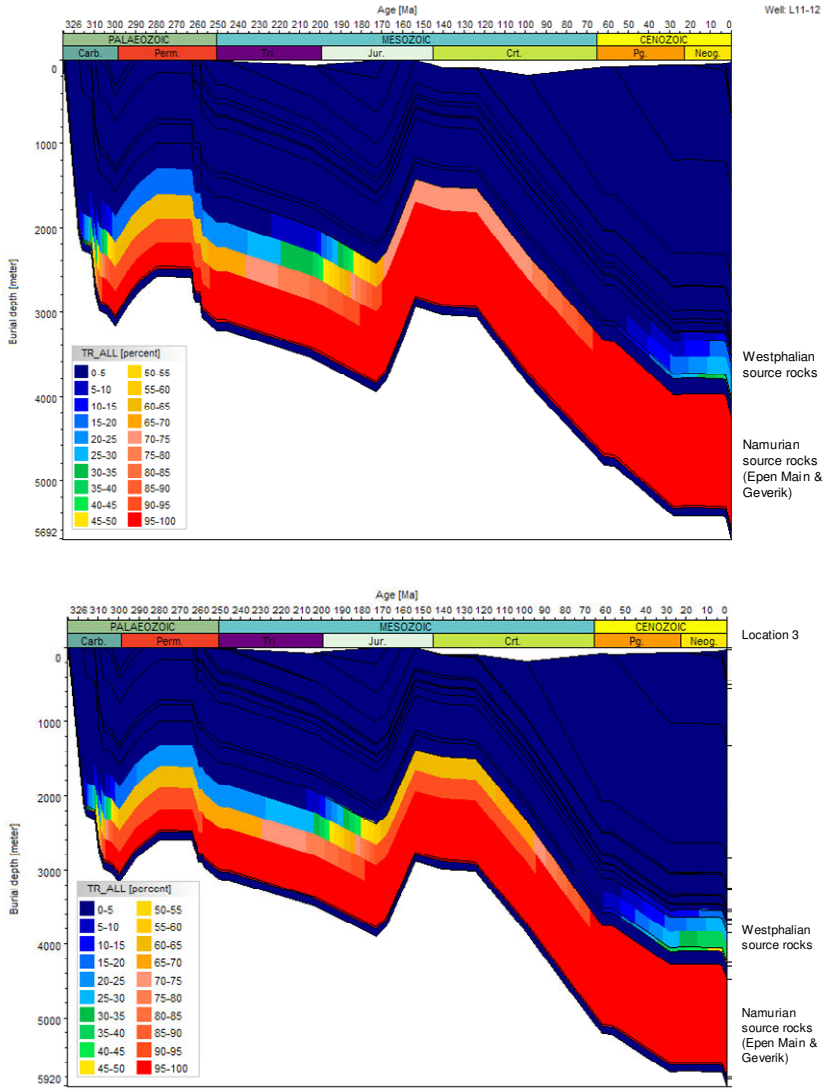

Figure 5.7(continued) 1D extraction at well L11-02 and at location 3 of the 3D simulated burial histories and history of transformation ratios of the assumed Namurian source rocks ('Epen Main' and Geverik) and the Westphalian source rocks modeling (scenario 2b) (see Figure 5.1 for location of the 1D extractions).

The calculated bulk hydrocarbon generation rates (Figure 5.8) reveal in more detail that the timing of hydrocarbon generation considering the Namurian 'Epen_Main + Geverik' as one source rock strongly depends on structural position and associated burial history of the source rock. The relatively minor Saalian erosion in combination with burial due to deposition of the Upper Rotliegend and Zechstein Groups trigger hydrocarbon generation at location 2 in Triassic times. Saalian erosion is more prominent at the other three locations. Here the assumed Namurian source rock reaches maximum bulk hydrocarbon generation rates in Jurassic times after reburial of the Namurian due to sedimentation from Upper Rotliegend to Early Jurassic times (see burial history for location 3; Figure 3.3). The hydrocarbon generation stops during Kimmerian uplift and erosion and resumes again because of reburial associated with deposition of the Rijnland Group and the thick package of chalk. Minor hydrocarbon generation from the Namurian continuous into the Early Tertiary in the eastern part of the area (e.g. L11-12).

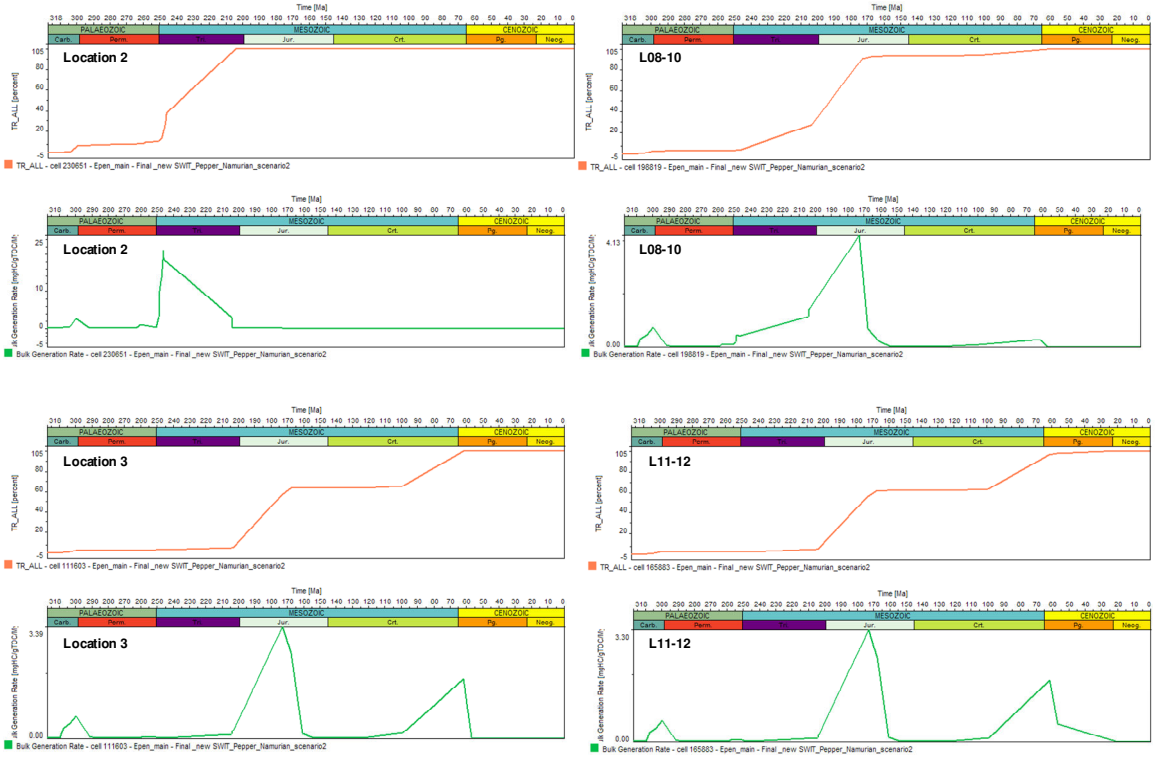

Figure 5.8 1D extractions at 4 locations of the 3D simulated histories of transformation ratio and bulk hydrocarbon generation rate of the assumed Namurian 'Main Epen' source rock (modeling scenario 2b)(see Figure 5.1 for location of the 1D extractions).

The deepest wells in the area do not reach the Namurian. The total thickness of the Namurian, the source rock properties and the location of the source intervals within the Namurian are not based on measured information. Therefore, the simulation runs provide results for hypothetical scenarios of Namurian conditions only. As such they show that within the area the regional variation in timing of hydrocarbon generation is strongly related to its structural position and to its location/depth within the Namurian. A transformation ratio of more than 90% is reached before the Tertiary at all depths and at all locations.

For the assumptions and conditions underlying the simulation scenarios 1, 2a and 2b, the results show that hydrocarbon generation from the Westphalian source rocks postdates that from the assumed Namurian source intervals.

6 Discussion

The 4D basin modeling of the Central Offshore Platform area provides a comprehensive simulation of a number of important interrelated basinal processes that lead to gas accumulations. Here we used the 4D simulations to increase the process-based understanding of the burial, temperature, maturity and hydrocarbon generation histories of the area, and to visualize these quantified histories. Focus was on Carboniferous source rocks: the Westphalian Baarlo, Ruurlo and Maurits Formations and assumed source intervals in the Namurian Epen Formation.

Basin modeling results depend on the fulfillment of the limiting assumptions and conditions underlying the approach, the chosen conceptual model of geological evolution of the area and a wide variety of additional input parameters and default relations between lithology and properties (Chapter 2). Below we review some important assumptions and conditions underlying the simulations in the Central Offshore Platform.

The temperature, maturity and hydrocarbon generation in the area were simulated assuming hydrostatic conditions. In reality the area is overpressured at present-day (Figures 1.10 and 1.11). Basin modeling programs simulate the temperature evolution using heat flow equations that are based, amongst other things, on lithology- and porosity-dependent thermal conductivities. As a consequence, the temperature evolution and the calculated present-day temperatures and source rock maturation will be affected by the porosity evolution. Hydraulic isolation (e.g. by evaporites) during burial results in overpressuring and undercompaction which is associated with relatively high porosities, and therefore lower thermal conductivities and higher temperatures below the seal in comparison with assumed hydrostatic compaction (Verweij et al., 2007). In order to avoid overestimation of porosities due to overpressuring, especially below the Zechstein salt, we decided to use hydrostatic modeling conditions for simulating the temperature and maturity history.

The results of the recently completed detailed mapping of the Central Offshore Platform (Witmans et al. , 2010) provided the conceptual model of the geological evolution required for the numerical modeling. The main uncertainties with respect to geological evolution concern the assumed erosional thicknesses, especially of the Upper Germanic Trias Group and the Altena Formation. Increasing or decreasing the original thicknesses of Triassic and Jurassic units may influence the timing and rates of hydrocarbon generation in the Carboniferous source rocks, but not their present-day burial depth and temperatures. The burial history plots (Figures 3.1, 3.3 and 4.7) indicate that for an increase of the original thicknesses of Triassic and Jurassic units of a few hundred metres, the present-day burial depth of the Westphalian source rocks will still be their maximum burial depth and the temperatures reached during the Mid-Miocene will still be their maximum temperatures reached during geological history.

There is uncertainty with respect to the total thickness of the Namurian Epen Formation and major uncertainty with respect to the distribution and properties of source intervals in the Namurian. The 3D modeling was run for two hypothetical scenarios.

Thermal boundary conditions directly influence the simulation of temperature and maturity history. In this study we compared a constant heat flow boundary with a variable basal heat flow boundary condition derived for K01-02 to study the effect on the maturity and hydrocarbon generation of the Westphalian source rocks (Section 4.3). The simulation results revealed differences in bulk hydrocarbon generation rates from the source rocks, but no to only minor changes in timing of hydrocarbon generation. Because the focus of the study is on investigating the timing of hydrocarbon generation, we selected the constant basal heat flow boundary conditions for running our models.

We also compared two recently reconstructed sediment water interface boundary conditions for the Tertiary and Quaternary times (Section 2.6). The only difference between these two boundary conditions is the temperature during Pleistocene times. It was found that the boundary condition with the more reduced Pleistocene temperatures provided a better fit with present-day temperatures, and showed no differences in the simulated present-day magnitudes of the maturities. This sediment water interface boundary condition with reduced Pleistocene temperatures was used in the study.

The choice of the kinetic model influences the timing and rates of hydrocarbon generation from source rocks. The effect of using two different kinetic models for the Westphalian source rocks (Burnham (1989)_T3 kinetic model and Pepper & Corvi (1995)_TIII-IV(F)) was treated in Section 4.1. The kinetic model of Pepper & Corvi (1995)_TIII-IV(F) was found to produce more conservative results. The Pepper & Corvi (1995)_TIII-IV(F) model was used for simulating the timing and bulk hydrocarbon generation rates of the Westphalian source rocks.

7 Synthesis

The recently in-house gathered, analyzed and mapped data and information on the Central Offshore Platform were used as input for a full 4D reconstruction of the burial history and history of temperature, source rock maturity and timing of hydrocarbon generation of the study area. The combination of available new data and information and new detailed Tertiary-Quaternary paleo temperature boundary conditions and 4D basin modeling has improved the 4D characterization and understanding of the burial, thermal and maturity history of the area and provided more detailed information on the timing of the main periods of hydrocarbon generation in the Westphalian Baarlo, Ruurlo and Maurits source rocks, and two scenerios for assumed Namurian source intervals.
A selection of the modeling results are presented below.

Modeling results: Burial history, temperature, source rock maturity and hydrocarbon generation Westphalian source rocks:

- The Westphalian source rocks of kerogen type II are at their maximum depth of burial at present-day;
- From Permian times onward, the burial depth and temperatures of Westphalian source rocks in the northern part of the area were higher than those in the central and southern part;
- The Westphalian source rocks reached maximum temperatures at Miocene times. Hence their present-day temperatures are lower than the temperatures reached in the Miocene;
- Present-day lateral variations in steady state temperatures are the combined result of burial depth and differences in bulk thermal conductivity of the sedimentary fill. These present-day lateral temperature differences reach 60 ^{o}C in the Baarlo Formation;
- The largest increase in source rock maturity occurs in Late Cretaceous-Tertiary times. Present-day maturities of the Maurits Formation varies from < 1 Ro% around the Texel-IJsselmeer High to values of approximately 1.3-1.5Ro% in a zone along the northeastern border of the area and locally in the northwest. The maturity of the Baarlo Formation reaches wet gas conditions in most of the area in Late Tertiary, while dry gas maturities develop locally along the northeastern border of the area;
- Simulated transformation ratios and bulk hydrocarbon generation rates show that hydrocarbon generation from Westphalian source rocks is concentrated in Tertiary times. The Maurits source rock starts to generate in Late Cretaceous times and peak generation rates were reached in Late Paleogene times. In contrast, in the more southern part of the area hydrocarbon generation starts in the Paleogene and peaks in Late Neogene times. This Neogene peak in hydrocarbon generation rate coincides with a period of only minor changes in burial depth of the source rock and the Mid-Miocene thermal maximum of the surface temperatures.

Modeling results: Burial history, temperature, source rock maturity and hydrocarbon generation assumed Namurian source rocks:
The deepest wells in the area do not reach the Namurian. The total thickness of the Namurian, the source rock properties and the location of the source intervals within the Namurian are not based on measured information. Therefore, the simulation runs provide results for hypothetical scenarios of Namurian conditions only.

- The assumed Namurian source rocks of kerogen type II, ‘Geverik’ (scenario 2a) and ‘Epen_Main + Geverik’ (scenario 2b), are at their maximum depth of burial at present-day;
- Hydrocarbon generation of the ‘Geverik’ source rock starts and ends in the Carboniferous and transformation ratios reach 100% at the end of the Carboniferous. The present-day maturity of the ‘Geverik’ is in the dry gas range;
- The timing of bulk hydrocarbon generation from the ‘Epen_Main + Geverik’ source rock strongly depends on structural position and associated burial history of the source rock. The

relatively minor Saalian erosion in combination with burial due to deposition of the Upper Rotliegend and Zechstein Groups trigger hydrocarbon generation in northern part of the area in Triassic times. Saalian erosion is more prominent in the remainder of the area. Here the assumed Namurian source rock reaches maximum bulk hydrocarbon generation rates in Jurassic times after reburial of the Namurian due to sedimentation from Upper Rotliegend to Early Jurassic times. The hydrocarbon generation stops during Kimmerian uplift and erosion and resumes again because of reburial associated with deposition of the Rijnland Group and especially the thick package of chalk. Minor hydrocarbon generation from the Namurian continuous into the Early Tertiary in the eastern part of the area (e.g. L11-12);

- The ‘Epen_Main + Geverik’ source rock reaches transformation ratios of > 90% before the Tertiary at all depths and all locations;

8 References

Burnham, A.K. 1989. A simple kinetic model of petroleum formation and cracking. Lawrence Livermoore National Laboratory Report UCID 21665, 11 p.

De Jager, J. & Geluk, M.C., 2007. Petroleum Geology. *In*: Th.E.Wong, D.A.J. Batjes and J. de Jager, eds, Geology of the Netherlands. Royal Dutch Academy of Arts and Sciences (Amsterdam), 241-264.

De Jager, J., 2007. Geological development. *In*: Th.E.Wong, D.A.J. Batjes and J. de Jager, eds, Geology of the Netherlands. Royal Dutch Academy of Arts and Sciences (Amsterdam), 5-26.

Donders, T.H., Weijers, J.W.H., Munsterman, D.K., Kloosterboer-van Hoeve, M.L., Buckles, L.K., Pancost, R.D., Schouten, S., Sinninghe Damsté, J.S., Brinkhuis, H., 2009. Strong climate coupling of terrestrial and marine environments in the Miocene of northwest Europe. Earth and Planetary Science Letters, v. 281, 215-225.

Doornenbal, J.C. & Stevenson, A.G., (eds), 2010. Petroleum Geological Atlas of the Southern Permian Basin Area. EAGE Publications b.v., Houten, the Netherlands.

Duin, E.J.T., Doornenbal, J.C., Rijkers, R.H.B., Verbeek, J.W., Wong, Th.E., 2006. Subsurface structure of the Netherlands - results of recent onshore and offshore mapping, Netherlands Journal of Geosciences - Geologie en Mijnbouw, v. 85-4, 245-276.

Geluk, M.C., 2007. Permian. Triassic. *In*: Wong, Th.E., Batjes, D.A.J., De Jager, J. (eds). Geology of the Netherlands. Royal Dutch Academy of Arts and Sciences (Amsterdam), p. 63-83; 85-106.

Geluk, M.C., Dusar, M., De Vos, W., 2007. Pre-Silesian. *In*: Wong, Th.E., Batjes, D.A.J., De Jager, J. (eds). Geology of the Netherlands. Royal Dutch Academy of Arts and Sciences (Amsterdam), 27-42.

Gerling, P., Geluk, M.C., Kockel, F., Lokhorst, A., Lott, G.K., Nicholson, R.A., 1999. NW European Gas Atlas – New implications for the Carboniferous gas play innthe western part of the Southern Permian Basin. In: Fleet, A.J. and S.A.R. Boldy, S.A.R. (eds). Petroleum geology of Northwest Europe. Proceedings of the 5th Conference. Geological Society London, 799-809.

Kombrink, H., 2008. The Carboniferous of the Netherlands and surrounding areas; a basin analysis. PhDThesis Utrecht University, Geologica Ultraiectina mededelingen van de Faculteit Geowetenschappen Universiteit Utrecht No. 294, 184 p.

Kombrink, H., Besly, B.M., Collinson, J.D., Den Hartog Jager, D.G., Drozdzewski, G., Dusar, M., Hoth, P., Pagnier, H.J.M., Stemmerik, L., Waksmundzka, M.I. & Wrede, V., 2010. Carboniferous. *In:* Doornenbal, J.C. & Stevenson, A.G. (eds). Petroleum Geological Atlas of the Southern Permian Basin Area. EAGE Publications b.v., Houten, the Netherlands, 81-99.

Kombrink, H., Leever, K.A., Van Wees, J-D., Van Bergen, F., David, P., Wong, Th. E. 2008. Late Carboniferous foreland basin formation and Early Carboniferous stretching in Northwestern Europe – Inferences from quantitative subsidence analyses in the Netherlands. Basin Research 20, 377-395.

Kombrink, H., Van Lochem, H., Van der Zwan, K.J., 2010b: Seismic interpretation of Dinantian carbonate platforms in the Netherlands; implications for the palaeogeographical and structural development of the Northwest European Carboniferous Basin. Journal of the Geological Society; v. 167, 99-108.

Lokhorst, A. (ed.), 1998. The Northwest European Gas Atlas. Netherlands Institute of Applied Geoscience TNO (Haarlem), ISBN 90-72869-60-5.

Mosbrugger, V., Utescher, T., Dilcher, D.L., 2005. Cenozoic continental climate evolution of Central Europe. Proc. Natl. Acad. Sci. USA, v. 102 (42), 14964-14969.

NITG, 1998. Geological atlas of the subsurface of the Netherlands (1:250.000). Explanation to map sheet X Almelo-Winterswijk. Netherlands Institute of Applied Geoscience TNO, Haarlem, 134 p.

Pearson, P.N., Van Dongen, B.E., Nicholas, C.J., Pancost, R.D., Schouten, S., Singano, J., Wade, B.S., 2007. Stable warm tropical climate through the Eocene Epoch. Geology, v. 35, 211-214.

Pepper, A.S. & Corvi, P.J., 1995. Simple kinetic models of pertoleum formation. Part I: oil and gas generation from kerogen. Marine and Petroleum Geology, v. 12, no. 3, 291-319.

Ramaekers, J.J.F., 2008. NCP2E Rotliegend Petrophysical analyses. TNO report 2008-U-R0605/A.

Sekiguchi, K., 1984. A method for determining terrestrial heat flow in oil basinal areas. Tectonophysics v. 103, 67-79.

Sluijs, A. & Brinkhuis, H., 2008. Rapid carbon injection and transient global warming during the Paleocene-Eocene thermal maximum. Netherlands Journal of Geosciences – Geologie en Mijnbouw, 87-3, 201-206.

Sluijs, A. et al., 2006. Subtropical Arctic Ocean temperatures during the Paleocene/Eocene thermal maximum. Nature, v. 441 (7093), 610-613.

Sweeney, J.J. & Burnham, A.K., 1990. Evaluation of a simple model of vitrinite reflectance based on chemical kinetics. AAPG Bulletin, v. 74, 1559-1570.

Van Adrichem Boogaert, H.A. & Kouwe, W.F.P. (eds), 1993 - 1997. Stratigraphic nomenclature of the Netherlands, revision and update by RGD and NOGEPA, Mededelingen Rijks Geologische Dienst, v. 50, The Netherlands.

Van Buggenum, J.M. & Den Hartog Jager, D.G., 2007. Silesian. *In*: Wong, Th.E., Batjes, D.A.J., De Jager, J. (eds). Geology of the Netherlands. Royal Dutch Academy of Arts and Sciences, Amsterdam, 43-62.

Verweij, H., David, P., Souto Carneiro Echternach, M., Van Wees, J-D., 2007. Simulation of coupled evolution of pore pressure, fluid flow, compaction and temperature: consequences for correct temperature and maturity prediction in unexplored arteas and unconventyional basin settings. Abstract AAPG Hedberg Conference Basin modeling perspectives: Innovative developments and novel applications, May 6-9, The Hague, The Netherlands.

Verweij, J.M., Souto Carneiro Echternach, M., Witmans, N., Abdul Fattah, R., 2010. Reconstruction of basal heat flow, surface temperature, source rock maturity and hydrocarbon generation in salt-dominated Dutch Basins. AAPG Hedberg special volume: Basin and Petroleum System Modeling: New horizons in research and applications (accepted).

Waples, D.W. & Waples, J.S., 2004. A review and evaluation of specific heat capacities of rocks, minerals and subsurface fluids. Part 2: fluids and porous rocks. Natural Resources Research, Vol 13., no. 2, 123-130.

Witmans, N., Van Gessel, S., Ten Veen, J.H., 2010. Central Offshore Platform and Vlieland Basin Mapping and Modeling – Area 2E. TNO Report TNO-034-UT-2010-01364.

Zachos, J.C., Dickens, G.R., Zeebe, R.E., 2008. An Early Cenozoic perspective on greenhouse warming and carbon-cycle dynamics. Nature, v. 451 (7176), 279-283.

9 Annexes

Annex 1: Gas Composition and fluid overpressure maps

Annex 2: Erosion maps

Annex 3: Lithology-related properties and relations

Annex 4: Calibration data

10 Signature

Utrecht, July 2010

TNO Built Environment and Geosciences

J.C. Doornenbal
Head of Department

Author
J.M. Verweij

ANNEX 1 a) Geochemical composition of the natural gas accumulations

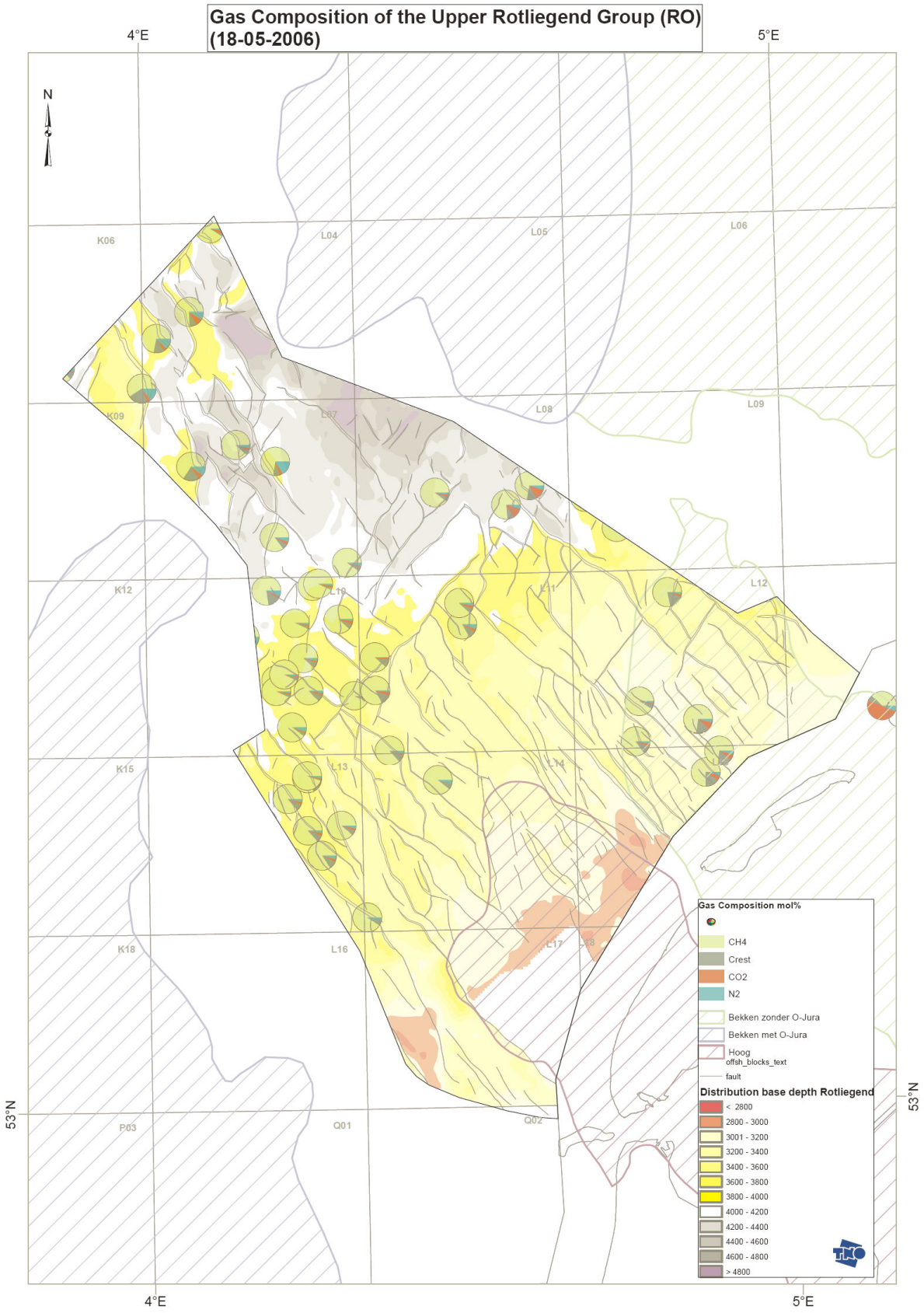

ANNEX 1 b) Distribution of all fluid overpressures in Upper Rotliegend Group

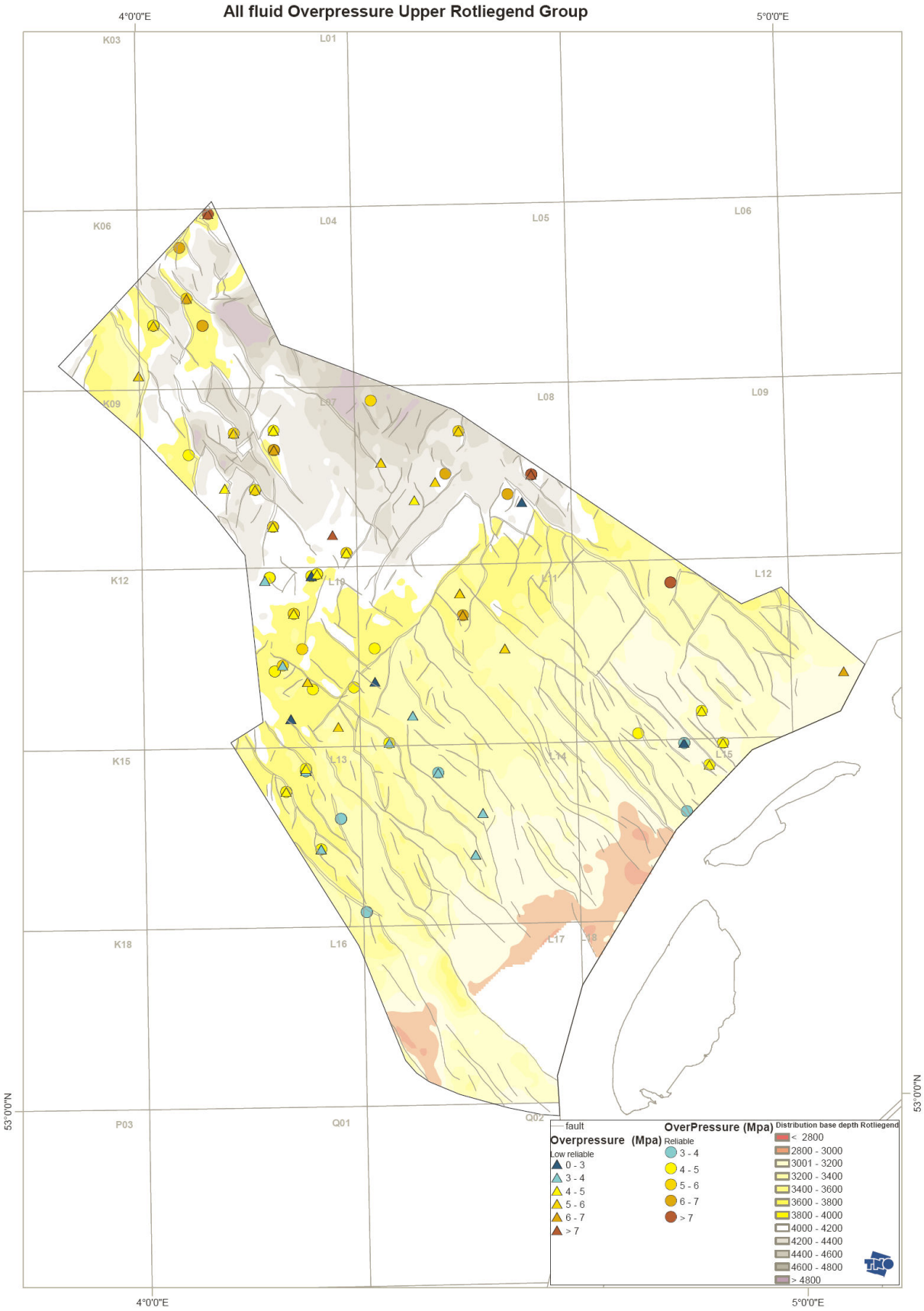

ANNEX 2 Erosion Maps

7 erosion maps (corresponding to the 7 stratigraphic layers affected by erosion) were created for input into the 3D basin model. The figures below show the reconstructed erosional thickness of the 7 stratigraphic layers affected by erosion.

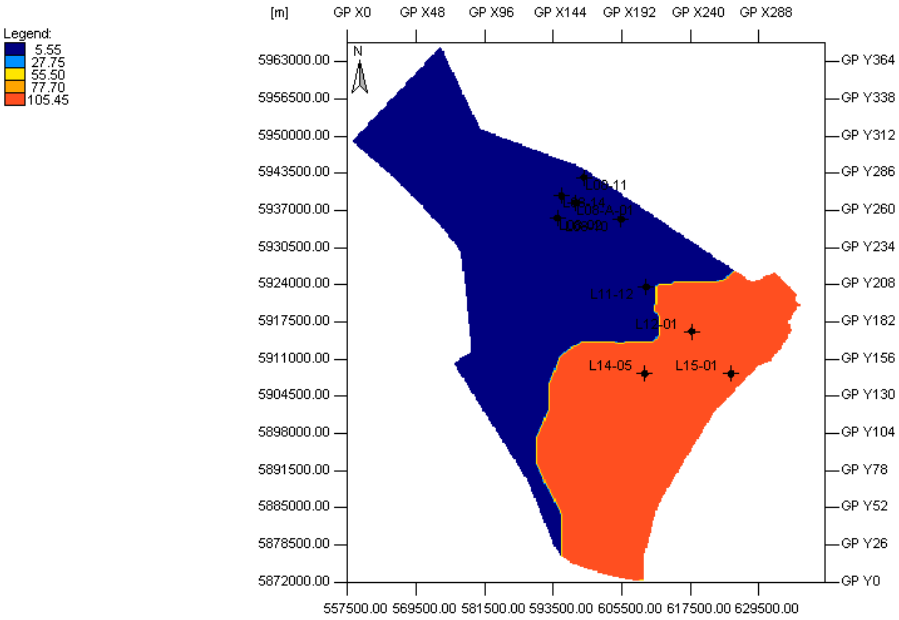

Annex 2_Figure 1. Present-day erosional thickness of the Ruurlo Formation of the Limburg Group. The reconstruction of the erosional thickness is based on an assumed original thickness of the Ruurlo Formation of 100m.

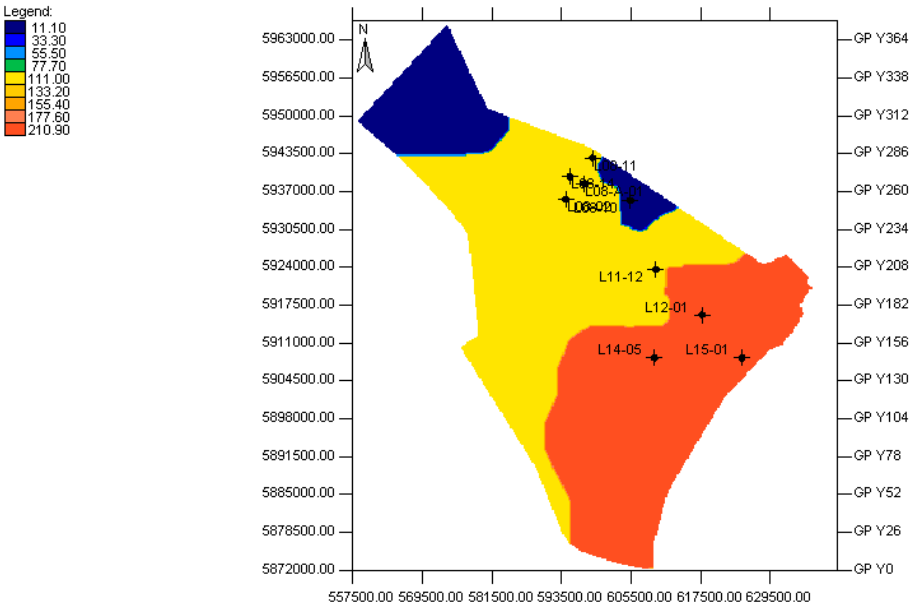

Annex 2_ Figure 2. Present-day erosional thickness of Maurits Formation. The reconstruction of the erosional thickness is based on an assumed original thickness of the Maurits Formation of 200m.

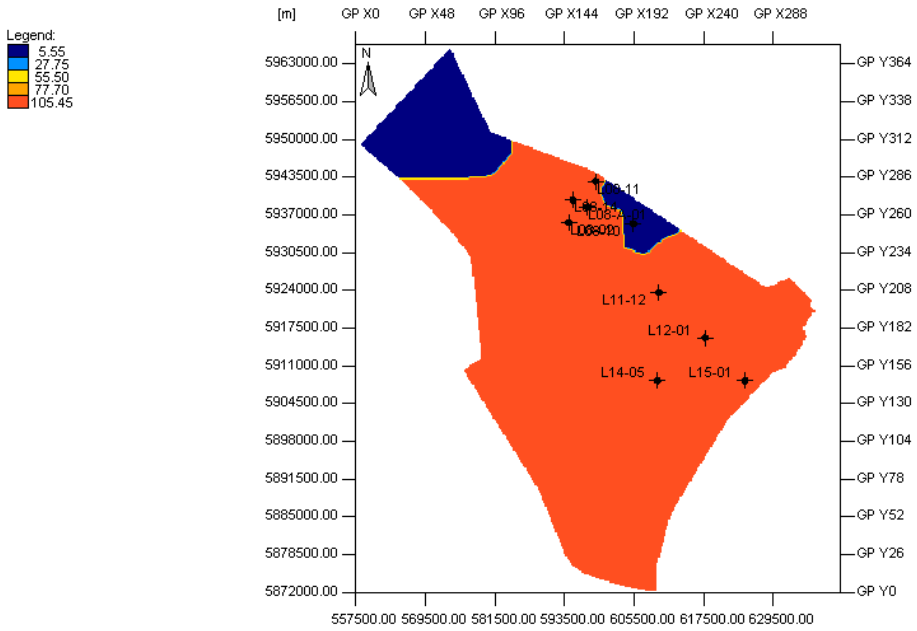

Annex 2_Figure 3. Present-day thickness and erosional thickness of the Hospital Ground Formation. The reconstruction of the erosional thickness is based on an assumed original thickness of the Hospital Ground Formation of 100m.

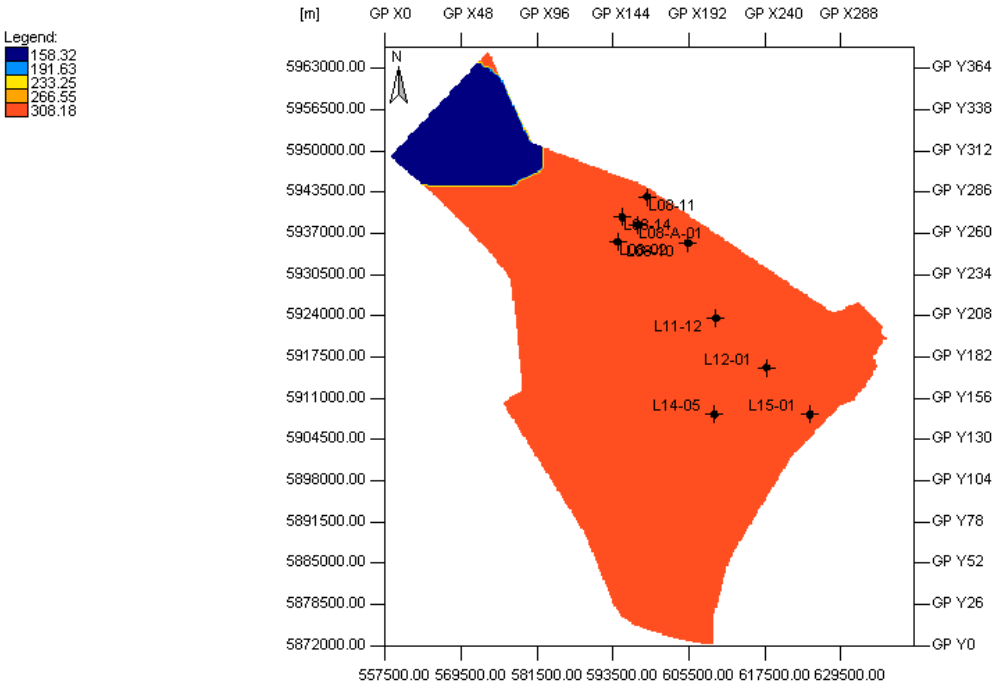

Annex 2_ Figure 4. Present-day erosional thickness of the Step Graben Formation. The reconstruction of the erosional thickness is based on an assumed original thickness of the Step Graben Formation of 300m.

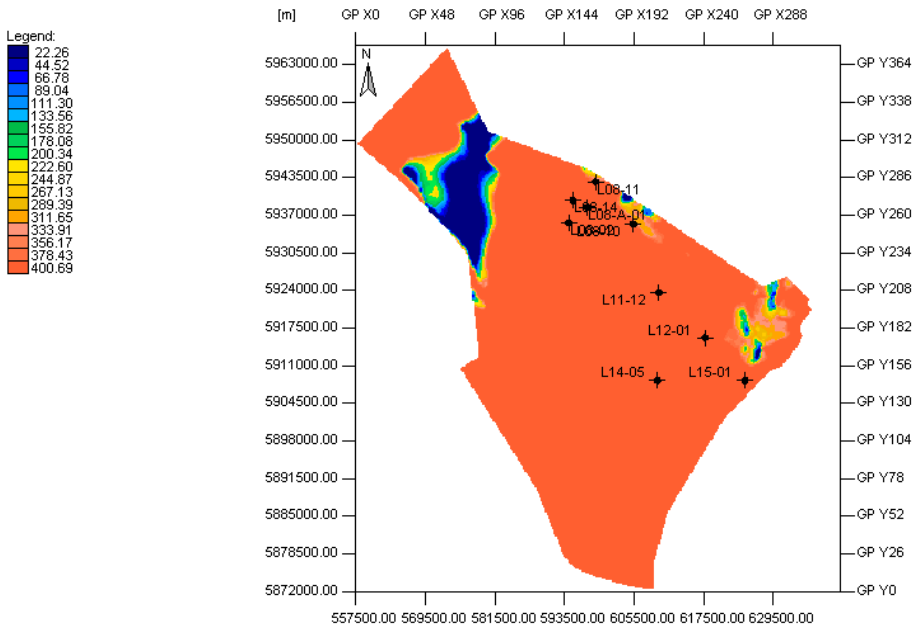

Annex 2_Figure 5. Present-day erosional thickness of the Lower Germanic Trias Group. The reconstruction of the erosional thickness is based on an assumed minimum original thickness of this unit of 400 m.

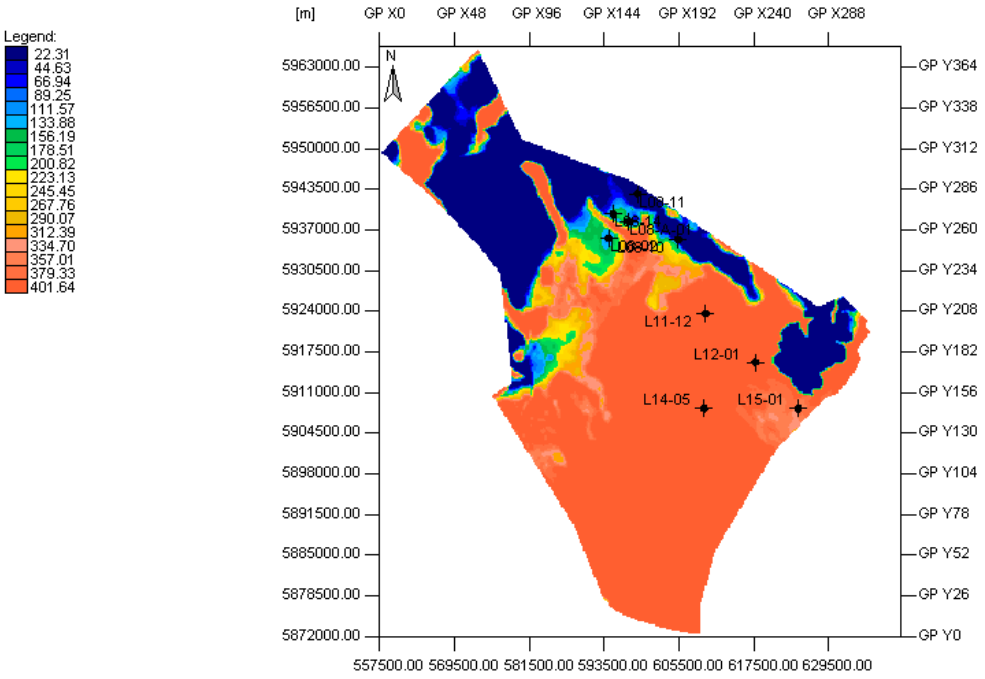

Annex2_Figure 6. Present-day erosional thickness of the Upper Germanic Trias Group. The reconstruction of the erosional thickness is based on an assumed minimum original thickness of 400m.

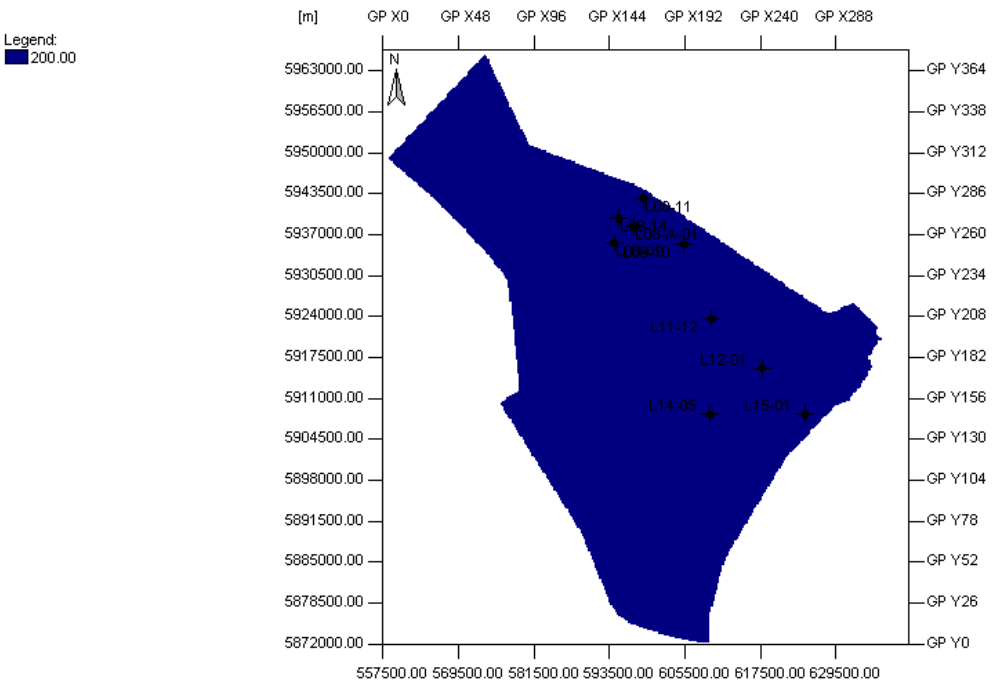

Annex2_Figure 7. Present-day erosional thickness of the Altena Group. The reconstruction of the erosional thickness is based on an assumed minimum original thickness of the Altena Group of 200m.

ANNEX 3 Lithology-related properties and relations

Annex 3_Table 1 Lithology related matrix thermal conductivities (Petromod version 10)

Lihology	Model	Matrix thermal conductivity W/m/K	
		at 20°C	at 100°C
100% Chalk	Sekiguchi Model	2.9	2.62
100% Salt	Sekiguchi Model	6.5	5.25
100% Shale	Sekiguchi Model	1.64	1.69
90% Shale 10% Sand	Sekiguchi Model	1.87	1.86
90% Sand 10% Shale	Sekiguchi Model	3.72	3.22
80% Shale 20% Sand	Sekiguchi Model	2.1	2.03
80% Shale 15% Silt 5% Limestone	Sekiguchi Model	1.77	1.79
80% Shale 15% Sand 5% Silt	Sekiguchi Model	2.01	1.96
80% Shale 15% Sand 5% Coal	Sekiguchi Model	1.92	1.89
80% Sand 20% Shale	Sekiguchi Model	3.49	3.05
78% Shale 20% Sand 2% Coal	Sekiguchi Model	2.08	2.01
75% Shale 25% Silt	Sekiguchi Model	1.74	1.77
75% Shale 25% Sand	Sekiguchi Model	2.22	2.12
75% Sand 25% Shale	Sekiguchi Model	3.37	2.96
65% Shale 25% Sand 10% Silt	Sekiguchi Model	2.26	2.15
60% Sand 20% Silt 18% Shale 2% Coal	Sekiguchi Model	3.08	2.74
50% Sand 50% Shale	Sekiguchi Model	2.79	2.54
49% Shale 49% Sand 2% Coal	Sekiguchi Model	2.75	2.5
48% Shale 25% Silt 25% Sand 2% Coal	Sekiguchi Model	2.29	2.17
Basement	Sekiguchi Model	2.72	2.35

Annex 3_Table 2 Lithology related radiogenic heat production (Petromod version 10)

Lithology	Model	Uranium ppm	Thorium ppm	Potassium ppm	Porosity	Radiogenic heat production (microW/m^3)
100% Chalk	Rybach equation	1.9	1.4	0.25	0	0.6
100% Salt	Rybach equation	0.02	0.01	0.1	0	0.02
100% Shale	Rybach equation	3.7	12	2.7	0	2.03
90% Shale 10% Sand	Rybach equation	3.46	11.15	2.56	0	1.9
90% Sand 10% Shale	Rybach equation	1.54	4.35	1.44	0	0.84
80% Shale 20% Sand	Rybach equation	3.22	10.3	2.42	0	1.77
80% Shale 15% Silt 5% Limestone	Rybach equation	3.31	10.4	2.32	0	1.79
80% Shale 15% Sand 5% Silt	Rybach equation	3.33	10.53	2.38	0	1.81
80% Shale 15% Sand 5% Coal	Rybach equation	3.23	10.28	2.38	0	1.73
80% Sand 20% Shale	Rybach equation	1.78	5.2	1.58	0	0.97
78% Shale 20% Sand 2% Coal	Rybach equation	3.18	10.12	2.38	0	1.73
75% Shale 25% Silt	Rybach equation	3.28	10.25	2.28	0	1.77
75% Shale 25% Sand	Rybach equation	3.1	9.88	2.35	0	1.7
75% Sand 25% Shale	Rybach equation	1.9	5.63	1.65	0	1.04
65% Shale 25% Sand 10% Silt	Rybach equation	2.93	9.18	2.18	0	1.6
60% Sand 20% Silt 18% Shale 2% Coal	Rybach equation	1.88	5.32	1.48	0	0.99
50% Sand 50% Shale	Rybach equation	2.5	7.75	2	0	1.37
49% Shale 49% Sand 2% Coal	Rybach equation	2.48	7.65	1.97	0	1.35
48% Shale 25% Silt 25% Sand 2% Coal	Rybach equation	2.63	7.94	1.88	0	1.4
Basement	Rybach equation	0	0	0	0	0

Annex 3_Table 3 Lithology related heat capacity (Petromod version 10)

Lithology	Model	Heat Capacity Kcal/kg/K	
		at 20°C	at 100°C
100% Chalk	Waples Model for Rock	0.203	0.234
100% Salt	Waples Model for Rock	0.206	0.238
100% Shale	Waples Model for Rock	0.206	0.238
90% Shale 10% Sand	Waples Model for Rock	0.206	0.238
90% Sand 10% Shale	Waples Model for Rock	0.204	0.236
80% Shale 20% Sand	Waples Model for Rock	0.206	0.238
80% Shale 15% Silt 5% Limestone	Waples Model for Rock	0.207	0.239
80% Shale 15% Sand 5% Silt	Waples Model for Rock	0.207	0.24
80% Shale 15% Sand 5% Coal	Waples Model for Rock	0.211	0.244
80% Sand 20% Shale	Waples Model for Rock	0.204	0.236
78% Shale 20% Sand 2% Coal	Waples Model for Rock	0.208	0.24
75% Shale 25% Silt	Waples Model for Rock	0.209	0.241
75% Shale 25% Sand	Waples Model for Rock	0.205	0.237
75% Sand 25% Shale	Waples Model for Rock	0.204	0.236
65% Shale 25% Sand 10% Silt	Waples Model for Rock	0.207	0.239
60% Sand 20% Silt 18% Shale 2% Coal	Waples Model for Rock	0.209	0.242
50% Sand 50% Shale	Waples Model for Rock	0.205	0.237
49% Shale 49% Sand 2% Coal	Waples Model for Rock	0.207	0.239
48% Shale 25% Silt 25% Sand 2% Coal	Waples Model for Rock	0.21	0.243
Basement	Waples Model for Rock	0.188	0.223

Annex 3_Table 4 Lithology related mechanical compaction relation (Petromod version 10)

Lithology	Model	Initial porosity	Minimum porosity	Athy's factor
				km^{-1}
100% Chalk	Athy's Law (Depth)	0.7	0.01	0.9
100% Salt	Athy's Law (Depth)	0.01	0.01	0
100% Shale	Athy's Law (Depth)	0.7	0.01	0.83
90% Shale 10% Sand	Athy's Law (Depth)	0.67	0.01	0.78
90% Sand 10% Shale	Athy's Law (Depth)	0.44	0.01	0.36
80% Shale 20% Sand	Athy's Law (Depth)	0.64	0.01	0.73
80% Shale 15% Silt 5% Limestone	Athy's Law (Depth)	0.67	0.01	0.67
80% Shale 15% Sand 5% Silt	Athy's Law (Depth)	0.66	0.01	0.76
80% Shale 15% Sand 5% Coal	Athy's Law (Depth)	0.66	0.01	0.73
80% Sand 20% Shale	Athy's Law (Depth)	0.47	0.01	0.41
78% Shale 20% Sand 2% Coal	Athy's Law (Depth)	0.64	0.01	0.72
75% Shale 25% Silt	Athy's Law (Depth)	0.66	0.01	0.75
75% Shale 25% Sand	Athy's Law (Depth)	0.63	0.01	0.7
75% Sand 25% Shale	Athy's Law (Depth)	0.48	0.01	0.44
65% Shale 25% Sand 10% Silt	Athy's Law (Depth)	0.61	0.01	0.67
60% Sand 20% Silt 18% Shale 2% Coal	Athy's Law (Depth)	0.5	0.01	0.45
50% Sand 50% Shale	Athy's Law (Depth)	0.55	0.01	0.57
49% Shale 49% Sand 2% Coal	Athy's Law (Depth)	0.56	0.01	0.57
48% Shale 25% Silt 25% Sand 2% Coal	Athy's Law (Depth)	0.59	0.01	0.61
Basement	Athy's Law (Depth)	0.05	0.05	0

Annex 3_Table 5 Lithology related porosity-permeability relation (Petromod version 10)

Lithology	Model	Permeability (log mD)	
		at 1% porosity	at 25% porosity
100% Chalk	Multi-Point Model	-6.75	-3.1
100% Salt	Multi-Point Model	-16	-16
100% Shale	Multi-Point Model	-8.52	-3
90% Shale 10% Sand	Multi-Point Model	-7.85	-2.4
90% Sand 10% Shale	Multi-Point Model	-2.47	2.4
80% Shale 20% Sand	Multi-Point Model	-7.18	-1.8
80% Shale 15% Silt 5% Limestone	Multi-Point Model	-7.87	-2.5
80% Shale 15% Sand 5% Silt	Multi-Point Model	-7.85	-2.4
80% Shale 15% Sand 5% Coal	Multi-Point Model	-7.22	-2.04
80% Sand 20% Shale	Multi-Point Model	-3.14	1.8
78% Shale 20% Sand 2% Coal	Multi-Point Model	-7.06	-1.78
75% Shale 25% Silt	Multi-Point Model	-7.96	-2.5
75% Shale 25% Sand	Multi-Point Model	-6.84	-1.5
75% Sand 25% Shale	Multi-Point Model	-3.48	1.5
65% Shale 25% Sand 10% Silt	Multi-Point Model	-6.62	-1.3
60% Sand 20% Silt 18% Shale 2% Coal	Multi-Point Model	-3.92	1.02
50% Sand 50% Shale	Multi-Point Model	-5.16	0
49% Shale 49% Sand 2% Coal	Multi-Point Model	-5.11	-0.04
48% Shale 25% Silt 25% Sand 2% Coal	Multi-Point Model	-6.16	-0.98
Basement	Multi-Point Model	-16	-16

ANNEX 4 Calibration data

Annex 4a: Calibration data: porosity

Tables 1 and 2 present reservoirproperties for the Upper and Lower Slochteren Sandstone of the Upper Rotliegend Group, respectively (from Ramaekers, 2008; TNO-rapport 2008-U-R0605/A)

Annex 4a_ Tabel 1 Reservoir properties Upper Slochteren Sandstone (based on cut-off's of 50% for clay volume,and 5% for porosity)

Reservoirsommatie	Top	Bottom	Top	Bottom	Gross	Net	n/g	phie	V_{cl}	Kb	Kb x h	S_w
Boring	**[m,MD]**	**[m,MD]**	**m,tvdss**	**m,tvdss**	**[m]**	**[m]**				**[mD]**	**[Dm]**	
L04-07												
L07-01	3644.00	3705.00	3617.53	3678.37	60.84	10.87	0.179	0.120	0.289	2.831	30.8	0.537
L07-04	3912.00	3982.00	3879.29	3949.22	69.93	7.64	0.109	0.116	0.347	0.153	1.2	0.640
L07-06	3876.00	3954.75	3841.72	3920.27	78.60	25.45	0.324	0.098	0.208	1.527	38.9	0.759
L08-01-S1	3952.53	4018.52	3925.02	3990.96	65.94	1.12	0.017	0.059	0.291	0.120	0.1	0.639
L08-P-01												
L08-P-03												
L10-01	3851.50	3958.50	3818.69	3925.66	106.96	92.57	0.865	0.173	0.222	6.807	630.1	0.391
L10-10	3778.50	3885.00	3739.23	3845.32	106.09	61.27	0.577	0.163	0.320	1.562	95.7	0.699
L10-A-01	3804.00	3948.00	3643.07	3781.05	137.98	105.79	0.767	0.092	0.263	0.388	41.0	0.533
L10-D-01-S1	3594.00	3735.00	3561.18	3702.01	140.84	120.41	0.855	0.143	0.203	2.183	262.5	0.362
L11B-A-01	3524.00	3604.00	3494.26	3574.25	79.99	22.25	0.278	0.113	0.278	1.499	33.4	0.562
L12-03	2912.00	2996.00	2884.49	2968.26	83.77	35.46	0.423	0.101	0.277	0.322	11.4	0.630
L12-05	3260.00	3279.00	3220.06	3239.04	18.98	5.69	0.300	0.121	0.334	1.072	6.1	0.683
L14-A-01	3212.00	3336.44	3180.68	3305.07	124.44	113.79	0.914	0.139	0.191	2.067	235.2	0.954
L15-01	2865.00	2989.00	2832.02	2956.00	123.98	59.49	0.480	0.110	0.191	0.475	28.3	0.425
M10-02	2787.00	2904.00	2677.52	2792.16	114.63	56.01	0.489	0.108	0.251	1.741	97.5	0.711

Annex 4a_Table 2 Reservoir properties Upper Slochteren Sandstone (based on cut-off's of 50% for clay volume,and 5% for porosity)

Reservoirsommatie	Top	Bottom	Top	Bottom	Gross	Net	n/g	phie	V_{cl}	Kb	Kb x h	S_w
Boring	**[m,MD]**	**[m,MD]**	**m,tvdss**	**m,tvdss**	**[m]**	**[m]**				**[mD]**	**[Dm]**	
L04-07	3832.92	3894.11	3761.67	3822.20	60.52	37.39	0.618	0.103	0.219	1.941	72.6	0.372
L07-01	3796.00	3871.34	3769.06	3844.03	75.01	52.36	0.698	0.121	0.164	6.923	362.5	0.803
L07-04	4097.52	4177.00	4064.61	4144.04	79.40	68.88	0.868	0.104	0.159	1.168	80.5	0.925
L07-06	4062.26	4130.00	4027.62	4095.15	67.58	37.51	0.555	0.106	0.122	1.567	58.8	0.838
L08-01-S1	4139.99	4213.00	4112.38	4185.33	72.96	33.68	0.462	0.080	0.161	0.479	16.1	0.354
L08-P-01	4278.00	4346.00	4181.77	4239.84	58.07	53.49	0.921	0.108	0.097	1.091	58.4	0.255
L08-P-03	4858.50	4934.00	4530.67	4602.33	71.66	47.84	0.668	0.096	0.097	0.941	45.0	0.286
L10-01	4003.00	4089.00	3970.14	4056.11	85.97	54.53	0.634	0.131	0.165	5.205	283.9	0.515
L10-10	3927.00	4017.50	3887.16	3977.32	90.16	52.70	0.585	0.123	0.258	1.322	69.7	0.934
L10-A-01	3994.00	4073.00	3825.17	3900.97	75.81	45.10	0.595	0.084	0.213	0.155	7.0	0.879
L10-D-01-S1	3774.50	3857.00	3741.47	3823.87	82.40	41.25	0.501	0.108	0.229	1.208	49.8	0.646
L11B-A-01	3696.00	3758.00	3666.23	3728.22	61.99	46.79	0.755	0.112	0.234	2.043	95.6	0.752
L12-03	3068.30	3120.30	3040.433	3092.38	51.95	3.70	0.071	0.066	0.356	0.215	0.8	0.702
L12-05	3430.00	3438.00	3389.92	3397.91	7.99	5.70	0.713	0.107	0.286	1.618	9.2	0.671
L14-A-01	3364.00	3422.00	3332.67	3390.67	58.00	36.60	0.631	0.107	0.231	1.668	61.0	0.913
L15-01	3090.00	3099.00	3056.99	3065.99	9.00	7.05	0.783	0.092	0.223	0.784	5.5	0.935
M10-02												

ANNEX 4 Calibration data

Annex 4b: Calibration data: pressures

WELL_NAME	WELL_ID	TVD_SS (m)	FORMATION_PRESSURE (Psia)	(MPa)	DATA_SOURCE
L04-03	7258	3659.81	6073.02	41.883	RFT
L04-03	7258	3664.78	6043	41.676	RFT
L04-03	7258	3668.26	6019.93	41.517	RFT
L04-03	7258	3677.71	6020.95	41.524	RFT
L04-03	7258	3687.85	6023.85	41.544	RFT
L04-03	7258	3694.12	5999.05	41.373	RFT
L04-03	7258	3694.62	6040.97	41.662	RFT
L04-03	7258	3695.61	6026.03	41.559	RFT
L04-03	7258	3702.77	6034	41.614	RFT
L04-03	7258	3707.54	6038.93	41.648	RFT
L04-03	7258	3711.02	6046.04	41.697	RFT
L04-03	7258	3716.99	6057.93	41.779	RFT
L04-03	7258	3725.93	6078.97	41.924	RFT
L04-06	8173	3649.28	6371.6	43.942	RFT
L04-06	8173	3649.29	6627.89	45.710	RFT
L04-06	8173	3650.77	6630.64	45.729	RFT
L04-06	8173	3654.24	6636.3	45.768	RFT
L04-06	8173	3659.69	6638.48	45.783	RFT
L04-06	8173	3665.64	6634.12	45.753	RFT
L04-06	8173	3675.55	6944.22	47.891	RFT
L04-06	8173	3693.4	6763.94	46.648	RFT
L04-06	8173	3693.89	6814.99	47.000	RFT
L04-06	8173	3695.88	6642.83	45.813	RFT
L04-06	8173	3695.89	6455.44	44.520	RFT
L04-06	8173	3696.37	6645.58	45.832	RFT
L04-06	8173	3696.86	6637.03	45.773	RFT
L04-06	8173	3696.86	6649.93	45.862	RFT
L04-06	8173	3698.35	6654.43	45.893	RFT
L04-06	8173	3698.55	6655.88	45.903	RFT
L04-06	8173	3698.85	6652.98	45.883	RFT
L04-06	8173	3707.27	7179.48	49.514	RFT
L04-06	8173	3707.76	7182.38	49.534	RFT
L04-06	8173	3945.29	6818.76	47.026	RFT
L04-06	8173	3945.78	6815.28	47.002	RFT
L04-06	8173	3945.79	6813.83	46.992	RFT
L04-06	8173	3945.8	6811.8	46.978	RFT
L04-06	8173	3946.76	6866.04	47.352	RFT
L04-06	8173	3948.24	6984.83	48.171	RFT
L04-06	8173	4036.91	6864.74	47.343	RFT
L04-06	8173	4037.89	6864.59	47.342	RFT
L04-06	8173	4040.82	6917.53	47.707	RFT
L04-06	8173	4043.27	6916.66	47.701	RFT
L04-06	8173	4047.18	6890.56	47.521	RFT
L04-06	8173	4048.65	6897.08	47.566	RFT
L04-06	8173	4051.58	6902.16	47.601	RFT
L04-06	8173	4055.99	6911.59	47.666	RFT
L04-06	8173	4056.48	6922.03	47.738	RFT
L04-07	8232	3770.54	6840.15	47.173	RFT
L04-07	8232	3794.53	6503.2	44.850	RFT
L04-07	8232	3797.58	6489.36	44.754	RFT
L04-07	8232	3801.03	6492.8	44.778	RFT
L04-07	8232	3807.53	6502.83	44.847	RFT
L04-07	8232	3807.54	6492.09	44.773	RFT
L04-07	8232	3809.04	6493.74	44.784	RFT
L04-07	8232	3812.55	6494.28	44.788	RFT
L04-07	8232	3816.85	6495.9	44.799	RFT
L04-07	8232	3818.05	6508.68	44.887	RFT
L04-07	8232	3824.56	6526.61	45.011	RFT
L04-07	8232	3824.66	6528.02	45.021	RFT
L04-07	8232	3833.57	6504.95	44.862	RFT
L04-07	8232	3848.56	6506.02	44.869	RFT
L04-07	8232	3848.57	6505.35	44.864	RFT
L04-07	8232	3849.54	6507.06	44.876	RFT
L04-07	8232	3933.14	6572.11	45.325	RFT
L04-07	8232	3954.63	6628.14	45.711	RFT
L04-07	8232	3955.15	6621.52	45.666	RFT
L04-07	8232	4027.66	7502.92	51.744	RFT
L04-A-01	7259	3761.35	6507.7	44.881	RFT
L04-A-01	7259	3773.03	6507.7	44.881	RFT
L04-A-01	7259	3794	6512.7	44.915	RFT
L04-A-01	7259	3806.97	6513.7	44.922	RFT
L04-A-01	7259	3816.96	6514.7	44.929	RFT
L07-10	7271	1820.73	3255.7	22.453	RFT
L07-10	7271	2301.25	3962.7	27.329	RFT
L07-10	7271	2327.74	4006.7	27.632	RFT
L07-10	7271	2406.23	4140.7	28.557	RFT
L07-10	7271	2413.72	4151.7	28.632	RFT
L07-10	7271	2423.72	4166.7	28.736	RFT
L07-10	7271	2432.22	4179.7	28.826	RFT
L07-10	7271	2438.72	4192.7	28.915	RFT
L07-10	7271	2449.72	4211.7	29.046	RFT

WELL_NAME	WELL_ID	TVD_SS (m)	FORMATION_PRESSURE (Psia)	(MPa)	DATA_SOURCE
L07-H-01	7756	3953.57	6725.4	46.382	RFT
L07-H-01	7756	4071.14	7134.4	49.203	RFT
L07-H-01	7756	4097.38	6839.98	47.172	RFT
L07-H-01	7756	4119.97	6803.72	46.922	RFT
L07-H-01	7756	4136.16	6808.07	46.952	RFT
L07-H-01	7756	4147.97	6819.67	47.032	RFT
L07-H-01	7756	4172.2	7285.24	50.243	RFT
L07-H-02	7943	3818.89	9911.2	68.353	RFT
L07-H-02	7943	3827.08	9935.2	68.519	RFT
L07-N-01	7593	3923.5	6772.59	46.708	RFT
L07-N-01	7593	3936.7	7003.84	48.302	RFT
L07-N-01	7593	3970	6580.28	45.381	RFT
L07-N-01	7593	3973.7	6600.76	45.522	RFT
L07-N-01	7593	3980.3	6583.83	45.406	RFT
L07-N-01	7593	4103.5	6721.33	46.354	RFT
L07-N-01	7593	4117.5	6727.73	46.398	RFT
L07-N-01	7593	4141.5	7172	49.462	RFT
L07-N-01	7593	4151.5	6736.26	46.457	RFT
L07-N-01	7593	4158.5	6740.4	46.486	RFT
L07-N-01	7593	4165.5	6742.23	46.498	RFT
L07-N-01	7593	4169.5	6753.44	46.575	RFT
L07-N-01	7593	4174.5	6774.46	46.720	RFT
L07-N-01	7593	4176	6808	46.952	RFT
L07-N-02	7840	4231.73	6933.43	47.817	RFT
L07-N-02	7840	4232.7	6941.41	47.872	RFT
L08-07	7627	4505	9188	63.366	RFT
L08-07	7627	4509	9283	64.021	RFT
L08-07	7627	4516	9022	62.221	RFT
L08-07	7627	4516.3	8819	60.821	RFT
L08-07	7627	4521	8483	58.503	RFT
L08-07	7627	4521.2	8491	58.559	RFT
L08-07	7627	4525	7371	50.834	RFT
L08-07	7627	4526.9	7386	50.938	RFT
L08-07	7627	4530.9	7382	50.910	RFT
L08-07	7627	4535	7409	51.097	RFT
L08-07	7627	4538.9	7421	51.179	RFT
L08-07	7627	4545.9	7396	51.007	RFT
L08-07	7627	4547	7400	51.034	RFT
L08-07	7627	4547.9	7396	51.007	RFT
L08-07	7627	4551	7402	51.048	RFT
L08-11	7969	4194.94	7403.6	51.059	RFT
L08-11	7969	4199.94	7317.3	50.464	RFT
L08-11	7969	4203.23	6904.6	47.618	RFT
L08-11	7969	4203.23	6905	47.621	RFT
L08-11	7969	4206.93	6928.8	47.785	RFT
L08-11	7969	4214.93	6933.5	47.817	RFT
L08-11	7969	4219.63	6962.1	48.014	RFT
L08-11	7969	4223.63	6960.6	48.004	RFT
L08-11	7969	4226.72	6963.7	48.026	RFT
L08-11	7969	4228.82	6971.2	48.077	RFT
L08-11	7969	4228.82	6971.4	48.079	RFT
L08-11	7969	4233.52	7092.6	48.914	RFT
L08-11	7969	4234.92	7107.6	49.018	RFT
L08-11	7969	4237.42	6961.2	48.008	RFT
L08-11	7969	4238.42	6964.4	48.030	RFT
L08-11	7969	4239.42	6965.1	48.035	RFT
L08-11	7969	4241.62	6981.6	48.149	RFT
L08-11	7969	4243.12	7063.1	48.711	RFT
L08-11	7969	4245.12	6974.8	48.102	RFT
L08-12	8018	4023.51	6899.7	47.584	RFT
L08-12	8018	4249.28	6927	47.772	RFT
L08-12	8018	4249.88	6928	47.779	RFT
L08-12	8018	4250.58	6929	47.786	RFT
L08-G-01	7564	4144.66	7451.7	51.391	RFT
L08-G-01	7564	4149.16	8028	55.366	RFT
L08-G-01	7564	4183.16	8885.9	61.282	RFT
L08-G-01	7564	4188.16	7292.96	50.296	RFT
L08-G-01	7564	4196.66	7284.8	50.240	RFT
L08-G-01	7564	4201.16	7285.4	50.244	RFT
L08-G-01	7564	4210.66	7397.3	51.016	RFT
L08-G-01	7564	4210.67	7635.4	52.658	RFT
L08-G-01	7564	4218.16	7411.1	51.111	RFT
L08-G-01	7564	4251.16	9044	62.372	RFT
L08-G-01	7564	4271.16	9100	62.759	RFT
L09-03	7792	3718.94	6616.73	45.633	RFT
L09-03	7792	3727.43	6616.73	45.633	RFT
L09-03	7792	3727.93	6616.73	45.633	RFT
L09-03	7792	3736.92	6622.53	45.673	RFT
L09-03	7792	3749.41	6626.88	45.703	RFT

Annex 4b (continued): Calibration data: pressures

WELL_NAME	WELL_ID	TVD_SS (m)	FORMATION_PRESSURE (Psia)	(MPa)	DATA_SOURCE	WELL_NAME	WELL_ID	TVD_SS (m)	FORMATION_PRESSURE (Psia)	(MPa)	DATA_SOURCE
L09-09	8159	3901.03	7120.3	49.106	RFT	L11-A-02-S1	8258	3973.61	5751.24	39.664	RFT
L09-09	8159	3901.04	7094.34	48.926	RFT	L11-A-02-S1	8258	4009.6	5474.78	37.757	RFT
L09-09	8159	3912.23	6869.09	47.373	RFT	L11-A-02-S1	8258	4046.6	5445.76	37.557	RFT
L09-09	8159	3912.23	6900.13	47.587	RFT	L11-A-02-S1	8258	4096.6	5490.93	37.868	RFT
L09-09	8159	3912.23	6902.6	47.604	RFT	L11-A-02-S1	8258	4117.6	5591.97	38.565	RFT
L09-09	8159	3915.83	6721.15	46.353	RFT	L11-A-02-S1	8258	4119.6	5567.31	38.395	RFT
L09-09	8159	3917.09	6828.77	47.095	RFT	L11-A-02-S1	8258	4126.6	5535.55	38.176	RFT
L09-09	8159	3917.09	6836.46	47.148	RFT	L11-A-02-S1	8258	4145.6	5571.87	38.427	RFT
L09-09	8159	3917.1	6828.77	47.095	RFT	L11-A-02-S1	8258	4158.6	6070.34	41.864	RFT
L09-09	8159	3920.01	6730.44	46.417	RFT	L11-A-02-S1	8258	4170.6	6122.77	42.226	RFT
L09-09	8159	3920.01	6758.86	46.613	RFT	L11B-A-01	7355	3495	5949.44	41.031	RFT
L09-09	8159	3920.01	6760.02	46.621	RFT	L11B-A-01	7355	3496.5	5950.89	41.041	RFT
L09-09	8159	3927.31	6767.57	46.673	RFT	L11B-A-01	7355	3499.7	5956.69	41.081	RFT
L09-09	8159	3932.18	6775.4	46.727	RFT	L11B-A-01	7355	3517.4	5943.64	40.991	RFT
L09-09	8159	3934.13	6777.14	46.739	RFT	L11B-A-01	7355	3517.4	5947.99	41.021	RFT
L09-09	8159	3936.17	6777.72	46.743	RFT	L11B-A-01	7355	3548.1	5985.7	41.281	RFT
L09-09	8159	3959.92	6657.34	45.913	RFT	L11B-A-01	7355	3672.2	6079.98	41.931	RFT
L09-09	8159	3961.19	6904.34	47.616	RFT	L11B-A-01	7355	3690.5	6169.9	42.551	RFT
L09-09	8159	3964.39	6874.03	47.407	RFT	L11B-A-01	7355	3714	6151.04	42.421	RFT
L09-09	8159	3964.39	6874.9	47.413	RFT	L11B-A-01	7355	3736.7	6188.75	42.681	RFT
L09-09	8159	3965.74	6871.27	47.388	RFT	L11B-A-01	7355	3760.7	6259.82	43.171	RFT
L10-31	8268	3508.88	5644.42	38.927	RFT	L12-03	7361	2886.76	5001.4	34.492	RFT
L10-31	8268	3509.85	5628.39	38.816	RFT	L12-03	7361	2903	4889.4	33.720	RFT
L10-31	8268	3527.88	5632.08	38.842	RFT	L12-03	7361	2903.4	4929.4	33.996	RFT
L10-31	8268	3540.36	5637.46	38.879	RFT	L12-03	7361	2903.4	4936.4	34.044	RFT
L10-31	8268	3565.36	5644.37	38.927	RFT	L12-03	7361	2934.31	4907.4	33.844	RFT
L10-31	8268	3566.38	5647.74	38.950	RFT	L12-03	7361	2947.28	4902.4	33.810	RFT
L10-31	8268	3580.39	5286.66	36.460	RFT	L12-03	7361	2966.24	4938.4	34.058	RFT
L10-31	8268	3589.4	5772.69	39.812	RFT	L12-05	7783	3048.2	6418.49	44.265	RFT
L10-31	8268	3621.21	5726.79	39.495	RFT	L12-05	7783	3187.08	6523.53	44.990	RFT
L10-31	8268	3626.42	5715.55	39.418	RFT	L12-05	7783	3349.94	6659.86	45.930	RFT
L10-31	8268	3754.35	5941.43	40.975	RFT	L12-05	7783	3459.85	6848.92	47.234	RFT
L10-A-06-S2	7310	3649	4971.7	34.288	RFT	L13-06	7369	3259.94	5594.1	38.580	RFT
L10-A-06-S2	7310	3659.66	5639.7	38.894	RFT	L13-06	7369	3271.9	5598.46	38.610	RFT
L10-A-06-S2	7310	3671.42	5244.7	36.170	RFT	L13-06	7369	3278.87	5592.65	38.570	RFT
L10-A-06-S2	7310	3723.98	5316.7	36.667	RFT	L13-06	7369	3278.88	5575.25	38.450	RFT
L10-G-01	7302	3815.2	6237.4	43.017	RFT	L13-06	7369	3293.82	5639.07	38.890	RFT
L10-G-01	7302	3825	6240.7	43.039	RFT	L13-06	7369	3304.08	5598.46	38.610	RFT
L10-G-01	7302	3837	6244.7	43.067	RFT	L13-06	7369	3319.73	5612.96	38.710	RFT
L10-G-01	7302	3881	6294.7	43.412	RFT	L13-06	7369	3327.7	5604.26	38.650	RFT
L10-G-01	7302	3885.5	6326.7	43.632	RFT	L13-06	7369	3347.15	5630.36	38.830	RFT
L10-G-01	7302	3889.7	6321.7	43.598	RFT	L13-06	7369	3356.12	5620.21	38.760	RFT
L10-G-01	7302	3901	6339.7	43.722	RFT	L13-06	7369	3368.58	5614.41	38.720	RFT
L10-G-01	7302	3904.5	6340.7	43.729	RFT	L13-06	7369	3378.56	5620.21	38.760	RFT
L10-K-02	7662	3687.34	5986	41.283	RFT	L13-06	7369	3389.02	5623.11	38.780	RFT
L10-K-02	7662	3703.79	5994	41.338	RFT	L13-06	7369	3439.87	5647.77	38.950	RFT
L10-K-02	7662	3717.3	6003	41.400	RFT	L13-06	7369	3455.63	5768.15	39.780	RFT
L10-K-02	7662	3747.95	6116	42.179	RFT	L13-06	7369	3460.92	5669.52	39.100	RFT
L10-K-02	7662	3748.38	6140	42.345	RFT	L13-06	7369	3473.48	5647.77	38.950	RFT
L10-K-02	7662	3748.82	6126	42.248	RFT	L13-06	7369	3477.27	5649.22	38.960	RFT
L10-K-02	7662	3754.01	6295	43.414	RFT	L13-08	7675	3479.48	5707.7	39.363	RFT
L10-K-02	7662	3754.02	6281	43.317	RFT	L13-08	7675	3490.47	5978.7	41.232	RFT
L10-K-02	7662	3757.92	6151	42.421	RFT	L13-08	7675	3538.93	5716.7	39.426	RFT
L10-K-02	7662	3757.93	6134	42.303	RFT	L13-08	7675	3562.91	5728.7	39.508	RFT
L10-K-02	7662	3758.77	5617	38.738	RFT	L13-08	7675	3596.88	5737.7	39.570	RFT
L10-K-02	7662	3769.16	6538	45.090	RFT	L13-08	7675	3601.38	5778.7	39.853	RFT
L10-K-02	7662	3782.15	6561	45.248	RFT	L13-08	7675	3676.83	5896.7	40.667	RFT
L10-K-02	7662	3871.32	6222	42.910	RFT	L13-08	7675	3680.32	5893.7	40.646	RFT
L10-K-02	7662	3906.82	6271	43.248	RFT	L13-08	7675	3692.82	5912.7	40.777	RFT
L11-04	7353	3453.59	5872.7	40.501	RFT	L13-09	7681	3403.93	5647	38.945	RFT
L11-04	7353	3453.89	5918.7	40.819	RFT	L13-09	7681	3408.46	5679	39.166	RFT
L11-04	7353	3453.89	5920.7	40.832	RFT	L13-09	7681	3428.86	5735	39.552	RFT
L11-04	7353	3515.89	6186.7	42.667	RFT	L13-09	7681	3433.89	5707	39.359	RFT
L11-04	7353	3620.39	5957.7	41.088	RFT	L13-09	7681	3489.21	5674	39.131	RFT
L11-04	7353	3642.69	6052.7	41.743	RFT	L13-09	7681	3493.2	5684	39.200	RFT
L11-05	7354	3421.65	5648.7	38.957	RFT	L13-09	7681	3578.46	5764	39.752	RFT
L11-05	7354	3514.97	5706.7	39.357	RFT	L13-09	7681	3578.47	5762.35	39.740	RFT
L11-05	7354	3524.26	5713.7	39.405	RFT	L13-09	7681	3588.43	5747	39.634	RFT
L11-05	7354	3524.36	5713.7	39.405	RFT	L13-09	7681	3597.9	5759	39.717	RFT
L11-05	7354	3524.46	5713.7	39.405	RFT	L13-09	7681	3626.33	5813	40.090	RFT
L11-05	7354	3548.53	5928.7	40.888	RFT	L13-09	7681	3641.29	5841	40.283	RFT
L11-05	7354	3554.03	5818.7	40.129	RFT						
L11-09	7358	3362.34	5482.7	37.812	RFT						
L11-09	7358	3362.84	5484.7	37.826	RFT						
L11-09	7358	3362.85	5429.7	37.446	RFT						
L11-09	7358	3368.94	5439.7	37.515	RFT						
L11-09	7358	3368.94	5440.7	37.522	RFT						
L11-09	7358	3395.34	5457.7	37.639	RFT						
L11-09	7358	3395.35	5459.7	37.653	RFT						
L11-09	7358	3420.34	5509.7	37.998	RFT						
L11-09	7358	3420.64	5506.7	37.977	RFT						
L11-09	7358	3431.84	5508.7	37.991	RFT						
L11-09	7358	3431.84	5516.7	38.046	RFT						
L11-09	7358	3553.73	5728.7	39.508	RFT						

Annex 4b (continued): Calibration data: pressures

WELL_NAME	WELL_ID	TVD_SS (m)	FORMATION_PRESSURE (Psia)	(MPa)	DATA_SOURCE
L13-16	8100	3248.56	5133.69	35.405	RFT
L13-16	8100	3250.06	5160.23	35.588	RFT
L13-16	8100	3259.06	5205.92	35.903	RFT
L13-16	8100	3261.06	5187.79	35.778	RFT
L13-16	8100	3376.1	5692.97	39.262	RFT
L13-16	8100	3376.51	5769.84	39.792	RFT
L13-16	8100	3376.9	5587.09	38.532	RFT
L13-16	8100	3407.6	5449.88	37.585	RFT
L13-16	8100	3413.99	5436.06	37.490	RFT
L13-16	8100	3490.02	5538.06	38.194	RFT
L13-16	8100	3519.99	5614.35	38.720	RFT
L13-16	8100	3526.06	5600.72	38.626	RFT
L13-16	8100	3542.53	5633.1	38.849	RFT
L13-16	8100	3542.62	5635.24	38.864	RFT
L13-17	8177	3249.56	5260.02	36.276	RFT
L13-17	8177	3259.46	5254.79	36.240	RFT
L13-17	8177	3259.47	5254.23	36.236	RFT
L13-17	8177	3259.48	5253.16	36.229	RFT
L13-17	8177	3260.66	5255.27	36.243	RFT
L13-17	8177	3270.75	5339.79	36.826	RFT
L13-17	8177	3283.15	5277.42	36.396	RFT
L13-17	8177	3334.95	5356.47	36.941	RFT
L13-17	8177	3334.96	5353.57	36.921	RFT
L13-17	8177	3344.25	5362.56	36.983	RFT
L13-17	8177	3356.14	5370.1	37.035	RFT
L13-17	8177	3364.34	5383.44	37.127	RFT
L13-17	8177	3411.21	5455.09	37.621	RFT
L13-17	8177	3435.59	5384.17	37.132	RFT
L13-17	8177	3452.08	5321.08	36.697	RFT
L13-17	8177	3475.15	5446.25	37.560	RFT
L13-FD-101	7608	3399.76	5725.7	39.488	RFT
L13-FD-101	7608	3420.96	5648.7	38.957	RFT
L13-FD-101	7608	3507.65	5680.7	39.177	RFT
L13-FD-101	7608	3515.48	5684.7	39.205	RFT
L13-FD-101	7608	3591.83	5769.7	39.791	RFT
L13-FD-101	7608	3596.8	5772.7	39.812	RFT
L13-FD-101	7608	3600.29	5770.7	39.798	RFT
L13-FD-101	7608	3600.3	5769.7	39.791	RFT
L13-FD-101	7608	3600.7	5771.7	39.805	RFT
L13-FD-101	7608	3602.77	5775.7	39.832	RFT
L13-FD-101	7608	3609.92	5776.7	39.839	RFT
L13-FD-101	7608	3611.74	5779.7	39.860	RFT
L13-FD-101	7608	3613.22	5780.7	39.867	RFT
L13-FD-101	7608	3634.58	5861.7	40.426	RFT
L13-FD-101	7608	3640.06	5824.7	40.170	RFT
L13-FD-101	7608	3644.03	5827.7	40.191	RFT
L13-FD-101	7608	3654.44	5861.7	40.426	RFT
L13-FE-101	7769	3320.73	5497.13	37.911	RFT
L13-FE-101	7769	3320.81	5456.51	37.631	RFT
L13-FE-101	7769	3365.14	5468.12	37.711	RFT
L13-FE-101	7769	3398	5478.27	37.781	RFT
L13-FE-101	7769	3423.75	5486.97	37.841	RFT
L13-FE-101	7769	3427.21	5507.28	37.981	RFT
L13-FE-101	7769	3447.48	5601.55	38.631	RFT
L13-FE-101	7769	3449.06	5732.09	39.532	RFT
L13-FE-101	7769	3488.26	5668.27	39.092	RFT
L13-FE-101	7769	3503.66	5663.92	39.062	RFT
L13-FE-101	7769	3504.07	5630.56	38.831	RFT
L13-FE-101	7769	3509.68	5594.3	38.581	RFT
L13-FE-101	7769	3524.02	5617.51	38.741	RFT
L13-FE-101	7769	3533.41	5672.62	39.122	RFT
L13-FE-102	7942	3470.56	5719.03	39.442	RFT
L13-FE-102	7942	3497.13	5721.93	39.462	RFT
L13-FE-102	7942	3522.49	5733.54	39.542	RFT
L13-FE-102	7942	3531.48	5736.44	39.562	RFT
L13-FE-102	7942	3549.46	5748.04	39.642	RFT
L13-FE-102	7942	3552.16	5748.04	39.642	RFT
L13-FE-102	7942	3563.95	5768.35	39.782	RFT
L13-FE-102	7942	3591.91	5755.29	39.692	RFT
L13-FE-102	7942	3667.84	5882.93	40.572	RFT
L13-FE-102	7942	3678.83	5890.18	40.622	RFT
L13-FH-101	7799	3249.5	5362.24	36.981	RFT
L13-FH-101	7799	3274.45	5370.94	37.041	RFT
L13-FH-101	7799	3317.37	5385.45	37.141	RFT
L13-FH-101	7799	3348.32	5391.25	37.181	RFT
L13-FH-101	7799	3439.16	5533.38	38.161	RFT
L13-FH-101	7799	3448.14	5530.48	38.141	RFT
L13-FH-101	7799	3458.13	5533.38	38.161	RFT
L13-FH-101	7799	3472.15	5546.44	38.251	RFT
L13-FH-101	7799	3501.1	5594.3	38.581	RFT
L13-FH-101	7799	3515.07	5617.51	38.741	RFT

WELL_NAME	WELL_ID	TVD_SS (m)	FORMATION_PRESSURE (Psia)	(MPa)	DATA_SOURCE
L14-06	8010	3051.08	4947.3	34.119	RFT
L14-06	8010	3070.47	4954.6	34.170	RFT
L14-06	8010	3070.57	4966.2	34.250	RFT
L14-06	8010	3088.87	4963.3	34.230	RFT
L14-06	8010	3114.73	5060.45	34.900	RFT
L14-06	8010	3174.41	5201.1	35.870	RFT
L14-06	8010	3234.6	5169.23	35.650	RFT
L14-06	8010	3254.49	5191	35.800	RFT
L14-06	8010	3276.38	5225.8	36.040	RFT
L14-A-02	7741	3257	5485.7	37.832	RFT
L14-A-02	7741	3268.86	5607.7	38.674	RFT
L14-A-02	7741	3278.14	5410.7	37.315	RFT
L14-A-02	7741	3278.46	5388.7	37.163	RFT
L14-A-02	7741	3278.57	5370.7	37.039	RFT
L14-A-02	7741	3288.16	5369.7	37.032	RFT
L14-A-02	7741	3310.81	5728.7	39.508	RFT
L14-A-02	7741	3312.43	5291.7	36.494	RFT
L14-A-02	7741	3312.53	5281.7	36.426	RFT
L14-A-02	7741	3360.52	5592.7	38.570	RFT
L14-A-02	7741	3397.19	5495.7	37.901	RFT
L15-03	7376	2945.34	4841.4	33.389	RFT
L15-03	7376	2958.82	4854.5	33.479	RFT
L15-03	7376	2969.8	4863.2	33.539	RFT
L15-03	7376	2998.72	4915.4	33.899	RFT
L15-03	7376	3176.7	5233	36.090	RFT
L15-04	7377	2884.8	4909.6	33.859	RFT
L15-04	7377	2935.09	4925.56	33.969	RFT
L15-04	7377	2980.77	4934.3	34.030	RFT
L15-04	7377	3005.2	4979.2	34.339	RFT
L15-04	7377	3009.48	5031.4	34.699	RFT
L15-04	7377	3009.68	5018.4	34.610	RFT
L15-FA-101	7375	2889.11	4873.3	33.609	RFT
L15-FA-101	7375	2910.59	5035.8	34.730	RFT
L15-FA-101	7375	2924.09	4900.9	33.799	RFT
L15-FA-101	7375	2932.08	4883.5	33.679	RFT
L15-FA-101	7375	2939.57	4886.4	33.699	RFT
L15-FA-101	7375	2939.58	4884.9	33.689	RFT
L15-FA-101	7375	2959.56	5099.6	35.170	RFT

ANNEX 4 Calibration data

Annex 4c: Calibration data: temperatures

WELL NAME	WELL_ID	TVD_ss (m)	TEMPERATURE (°C)	DATA_SOURCE
K06-02	7089	3472.7	106	BHTX
K09C-A-01	7624	3869.27	122.23	DST_EXT
K11-FA-103	7929	3208.16	109	BHTX
L04-06	8173	3613.4	121.85	DST_EXT
L04-07	8232	3755.96	124	BHTX
L07-01	7264	3561.96	114	BHTX
L07-01	7264	3891	117	BHTX
L07-04	7265	3826.43	109	BHTX
L07-06	7267	3806.91	107	BHTX
L07-07	7268	3804.27	114	BHTX
L07-08	7269	3985.44	116	BHTX
L07-C-01	7277	4083.8	123	BHTX
L07-N-01	7593	4165.5	133	BHTX
L08-02	7279	3965.16	125	BHTX
L08-02	7279	4271.29	136	BHTX
L08-03	7280	4025.6	115	BHTX
L08-03	7280	4397.75	134	BHTX
L08-11	7969	4323.4	133	BHTX
L08-12	8018	4335.23	134	BHTX
L08-A-01	7628	4035.31	130.68	DST_EXT
L08-A-01	7628	4054.92	130.38	DST_EXT
L08-A-01	7628	4064.77	131.78	DST_EXT
L08-A-01	7628	4077.43	132.06	DST_EXT
L08-G-01	7564	4138.06	145.85	DST_EXT
L08-G-01	7564	4151.96	143.48	DST_EXT
L08-G-02-S1	7576	4272.33	144.9	DST_EXT
L08-G-02-S1	7576	4331.79	148.79	DST_EXT
L08-H-01	7659	4004.57	132.4	DST_EXT
L08-H-01	7659	4040.39	134.69	DST_EXT
L08-H-01	7659	4089.15	137.25	DST_EXT
L08-H-01	7659	4098.03	132.49	DST_EXT
L08-H-01	7659	4164.45	130	BHTX
L09-03	7792	3718.14	134.33	DST_EXT
L10-10	7289	4001.3	119	BHTX
L10-G-01	7302	3780.5	123.9	DST_EXT
L11-04	7353	3711.43	126	BHTX
L11-05	7354	3583.5	124	BHTX
L11-A-02-S1	8258	4234.6	120	BHTX
L12-03	7361	2838.06	103	BHTX
L12-03	7361	3120.44	114	BHTX
L12-05	7783	3241.53	115.9	DST_EXT
L12-05	7783	3241.54	117.5	DST_EXT
L12-05	7783	3302.98	117	DST_EXT
L13-06	7369	3632.37	120	BHTX
L13-11	7802	3575.16	128	BHTX
L13-FD-101	7608	3626.64	117	BHTX
L13-FE-101	7769	3415.34	122.36	DST_EXT
L13-FE-101	7769	3587.93	128	BHTX
L14-06	8010	3334.17	107	BHTX
L14-A-01	7370	3405.4	115	BHTX
L17-03	7838	3051.09	103	BHTX

ANNEX 4 Calibration data

Annex 4d: Calibration data: vitrinite reflectance

Vitrinite reflectance values for the Central Offshore Platform used for calibration purposes.

The results of the vitrinite reflectance measurements are presented by their statistics (average value, standard deviation and number of measurements per sample) and a label describing the reliability of the measurement.

On the basis of the number of measurements and the standard deviation a statement can be made on the 'reliability' of the measurement. The criteria are given in the table below.

A	High reliability, (Stdv ≤ 0.05; N ≥ 40)
B	Average reliability, (0.05 ≤ Stdv ≥ 0.10; 15 ≤ N ≥ 40)
C	Low reliability, (Stdv ≥ 0.10; N ≤ 15)

Summary of the vitrinite reflectance measurements. %Rr = mean random reflectance; SD = standard deviation; N = number of measurements; A = high reliability; B = average reliability C = low reliability; mp = multiple populations. Areas indicated in grey represent the individual populations as calculated from the values of the original sample.

WELL_NAME	SAMPLE DEPTH	%Rr	SD	N	Reliability	Stratigraphy
	Top (m)					
L11-12	2936	0.8	0.54	17	C	RBSHM
L11-12	2988	0.78	0.28	8	C	RBSHM
L11-12	3112	0.68	0.24	63	C	ZEZC1
L11-12	3446	1.56	0.13	88	C	DCCR
L11-12	3458	1.11	0.35	100	C	DCCR
L11-12	3466	0.96	0.25	100	C	DCCR
L11-12	3506	0.84	0.09	100	B	DCCR